



Engineering Geology  
Royal Institute of Technology

Doctoral Thesis  
— 1993 —

# Mechanics of Fractures and Intervening Bridges in Hard Rocks

Baotang Shen

Stockholm, Sweden

# **Mechanics of Fractures and Intervening Bridges in Hard Rocks**

Baotang Shen

Engineering Geology  
Royal Institute of Technology  
S-100 44 Stockholm

AKADEMISK AVHANDLING

som med tillstånd av Kungliga Tekniska Högskolan i Stockholm framläggs till offentlig granskning för avläggande av tekniska doktorexamen i Teknisk Geologi, 1 december 1993 kl 10.00 i Kollegiesalen, Administrationsbyggnaden, KTH, Valhallavägen 79, Stockholm. Avhandlingen försvaras på engelska.

**"Mechanics of Fractures and Intervening Bridges in Hard Rocks"** by *B. Shen*,  
Engineering Geology, Royal Institute of Technology, Doctoral Thesis (1993), ISBN  
91-7170-140-0

### ABSTRACT

This study is about the mechanical behaviour of rock fractures and bridges in relation to the deformability and strength of fractured rock masses. The work deals with sliding, propagation and coalescence of rock fractures.

Depending upon different compressive loading levels, the fracture behaviour is divided into three phases: (a) at low stress level, rock fractures have only sliding deformation; (b) at intermediate stress level, fractures undergo sliding and mode I fracture propagation; and (c) at high stress level, intact rock between fractures—rock bridges—fail and rock fractures coalesce. For each phase, different models are developed to explain and predict the behaviour of rock fracture-bridge systems, namely the conceptual model, the tensile failure model and the coalescence model.

The conceptual model of fracture deformation is developed for the low stress loading and it considers the sliding of rock fractures and the interaction between fractures and bridge. This model explains the hysteretic loading and unloading characteristic of a fractured rock mass.

The tensile failure model is established for intermediate stress loading and it uses the Displacement Discontinuity Method (DDM). The model takes into account the fracture sliding and mode I fracture propagation. Both the non-linearity during loading and the hysteresis during unloading of a fractured rock mass are reproduced with the tensile failure model.

To study the failure mechanism of rock bridge at high compressive loading, experimental investigation of coalescence between two open and closed fractures was carried out by using uniaxial compressive loading test of pre-fractured gypsum samples. It is unveiled that closed fractures can coalesce when fracture friction resistance is exceeded. Fracture coalescence can develop by tensile failure, shear failure and mixed tensile and shear failure. The failure mode depends upon the relative position of the two fractures. When the fractures are almost overlapping in the direction of loading, fracture coalescence can easily occur by mixed tensile and shear failure of the rock bridge. The mixed mode of failure controls the strength of fractured rock masses.

The coalescence model explains and predicts the fracture coalescence at high loading level. To simulate both tensile and shear failure, a fracture criterion which considers both mode I and II surface energy is proposed and implemented in the numerical method DDM. Application of a modified G-criterion and DDM to the experiments produces excellent agreement with the experimental results. The fracture coalescence model explains well the complicated mechanism of fracture coalescence of earth materials.

**Key words:** Rock fracture, rock bridge, fracture mechanics, fracture propagation, mode I, mode II, fracture coalescence, numerical modelling, physical experiment.

*One can never stop learning, whenever and wherever*

*To my wife and my little daughter*

## Acknowledgements

I wish to express my sincere thanks to the following persons who gave me a lot of help and encouragement — in one way or another — during my doctoral studies for nearly two years at the Division of Rock Mechanics, Luleå University of Technology and three years at Engineering Geology, Royal Institute of Technology:

Professor Ove Stephansson at Engineering Geology, Royal Institute of Technology, previously at the Division of Rock Mechanics, Luleå University of Technology, who gave me the opportunity to study at Luleå University of Technology and brought me to the Royal Institute of Technology; who gave me his supervision and guidance in my research work; and who always gave me much freedom and trust in my work.

Professor Herbert Einstein at the Department of Civil Engineering, Massachusetts Institute of Technology (MIT), who gave me the opportunity to visit him and perform my experimental tests in his laboratory. Mr. Bidjan Ghahreman at the same department who gave me a lot of help during the experiments.

Professor Wang Yongjia, Northeast University, China, who sent me to Sweden for the Sino-Swedish co-operation in mining and metallurgy and made my study in Sweden possible.

My colleagues at Engineering Geology (KTH) who created a kind environment for studying and who shared my happiness when I had success in my research work and who always gave me encouragement at the time when I was not so successful.

My former colleagues at the Division of Rock Mechanics, Luleå University of Technology, who gave me a lot of help at the difficult time when I had just arrived in Sweden and nothing was familiar to me.

The Swedish National Board for Industrial and Technical Development (NUTEK) provided the financial support. The research work is part of the Sino-Swedish Co-operation on Metallurgy and Mining, Project 2.3, Numerical Modelling for Rock Engineering Design.

# Contents

Abstract	iv
1. Introduction	1
2. A conceptual model of a fracture-rock bridge system	5
2.1 Loading	6
2.2 Initial unloading	7
2.3 Final unloading	7
3. A tensile failure model	9
3.1 The Displacement Discontinuity Method (DDM)	9
3.2 Simulation of fracture initiation and propagation	12
3.3 Application of the numerical model to the fracture-bridge system	13
4. A modified G-criterion for fracture propagation in mode I and mode II	15
4.1 The modified G-criterion	15
4.1.1 The original G-criterion	16
4.1.2 Numerical calculation of G-value	16
4.1.3 The insufficiency of the original G-criterion	17
4.1.4 Modification of the G-criterion	18
4.2 Application of the modified G-criterion to mixed mode fracture propagation	19
5. Experimental and numerical study of fracture coalescence	22
5.1 Experimental investigation of fracture coalescence	22
5.1.1 The process of coalescence	22
5.1.2 Failure mode of the bridge	25
5.1.3 Load of coalescence	25

5.2	Numerical simulation and interpretation	26
5.2.1	Stress analysis	26
5.2.2	Modelling by using the modified G-criterion and DDM	28
6.	Conclusions and recommendations for future work	33
6.1	Conclusion	33
6.2	Recommendations for future study	33
	References	35

## Appendix: Dissertation Papers

Paper A: A1-A5

**Cyclic loading characteristics of joints and rock bridges in a jointed rock specimen.**

By: Shen B. and Stephansson O.

Published in: *Proc. Int. Symp. on Rock Joints, Leon, Norway, pp.715-729.(1990)*

Paper B: B1-B15

**Deformation and propagation of finite joints in rock masses.**

By: Shen B. and Stephansson O.

Published in: *Proc. Int. Conf. on Fractured and Jointed Rock Masses, Lake Tahoe, U.S.A., Vol.2, pp.312-318. (preprints) (1992)*

Paper C: C1-C17

**Modification of the G-criterion for crack propagation subjected to compression.**

By: Shen B. and Stephansson O.

Published in: *Int. J. of Engineering Fracture Mechanics (in press) (1993).*



Paper D:

D1-D17

**Numerical analysis of Mode I and Mode II propagation of rock fractures.**

By Shen B. and Stephansson O.

Published in: *Int. J. Rock Mech. Min. Sci.* (special issue for the 34th U.S. Symposium on rock mechanics) (in press) (1993).

Paper E:

E1-E23

**Coalescence of open and closed cracks — A laboratory investigation.**

By: Shen B., Stephansson O., Einstein H. and Ghahreman B.

Submitted to: *Int. J. Rock Mech. Min. Sci.* (1993)

Paper F:

F1-F19

**The mechanism of fracture coalescence in compression — Experimental study and numerical simulation.**

By: Shen B.

Submitted to: *Int. J. Eng. Frac. Mech.* (1993)

## Abstract

This study is about the mechanical behaviour of rock fractures and bridges in relation to the deformability and strength of fractured rock masses. The work deals with sliding, propagation and coalescence of rock fractures.

Depending upon different compressive loading levels, the fracture behaviour is divided into three phases: (a) at low stress level, rock fractures have only sliding deformation; (b) at intermediate stress level, fractures undergo sliding and mode I fracture propagation; and (c) at high stress level, intact rock between fractures—rock bridges—fail and rock fractures coalesce. For each phase, different models are developed to explain and predict the behaviour of rock fracture-bridge systems, namely the conceptual model, the tensile failure model and the coalescence model.

The conceptual model of fracture deformation is developed for the low stress loading and it considers the sliding of rock fractures and the interaction between fractures and bridge. This model explains the hysteretic loading and unloading characteristic of a fractured rock mass.

The tensile failure model is established for intermediate stress loading and it uses the Displacement Discontinuity Method (DDM). The model takes into account the fracture sliding and mode I fracture propagation. Both the non-linearity during loading and the hysteresis during unloading of a fractured rock mass are reproduced with the tensile failure model.

To study the failure mechanism of rock bridge at high compressive loading, experimental investigation of coalescence between two open and closed fractures was carried out by using uniaxial compressive loading test of pre-fractured gypsum samples. It is unveiled that closed fractures can coalesce when fracture friction resistance is exceeded. Fracture coalescence can develop by tensile failure, shear failure and mixed tensile and shear failure. The failure mode depends upon the relative position of the two fractures. When the fractures are almost overlapping in the direction of loading, fracture coalescence can easily occur by mixed tensile and shear failure of the rock bridge. The mixed mode of failure controls the strength of fractured rock masses.

The coalescence model explains and predicts the fracture coalescence at high loading level. To simulate both tensile and shear failure, a fracture criterion which considers both mode I and II surface energy is proposed and implemented in the numerical method DDM. Application of a modified G-criterion and DDM to the experiments produces excellent agreement with the experimental results. The fracture coalescence model explains well the complicated mechanism of fracture coalescence of earth materials.

**Key words:** Rock fracture, rock bridge, fracture mechanics, fracture propagation, mode I, mode II, fracture coalescence, numerical modelling, physical experiment.

# 1. Introduction

Rock masses on a large scale contain faults, shear zones, dikes and other major discontinuities generated by tectonic processes. On engineering scales, rock masses are composed of intact rock and joints, bedding planes, fissures and similar minor discontinuities. Intact rocks, on the other hand, usually have voids, cracks and flaws. All these discontinuities in rock on different scales are named "rock fractures". Rock fractures of finite length often exist in rocks and rock masses and they are separated by intact rock. The intact parts of rock between fractures are named "rock bridges" (see Fig.1.1).

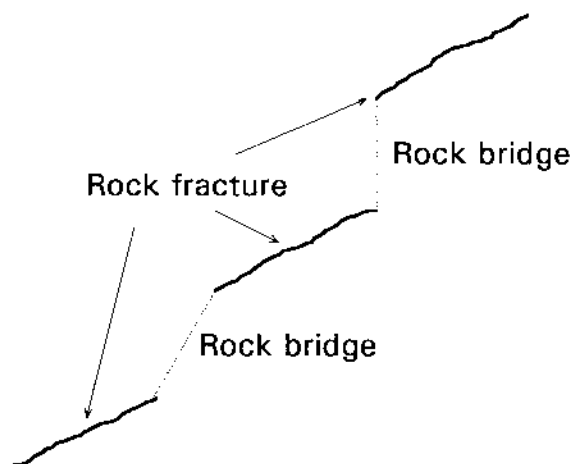


*Fig.1.1. Rock fractures and rock bridges in fractured rock mass.*

The existence of rock fractures and rock bridges is the main reason for the complicated mechanical response of brittle rocks to stress loading. Microcrack growth and interaction cause non-linear stress-strain relation and hysteresis (Griffith, 1921; Kachanov, 1982; Kemeny & Cook, 1991; Kemeny, 1991; Li, 1993), and induce splitting failure or shear failure of rock samples under compressive loading (Wong, 1982; Horii & Namat-Nasser, 1985, 1986; Lockner et al, 1992). Joint and bridge interaction can reduce the average elastic modulus (Kulatilake, 1992) and cause a strong hysteresis in the loading and unloading curve at testing jointed rock masses (Brady et al., 1986). The failure of the rock bridges can lead to the failure of rock slopes (Einstein, 1983) and other rock excavations, and create shear zones of faults which are usually accompanied by earthquakes (Segall & Pollard, 1983; Deng & Zhang, 1984). The fracture-bridge interaction and bridge failure dominates the mechanical behaviour of fractured rock masses and the stability of rock excavations.

A number of experimental and analytical works have been reported in the past decades on the behaviour of fractures and rock bridges. Among the experimental studies, Lajtai (1969) conducted direct shear tests on natural rock with two lined slots and studied the failure mode and shear strength of the bridge; Savilahti et al (1990) carried out shear box tests to study the failure pattern of the bridges between two stepped fractures; Brace & Byerlee (1967) performed uniaxial compression tests of glass samples with multiple en-echelon flaws to observe the crack propagation and interaction; Wang et al. (1987) used holograms to study the stress and strain field in the process of coalescence of two overlapping flaws in marble samples; Reyes & Einstein (1991) tested gypsum samples in uniaxial compression to study the coalescence between two non-overlapping flaws under uniaxial compressive load. Among the theoretical and numerical studies, Segall & Pollard (1980) analysed the stress field in the bridge between two stepped fractures; Hamajima et al. (1985) used a rigid block spring model to simulate the multi-crack interaction. A large number of numerical studies have been conducted by using the finite element method (Ingraffea, 1987, Boone et al., 1987), the boundary element method (Aliabadi & Bookey, 1991) and the discrete element method (Jirasek & Bazant, 1993) to simulate fracture propagation and fracture coalescence.

The achievements of previous studies can be summarized as the follows:

- 1). The stress state inside the rock bridge is very complicated. The methods to estimate the equivalent elastic properties of jointed rock mass by assuming persistent joints (Singh, 1973; Stephansson, 1981) cannot be applied to the fracture-rock bridge system. Failure criteria for intact rocks based on the assumption of a uniform stress distribution, such as tensile strength criterion, Coulomb's shear strength criterion (Brady & Brown, 1985) and Hoek & Brown's shear strength criterion (Hoek & Brown, 1980), do not predict the failure of rock bridges.
- 2). The mechanism of the failure of the rock bridges is complicated. It has been observed from laboratory tests that the failure of rock bridges can be caused by tension, by shearing or by mixed tension and shearing. However, there is still not a comprehensive understanding of when and how the different failure modes will occur.

3). Experimental tests conducted on polymer, glass etc. produced only tensile fracture propagation and only the bridges between overlapping fractures can fail. On the other hand, tests with samples made of rocks, gypsum, concrete etc. showed that shear failure can occur in the bridge between two non-overlapping fractures. This material-dependent characteristic means that, for different type of materials, the failure mode of the bridges may be different. The reason why different failure modes can occur in different materials is still not fully understood.

4). In studying the failure of rock bridges by using a fracture mechanics approach, the existing fracture criteria have been successfully applied in different numerical methods to predict the tensile (mode I) failure. However, so far the prediction of shear (mode II) failure of the bridges by using the existing fracture criteria has not been found successful.

The aim of the thesis is to give a better understanding of the complicated behaviour of rock fractures and rock bridges. The study to be described in this thesis is performed experimentally, analytically and numerically, and it starts with a simple conceptual model and ends with a complicated coalescence model, correspondent to different stress levels (Fig.1.2). In short, the thesis is composed of five major parts:

1. A conceptual model of a fracture-bridge system to study the deformability of rock samples under cyclic loading at low stress level due to fracture sliding. (Chapter 2)
2. A tensile failure model to study rock mass deformability at intermediate stress level. (Chapter 3)
3. Development of a fracture criterion for the bridge failure in shearing at high stress level. (Chapter 4)
4. Experimental and numerical study of fracture coalescence (Chapter 5).
5. Conclusions and recommendation for future works (Chapter 6).

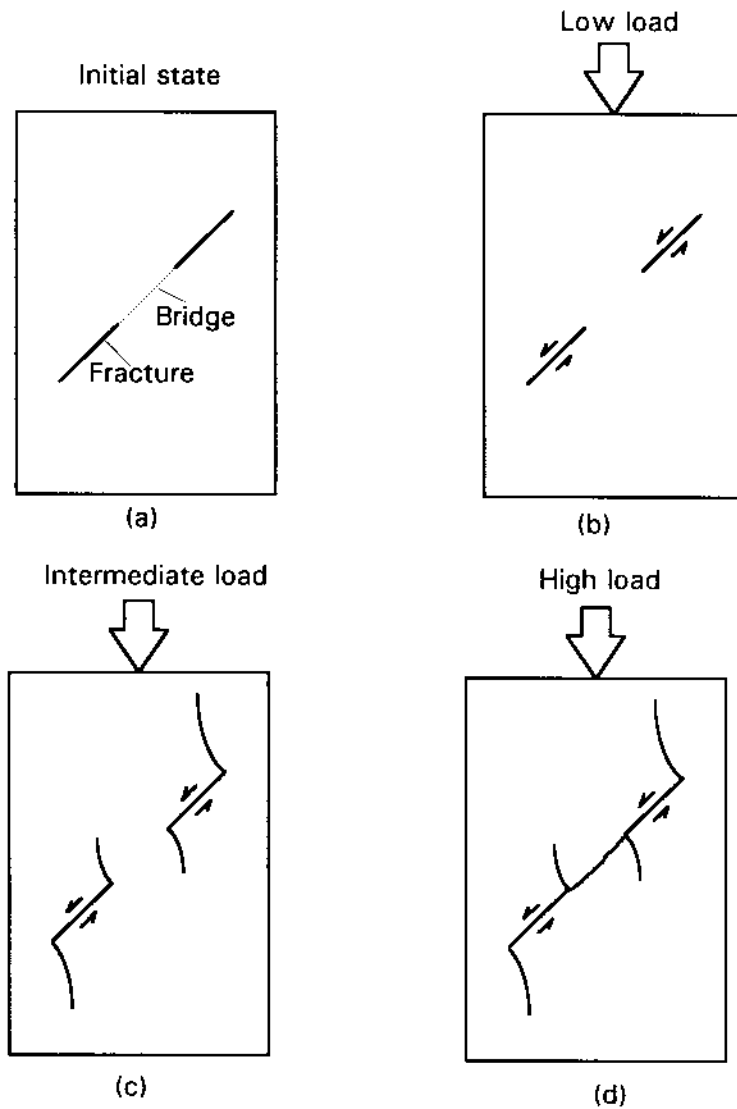


*Fig.1.2. Models of fracture response at different levels of loading stress. (a) Initial fracture-bridge system; (b) fracture deformation at low load; (c) tensile failure at intermediate load; and (d) fracture coalescence at high load.*

## 2. A conceptual model of a fracture-rock bridge system

A typical stress-strain curve of rocks or rock masses is non-linear during loading and shows hysteresis during unloading. Brady et al. (1985) reported the load-displacement relation of a heavily jointed, large rock block (dimensions  $2.2 \times 2.2 \times 2.0$  m) during a loading-unloading cycle (see Fig.2.1). Non-linearity and strong hysteresis was found. To explain this phenomenon, one has to consider the existence of fractures and rock bridges inside the rock masses and the sliding of the fractures.

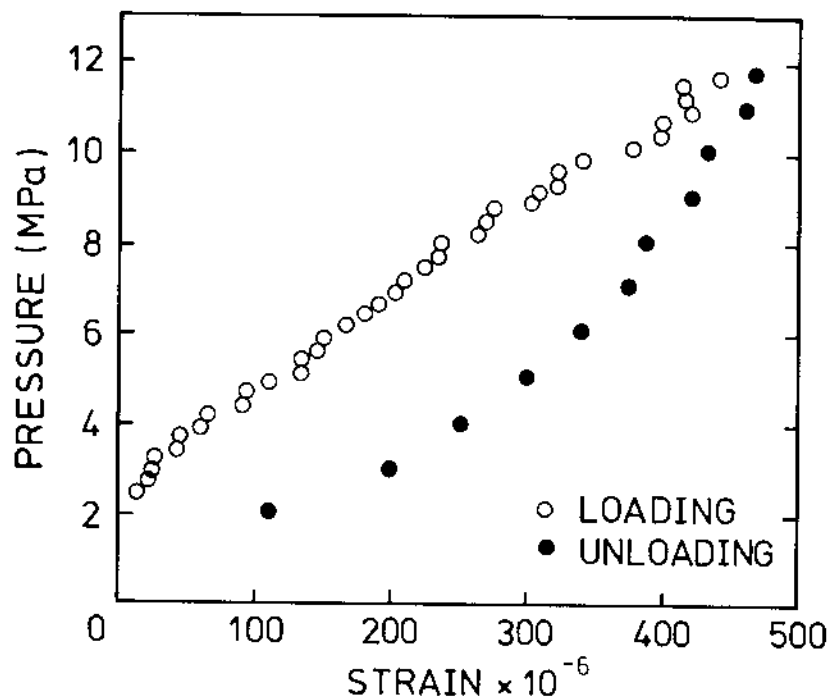


Fig.2.1. Load-displacement curve of a large basalt rock block ( $2.2 \times 2.2 \times 2.0$  m) during a loading and unloading cycle (Brady et al. 1985).

Consider a sample containing a fracture inside the sample and apply an uniaxial loading. We assume a plane cutting through the sample and the plane is then divided into the rock bridge part and the fracture part. The deformability of the bridges is considered by introducing the equivalent normal and shear stiffness ( $K_n^b$  and  $K_s^b$ ). The fracture is simulated by its true stiffness ( $K_n^f$  and  $K_s^f$ ) and friction angle ( $\phi$ ). The deformability of the intact rock is presented by an equivalent stiffness ( $k$ ). The sliding or locking of the fracture during a loading and an unloading cycle divides the whole process into three stages: loading stage, initial unloading stage, and final unloading stage (see Fig.2.2).



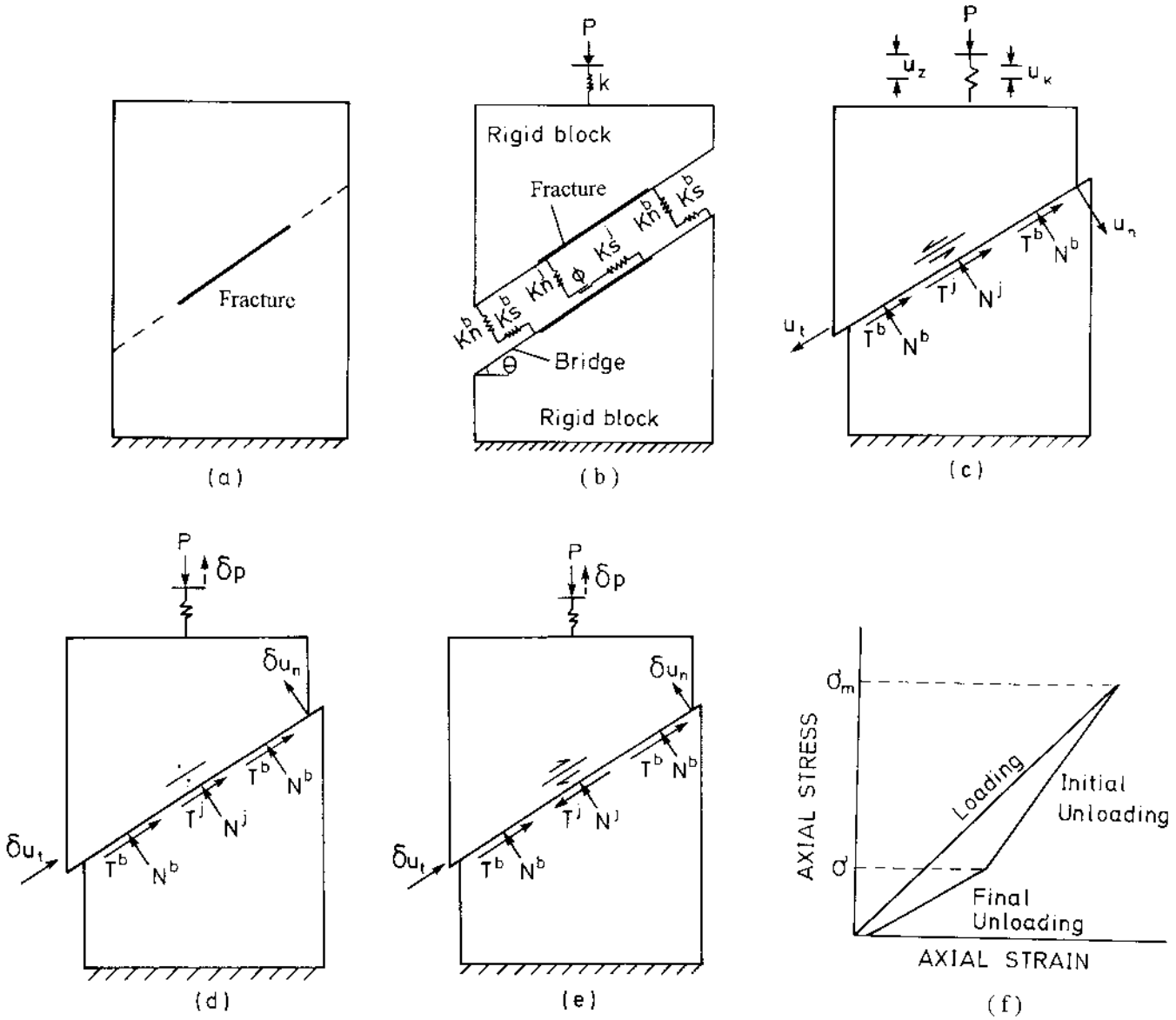


Fig.2.2. Conceptual model of a fracture-bridge system and its deformation process during a loading and unloading cycle. (a) A sample containing a fracture; (b) the conceptual model; (c) loading stage; (d) initial unloading stage; (e) final unloading stage; and (f) average stress-strain curve for the conceptual model

## 2.1 Loading

When the inclination of the fracture ( $\theta$ ) exceeds the critical value, i.e.

$$\theta \geq \tan^{-1} \left[ \frac{K_s^j + 2K_s^b}{K_n^j + 2K_n^b} \cdot \frac{K_n^j}{K_s^j} \cdot \tan \phi \right] \quad (2.1)$$

the fracture is sliding in the loading stage. With fracture sliding the deformation of the fracture-bridge system is not elastic. The average stress-strain relation is represented by

$$\frac{d\sigma}{d\varepsilon} = L \cdot \left[ \frac{L}{E'} + \frac{\cos^2 \theta}{K_n^j + 2K_n^b} + \frac{\sin \theta}{2K_s^b} \left( \sin \theta - \frac{K_n^j}{K_n^j + 2K_n^b} \cdot \tan \phi \cdot \cos \theta \right) \right]^{-1} \quad (2.2)$$

where  $L$ =height/width ( $H/W$ ) of the rock sample containing the fracture-bridge system;  $E'$ =Young's modulus of the intact rock for the plane stress condition ( $E' = k/H$ ).

## 2.2. Initial unloading

When the loading stress reaches the maximum and starts to decline, the fracture-bridge system is in the initial unloading stage. At this stage, the fracture undergoes a reversed shearing and it is temporarily locked. The deformation in this stage is elastic, and the stress-strain relation depends on the Young's modulus of intact rock and the shear and normal stiffness of both the fracture and bridges. It is given by:

$$\frac{d\sigma}{d\varepsilon} = L \cdot \left[ \frac{L}{E'} + \frac{\cos^2 \theta}{K_n^j + 2K_n^b} + \frac{\sin^2 \theta}{K_s^j + 2K_s^b} \right]^{-1} \quad (2.3)$$

## 2.3 Final unloading

When the loading stress decreases to a critical value ( $\sigma_c$ ), the shear stress developed in the fracture will cause the joint to slide again in the reversed direction. Therefore, the final unloading stage is also non-elastic. The ratio of the critical stress to the maximum loading stress is obtained as:

$$\frac{\sigma}{\sigma_m} = \frac{\alpha_1 \sin \theta - \alpha_2 \cos \theta \tan \phi}{\alpha_1 \sin \theta + \alpha_2 \cos \theta \tan \phi} \quad (2.4)$$

where  $\sigma$  — critical stress when the fracture starts to slide,

$\sigma_m$  — maximum stress applied in loading stage,

$\alpha_1$  —  $K_s^j / (K_s^j + 2K_s^b)$ , and

$\alpha_2$  —  $K_n^j / (K_n^j + 2K_n^b)$ .

The stress-strain relation when the applied stress is less than the critical stress in the final unloading stage is given by:

$$\frac{d\sigma}{d\varepsilon} = L \cdot \left[ \frac{L}{E'} + \frac{\cos^2 \theta}{K_n^j + 2K_n^b} + \frac{\sin \theta}{2K_s^b} \left( \sin \theta + \frac{K_s^j}{K_n^j + 2K_n^b} \cdot \tan \phi \cdot \cos \theta \right) \right]^{-1}. \quad (2.5)$$

Equations (2.2),(2.3) and (2.5) define a complete stress-strain curve of a complete loading and unloading cycle (Fig.2.2f). Only the initial unload stage is elastic, and the stress-strain relation in all the three stages is related to the shear and normal stiffness of the fracture and bridges. The analytical stress-strain curve also exhibits an evident hysteretic phenomenon in the unloading stage.

To check the validity of the conceptual model, a numerical simulation for a simple problem as shown in Fig.2.3 is carried out by using the distinct element code UDEC (Cundall, 1980). Excellent agreement between the numerical results and the analytical results is obtained, which proves that the conceptual model is able to simulate the hysteresis due to fracture-rock bridge interaction.

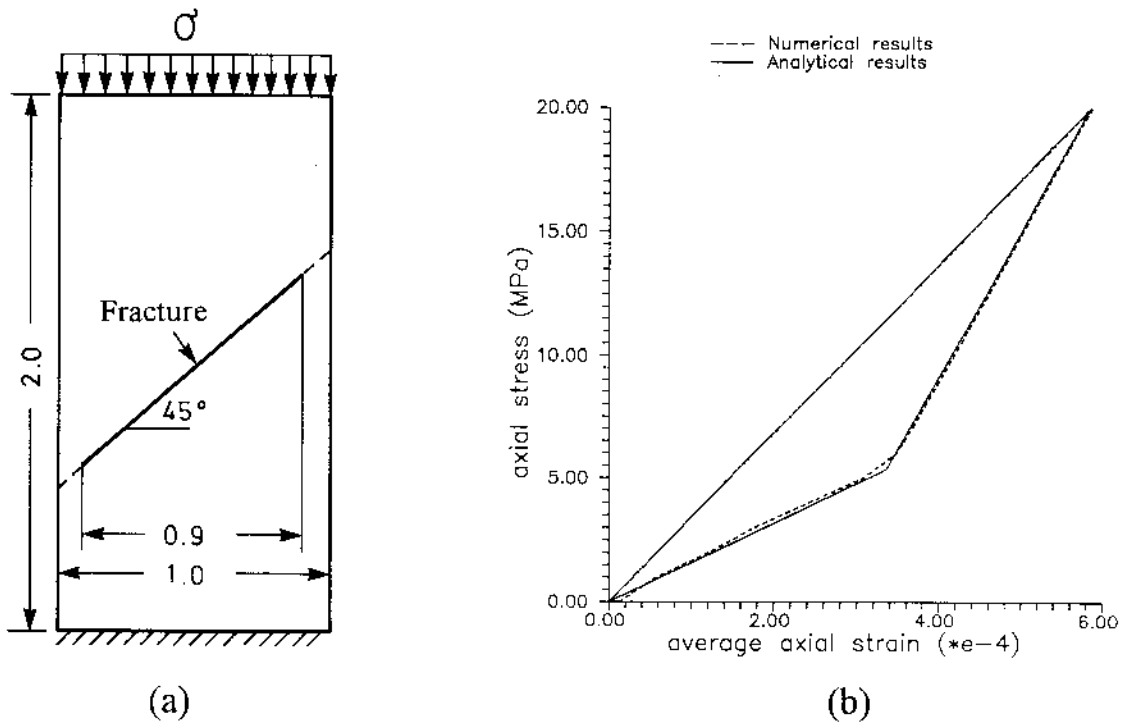


Fig.2.3. Comparison between the analytical results and the UDEC results for a uniaxial loading and unloading test of the fracture-bridge system. (a) Rock sample; (b) analytical and numerical stress-strain curves. Assigned properties:  $E' = 95\text{GPa}$ ,  $K_n^j = K_s^j = 55\text{GPa/m}$ ,  $K_n^b = K_s^b = 55\text{GPa/m}$ ,

### 3. A tensile failure model

If the applied compressive load is increased beyond the level of fracture deformation, the pre-existing fractures in a rock mass may propagate. Fracture propagation weakens the rock mass and therefore it has to be taken into account in estimating the stress-strain relation. Fracture propagation is a complicated process. In most cases numerical methods are needed to predict and simulate the fracture initiation and propagation. Between the two most commonly used numerical methods (the finite element method and the boundary element method), the boundary element method is selected in this study. This is not only because of its high accuracy in calculating the stress state near a fracture tip but also due to the convenience in simulating the progressive fracture propagation. The Displacement Discontinuity Method (DDM), which is one of the boundary element techniques, is used.

#### 3.1. The Displacement Discontinuity Method (DDM).

The Displacement Discontinuity Method (DDM) was initially developed by Crouch (1976) and later widely used in rock mechanics and fracture mechanics. The advantage of DDM in simulating fracture propagation, compared with other boundary element techniques, is its direct presentation of the fracture as fracture elements, without considering the separated fracture surfaces. The displacement discontinuities,  $D_s$  in shear direction and  $D_n$  in normal direction across a fracture, are directly presented as unknowns. For the problem with one fracture in an infinite elastic body (Fig.3.1), the system of governing equations of DDM can be written as:

$$\begin{aligned}\sigma_s^i &= \sum_j (A_{ss}^{ij} D_s^j + A_{sn}^{ij} D_n^j) - (\sigma_s^i)_0 \\ \sigma_n^i &= \sum_j (A_{ns}^{ij} D_s^j + A_{nn}^{ij} D_n^j) - (\sigma_n^i)_0\end{aligned}\tag{3.1}$$

where  $\sigma_s^i$  and  $\sigma_n^i$  represent the shear and normal stresses of the  $i$ th element, respectively;  $(\sigma_s^i)_0, (\sigma_n^i)_0$  are the far-field stresses transformed in the fracture shear and normal directions.  $A_{ss}^{ij}, \dots, A_{nn}^{ij}$  are the influence coefficients, and

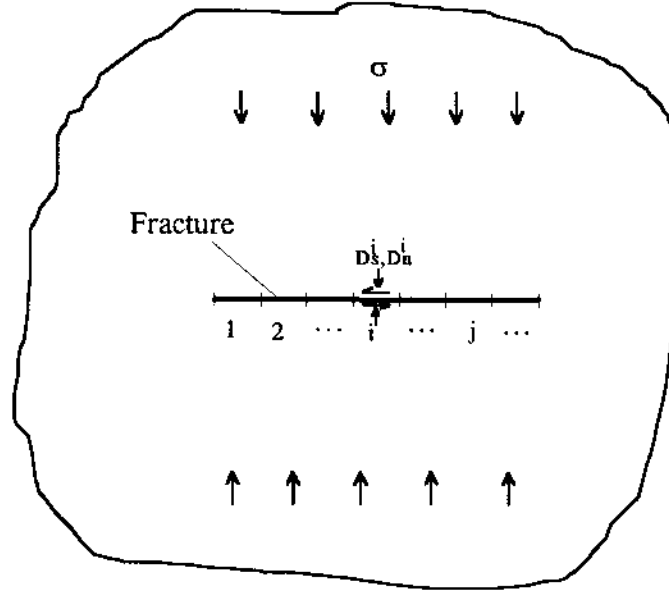


Fig.3.1. DDM discretization of a fracture inside an elastic medium.

$D_s^j, D_n^j$  represent displacement discontinuities of  $j$ th element which are unknowns in the system of equations.

A fracture has three states: open, elastic contact or sliding contact. For different states the system of governing equations can be represented in the following ways, depending on the shear and normal stresses ( $\sigma_s^i$  and  $\sigma_n^i$ ) of the fracture.

1). For an open fracture  $\sigma_s^i = \sigma_n^i = 0$ , and therefore the system of governing equations (3.1) can be rewritten as:

$$\sigma_s^j = 0 = \sum_j (A_{ss}^{ij} D_s^j + A_{sn}^{ij} D_n^j) - (\sigma_s^j)_0 \quad (3.2)$$

$$\sigma_n^j = 0 = \sum_j (A_{ns}^{ij} D_s^j + A_{nn}^{ij} D_n^j) - (\sigma_n^j)_0$$

2). When the two fracture surfaces are in elastic contact,  $\sigma_s^i$  and  $\sigma_n^i$  depend upon the fracture stiffness ( $K_s, K_n$ ) and the displacement discontinuities ( $D_s^i, D_n^i$ )

$$\sigma_s^i = K_s D_s^i \quad (3.3)$$

$$\sigma_n^i = K_n D_n^i \quad (3.4)$$

Substituting Equations (3.3) and (3.4) into Equation (3.1) and carrying out a simple mathematical manipulation, the system of governing equations becomes:

$$0 = \sum_j (A_{ss}^{ij} D_s^j + A_{sn}^{ij} D_n^j) - (\sigma_s)_0 - K_s D_s^i \quad (3.5)$$

$$0 = \sum_j (A_{ns}^{ij} D_s^j + A_{nn}^{ij} D_n^j) - (\sigma_n)_0 - K_n D_n^i$$

3). For a fracture with its surfaces sliding

$$\sigma_n^i = K_n D_n^i$$

$$\left| \sigma_s^i \right| = \sigma_n^i \tan \phi = K_n D_n^i \tan \phi \quad (3.6)$$

where  $\phi$  is the friction angle and  $c$  is the cohesion of the fracture. The sign of  $\sigma_s^i$  depends on the sliding direction. Consequently, the system of Equation (3.1) can be presented as:

$$0 = \sum_j (A_{ss}^{ij} D_s^j + A_{sn}^{ij} D_n^j) - (\sigma_s)_0 \pm K_n D_n^i \tan \phi \quad (3.7)$$

$$0 = \sum_j (A_{ns}^{ij} D_s^j + A_{nn}^{ij} D_n^j) - (\sigma_n)_0 - K_n D_n^i$$

The displacement discontinuities ( $D_s^i, D_n^i$ ) of the fracture are obtained by solving the system of governing equations using conventional numerical techniques, e.g. Gauss elimination method. If the fracture is open, the stresses ( $\sigma_s^i, \sigma_n^i$ ) are zero, otherwise if the fracture is in elastic contact or sliding, they can be calculated by Equations (3.3), (3.4) or (3.6).

### 3.2. Simulation of fracture initiation and propagation

Consider that only tensile (mode I) failure can occur at the intermediate stress level. The fracture propagation is then determined by the Maximum Tensile Stress Criterion (Eordgan & Sih, 1963), i.e.

$$K_I \geq K_{Ic} \quad (3.8)$$

where  $K_I$  is the mode I stress intensity factor at the fracture tip, and  $K_{Ic}$  is the mode I fracture toughness. When the fracture is angled from the loading direction (Fig.3.2), the mode I stress intensity factor in Equation (3.8) should be replaced by the equivalent intensity factor  $(K_I)_e$ .

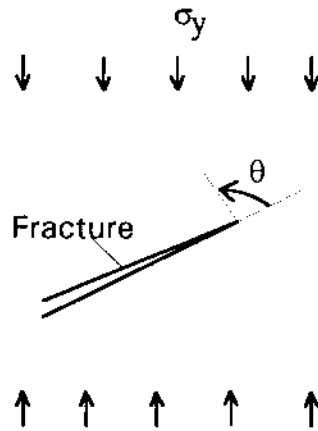


Fig.3.2. An inclined fracture under uniaxial compression.

$$(K_I)_e = K_I \cos^3\left(\frac{\theta}{2}\right) - 3K_{II} \cos^2\left(\frac{\theta}{2}\right) \sin\left(\frac{\theta}{2}\right) \quad (3.9)$$

In Equation (3.9),  $\theta$  is the direction of fracture propagation. It is calculated by

$$\tan\left(\frac{\theta}{2}\right)_{1,2} = \frac{1}{4} \left[ \frac{K_I}{K_{II}} \pm \sqrt{\left(\frac{K_I}{K_{II}}\right)^2 + 8} \right] \quad (3.10)$$

where  $K_{II}$  is the mode II stress intensity factor. The note (1,2) presents the direction of two principal stresses ( $\sigma_1$  and  $\sigma_2$ ).  $\theta$  is the direction of the maximum compressive principal stress.

Using the DDM, the stress intensity factors at a fracture tip can be estimated from the displacement discontinuities of the element at the fracture tip (Schultz, 1988):

$$K_I = \frac{E}{8\pi(1-\nu^2)} \sqrt{\frac{2\pi}{d}} D_n$$

$$K_{II} = \frac{E}{8\pi(1-\nu^2)} \sqrt{\frac{2\pi}{d}} D_s$$
(3.11)

Knowing the loading stress and the fracture toughness ( $K_{IC}$ ), it can then be calculated whether fracture propagation occurs and in which direction. Once a propagation is determined, a new element will be added to the tip in the direction of propagation. In the next calculation step, the new element will be considered as the fracture tip element to determine further possible propagation.

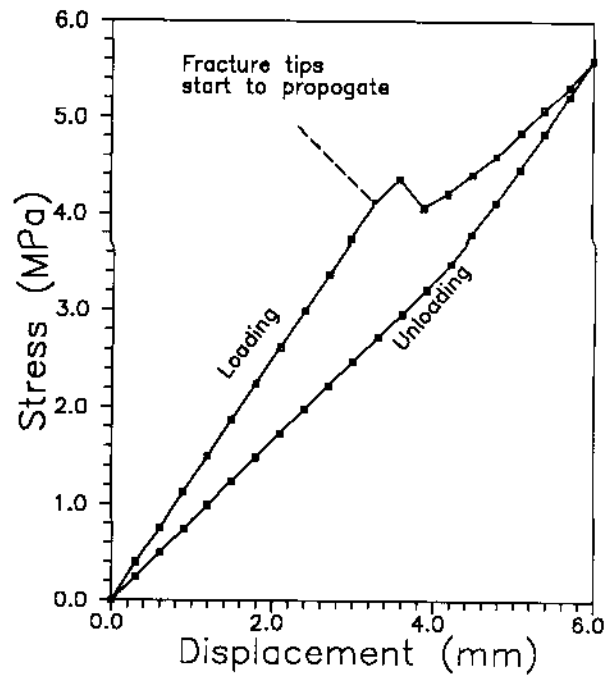
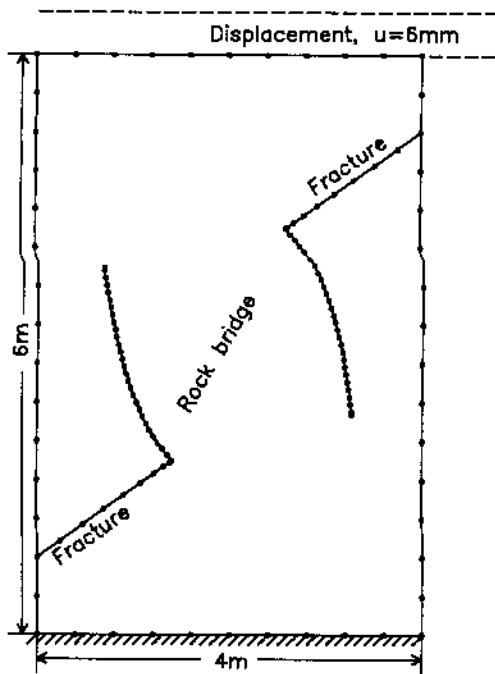
### 3.3. Application of the numerical model to the fracture-bridge system.

Consider a rock sample containing two fractures and under uniaxial compression (Fig.3.3). The mechanical properties of the intact rock and fractures are:

- Young's modulus  $E = 10$  GPa
- Poisson's ratio  $\nu = 0.15$
- Fracture stiffness  $K_n = K_s = 3$  GPa/m
- Fracture friction angle  $\phi = 25^\circ$
- Cohesion  $c = 0$
- Fracture toughness  $K_{IC} = 3.16$  MPa m<sup>1/2</sup>

The simulated results are shown in Fig.3.3. The non-linearity in loading and hysteresis in unloading are obtained numerically.





(a)

(b)

Fig.3.3. A rock block with two fractures loaded in uniaxial compression. Displacement control is applied on the top surface. (a) Geometry of the block with initial fractures and new developed fractures after peak displacement; (b) average uniaxial stress versus displacement.

## 4. A modified G-criterion for fracture propagation in mode I and mode II

The conceptual model presented in Chapter 2 considers only the sliding of the rock fractures, and it is applicable to the low stress level which would not induce any fracture propagation. The tensile failure model presented in Chapter 3 takes into account both fracture sliding and mode I fracture propagation, and it is for the intermediate stress loading on which only mode I fracture propagation occurs. Some researchers have reported that fractures in rock or materials similar to rock can propagate in shear mode (mode II) when the compressive load is substantially high, following the occurrence of mode I fracture propagation (Lajtai, 1974; Petit & Barquins, 1988). See Fig.4.1. For this high loading level, neither the conceptual model nor the tensile failure model is sufficient to predict the behaviour of the fracture-bridge system. Mode II fracture propagation has to be considered and a suitable fracture criterion has to be used.

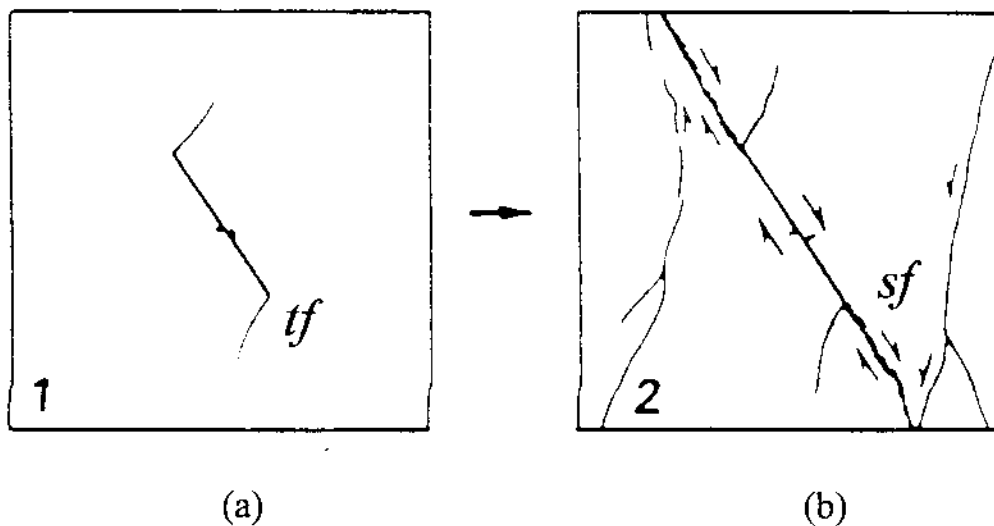


Fig.4.1. Fracture propagation from a single-inclined flaw in high porosity sandstone under uniaxial compression. (a) Low stress; (b) high stress. *tf* — tensile fracture; *sf* — shear fracture. After Petit & Barquins (1988)

### 4.1. The modified G-criterion.

There are many fracture criteria in fracture mechanics. The most commonly used criteria are the Maximum Tensile Stress Criterion (Eordgan & Sih, 1963), the Maximum Strain Energy Release Rate Criterion (G-criterion)(Griffith, 1913) and the Minimum Strain Energy Density Criterion (Sih, 1974). The maximum tensile stress criterion is based on the concentration of tensile stress at the fracture tips.

It is a conventional method to predict Mode I fracture propagation but cannot be used to simulate the shear failure. The G-criterion and the S-criterion, which are conceptually based on the strain energy in a crack system, seem to be applicable to predicting both tensile and shear fracture because the strain energy is related to all the three stress components in two dimensions. However, for an inclined fracture subjected to compression, the S-criterion only predicts two minimum S-values, one approximately in the direction of maximum tensile stress and the other in the direction of maximum compressive stress. Neither of the two minimum S-values are in the direction of shear failure. The study is then focused on the G-criterion.

#### 4.1.1 The original G-criterion

The G-criterion states: when the strain energy release rate ( $G$ ) in an elastic medium is equal to or larger than the surface energy required to separate the material ( $G_c$ ), a fracture tip will propagate, i.e.

$$G \geq G_c \quad (4.1)$$

The G-criterion has many mathematical difficulties in its application because the G-value in an arbitrary direction is difficult to present analytically. Hussain et al. (1974) and Melin (1985) have successfully presented the G-value, using the stress intensity factors ( $K_I$  and  $K_{II}$ ). However, Hussain's formula has been shown to be inaccurate in predicting compressive fracture propagation (Chiang, 1977; El-Tahan, 1990), and Melin's results are only for tensile fracture propagation. In this study the DDM is used to calculate the G-value and to examine the applicability of the G-criterion.

#### 4.1.2. Numerical calculation of G-value

The G-value, by definition, is the change of the strain energy in an elastic body when the fracture has grown one unit of length. To obtain the G-value in an arbitrary direction in the numerical method, we add a small element to the fracture tip in the direction  $\theta$  (Fig.4.2). Then the G-value in this direction can be estimated by:

$$G(\theta) = \frac{\partial W}{\partial a} \approx \frac{[W(a + \Delta a) - W(a)]}{\Delta a} \quad (4.2)$$

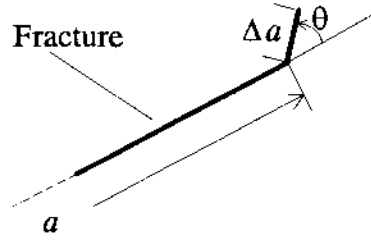


Fig.4.2. Small element added to the fracture tip to simulate its growth.

where  $W$  is the elastic strain energy of the elastic medium;  $\Delta a$  is the length of the small element;  $W(a+\Delta a)$  and  $W(a)$  are the strain energy with and without the fracture growth. The strain energy can be obtained from work done by external forces and displacement. In cases where the fracture is under far-field loading, the strain energy is

$$W(a) = \frac{1}{2} \int_0^a [(\sigma_s - (\sigma_s)_0)D_s + (\sigma_n - (\sigma_n)_0)D_n] da \quad (4.3)$$

where  $a$  is the fracture length,  $\sigma_s, \sigma_n$  are the stress and displacement in tangential and normal direction along the fracture.  $(\sigma_s)_0$  and  $(\sigma_n)_0$  are the far-field stresses.  $D_s$  is the shear displacement discontinuity and  $D_n$  is the normal displacement discontinuity of the fracture. In terms of DDM elements, it is

$$W(a) \approx \frac{1}{2} \sum_{i=1}^m (a^i (\sigma_s^i - (\sigma_s^i)_0) D_s^i + a^i (\sigma_n^i - (\sigma_n^i)_0) D_n^i) \quad (4.4)$$

$i$  is the element number and  $m$  is the total number of the DDM elements.

#### 4.1.3 The insufficiency of the original G-criterion

Applying the G-criterion to an inclined fracture under uniaxial compression, the G-value in different directions from a fracture tip is plotted in Fig.4.3. The maximum G-value appears in a direction almost parallel to the pre-existing fracture plane. This direction is actually the direction of shear failure. In the direction of tensile failure, i.e., about  $90^\circ$  away from the fracture plane, there is no obvious local maximum G-value. According to the G-criterion, in this case, a mode II fracture propagation will occur prior to any mode I fracture propagation. This prediction does not agree with experimental observation that mode I fractures always appear first. To be able to predict both mode I and mode II fracture propagation, modification of the G-criterion is necessary.

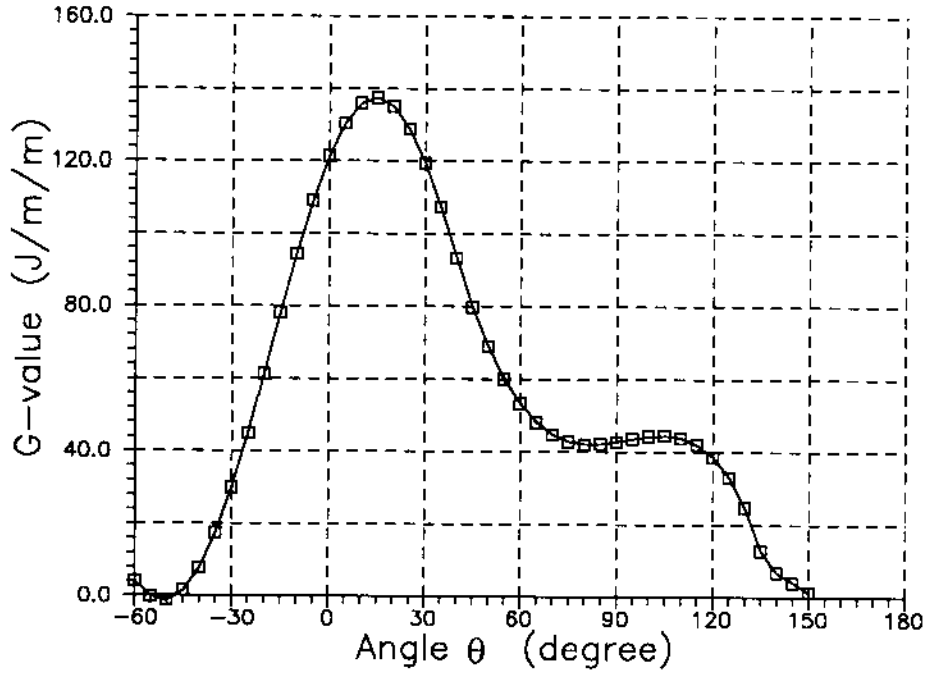


Fig.4.3. G-value in different directions from a fracture tip when the fracture is in an infinite elastic medium and under far-field uniaxial compression. The fracture length = 20mm, fracture inclination = 45°, uniaxial load = 10 MPa,  $E=6200\text{MPa}$ ,  $\nu=0.28$ .

#### 4.1.4 Modification of the G-criterion.

Considering a dimensionless factor (F). The value of F in a direction ( $\theta$ ) is determined by:

$$F(\theta) = \frac{G_I(\theta)}{G_{Ic}} + \frac{G_{II}(\theta)}{G_{IIc}} \quad (4.5)$$

where  $G_{Ic}$  and  $G_{IIc}$  are fracture surface energy in mode I failure and in mode II failure, respectively.  $G_I(\theta)$  is the energy release rate when the growth part of a fracture only has open displacement, while  $G_{II}(\theta)$  is the energy release rate when the growth part only has shear displacement.

For most rocks,  $G_{IIc}$  is reported to be much higher than  $G_{Ic}$  (about two orders of magnitude higher according to Li, 1991). Assuming  $G_{IIc} = 10 \times G_{Ic} = 500 \text{ J/m}^2$ , the F-value in different direction for the sample problem as shown in Fig.4.3 is calculated and plotted in Fig.4.4. Two maximum F-values are found, one in the direction of the tensile failure and another in the direction of the shear failure as shown in Fig.4.1. The maximum F-value in the direction of tensile failure is the global maximum. This result shows that the F-value can be used to

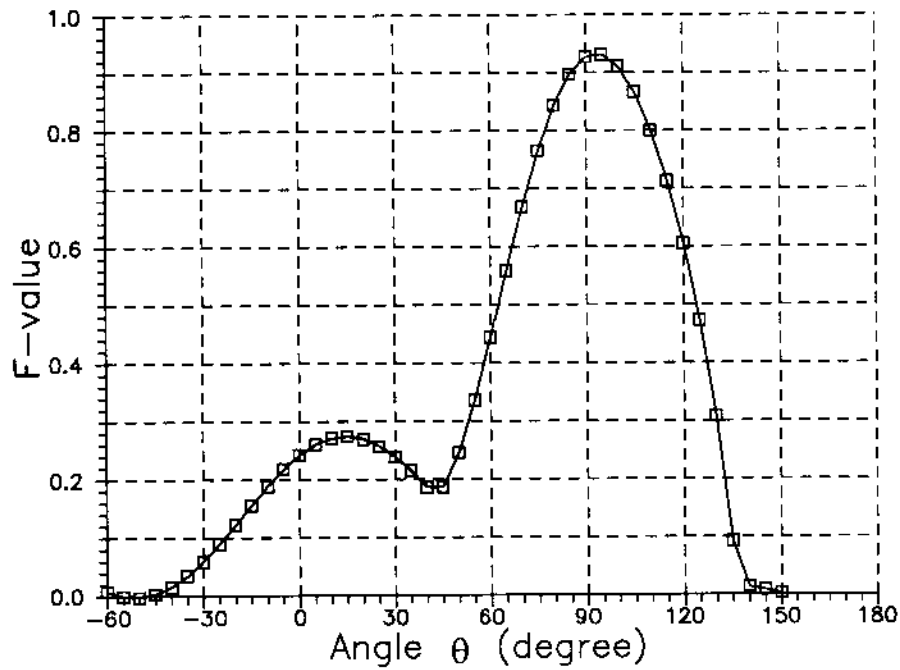


Fig.4.4.  $F$ -value in different directions from a fracture tip when the fracture is in an infinite elastic medium and under far-field compression. Assumption:  $G_{Ic} = 50 \text{ J/m}^2$  and  $G_{IIc} = 500 \text{ J/m}^2$ .

predict the mode I and mode II failure. Then a modified G-criterion is proposed, i.e.,

- (1) In any direction of a fracture tip, there exists a dimensionless parameter  $F$ .  $F$  is determined by Equation (4.5);
- (2)  $F$  reaches a maximum value in a certain direction;
- (3) If the maximum  $F$  reaches the unit value (1.0), i.e.,  

$$F_{\max} \geq 1.0$$
the fracture tip will propagate in the direction of maximum  $F$ .

#### 4.2. Application of the modified G-criterion to mixed mode fracture propagation.

An inclined fracture in an infinite elastic medium subjected to uniaxial compression is simulated by using the modified G-criterion and DDM. The fracture length is 1.0 cm and is inclined  $45^\circ$  from the loading direction. The mechanical properties of the medium are taken as follows:

Young's modulus,  $E = 6200 \text{ MPa}$

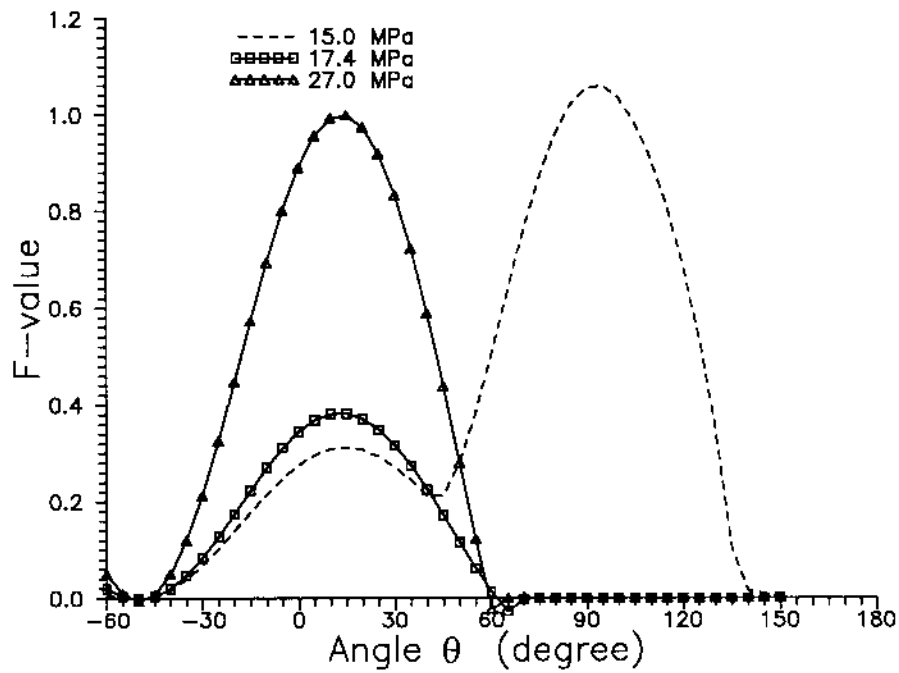
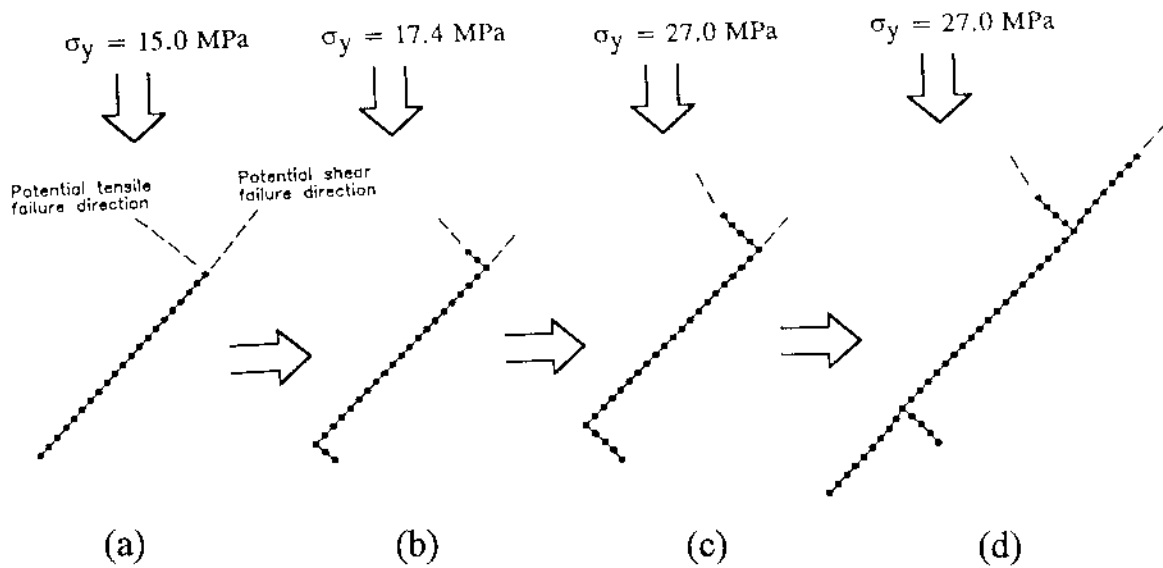
Poisson's ratio,  $\nu = 0.28$

Mode I fracture surface energy,  $G_{Ic} = 50 \text{ J/m}^2$

Mode II fracture surface energy,  $G_{IIc} = 500 \text{ J/m}^2$ .

The mode I and mode II fracture propagation from the existing crack tips is predicted by the  $F$  versus  $\theta$  plot (Fig.4.5). When the compressive stress is less than 15 MPa, there exist two maxima in the  $F$ - $\theta$  plot: one associated with the potential tensile failure which is approximately perpendicular to the pre-existing fracture, and one associated with the potential shear failure in the same direction as the pre-existing fracture. When the compressive stress exceeds 15 MPa the  $F$ -value in the direction of potential tensile failure is the first to satisfy the propagation criterion,  $F_{\max} \geq 1.0$ , and therefore Mode I propagation occurs. This results in the release of tensile stress at the fracture tip and therefore the maximum  $F$ -value due to tension disappears. The tensile fracture has minor influence on the shear stress and the maximum  $F$ -value due to shearing still exists. In order to maintain mode I propagation, the load must be constantly increased. With increasing load, the maximum  $F$ -value in the direction of maximum shearing is also increased. When it satisfies the criterion  $F_{\max} \geq 1.0$  at the stress level of 27 MPa, mode II propagation is initiated in the direction of the initial fracture. This simulated mixed mode I and II propagation process is consistent with the actual observations in laboratory experiments (Fig.4.1).

The modified  $G$ -criterion and DDM will be used to simulate the fracture coalescence in Chapter 5.



(e)

*Fig.4.5. Stages of fracture propagation in uniaxial compression and corresponding F- $\theta$  curves. (a) Initial state; (b) and (c) tensile fractures are initiated and propagate; (d) shear fractures develop and the tensile fractures stop; and (e) curves of F versus  $\theta$  at the upright tip of the inclined fracture for stage (a), (b) and (c).*



## 5. Experimental and numerical study of fracture coalescence

Fracture coalescence is caused by the failure of rock bridges. It usually occurs at high stress level and triggers an entire failure of fractured rock masses. Reyes & Einstein (1991) studied experimentally the coalescence between two flaws in gypsum samples subjected to uniaxial compression and observed the coalescence between non-overlapping flaws. However, whether and how fractures in surface contact and friction coalesce is still not answered. To provide better understanding of the mechanism of rock fracture coalescence, further experimental investigation and numerical simulation have been carried out in this study.

### 5.1 Experimental investigation of fracture coalescence.

The experimental investigation is performed with pre-fractured gypsum samples under uniaxial compression. The fractures and rock bridges are modelled by two central cracks separated by the bridges (see Fig.5.1). A number of different crack inclinations ( $\alpha$ ) and bridge inclinations ( $\beta$ ) are used to investigate their influence on the failure mode and coalescence load. The selected crack inclination is  $30^\circ$ ,  $45^\circ$  and  $60^\circ$ . The selected bridge inclination is  $45^\circ$ ,  $60^\circ$ ,  $75^\circ$ ,  $90^\circ$ ,  $105^\circ$  and  $120^\circ$ . Two types of cracks are used: the closed cracks (i.e., cracks with surface contact and friction) and open cracks (cracks without surface contact). The open cracks are actually the slots created by removing pre-installed steel sheets *after* curing. The closed cracks are created by pulling out pre-installed thin polyethylene sheets *during* curing. The failure process is monitored by a microscope and a video recorder.

#### 5.1.1. The process of coalescence.

During the tests, crack coalescence occurs in the samples with crack inclinations of  $45^\circ$  and  $60^\circ$  and different bridge inclinations, for both open and closed cracks. When the crack inclination is  $30^\circ$ , closed cracks do not slide and consequently no coalescence occurs. Samples with different bridge inclinations show different processes of failure. When the bridge inclination is  $45^\circ$  and  $60^\circ$ , the coalescence is caused by two secondary cracks which are developed from the tips of pre-existing cracks and propagate to the center of the bridge, see Fig.5.2. When the bridge inclination is  $75^\circ$  and  $90^\circ$ , however, the secondary crack does not start from the tips of pre-existing cracks but from the center of the bridge (see

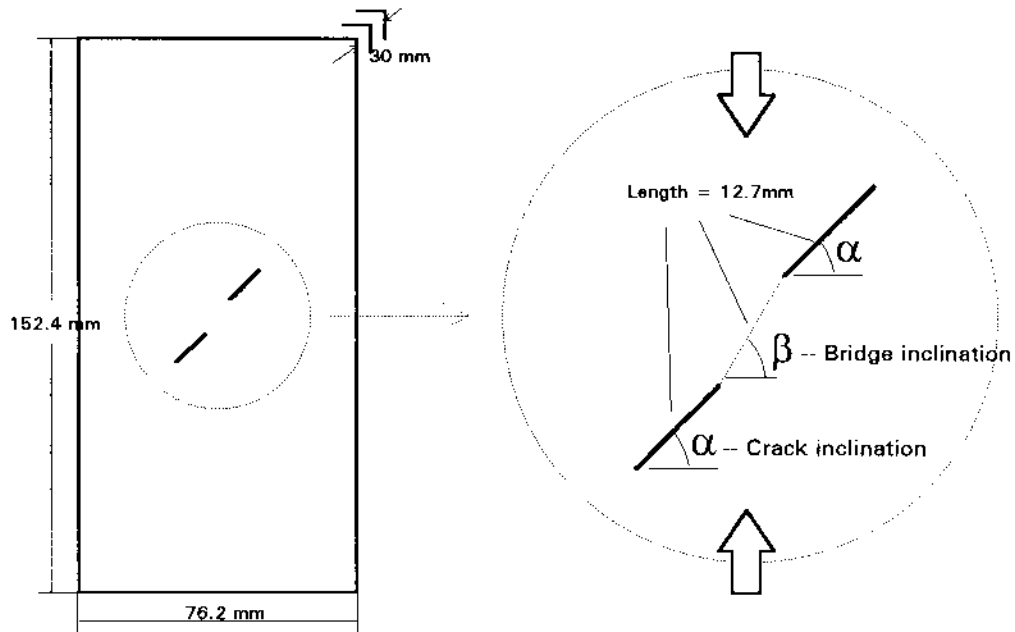


Fig.5.1. Geometry of the sample and cracks.

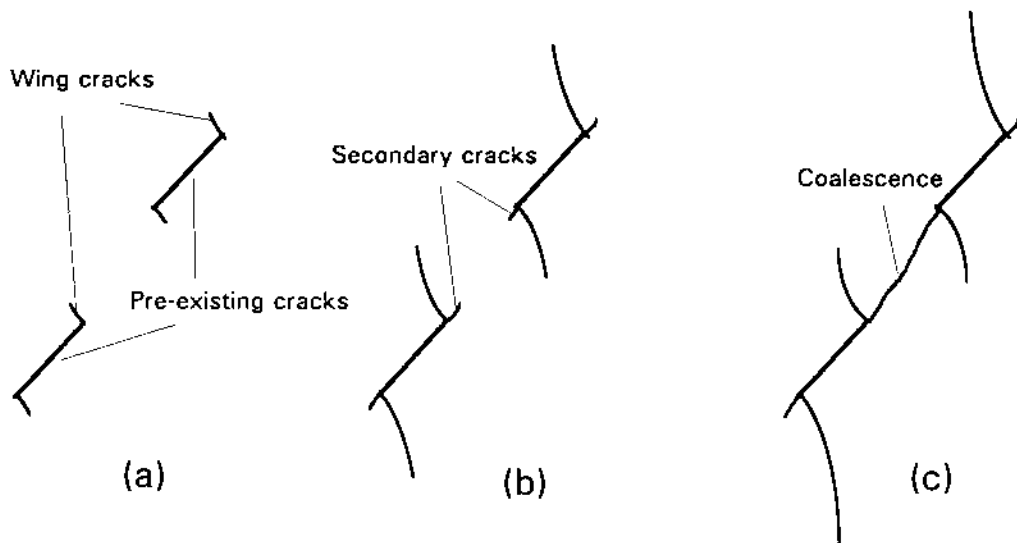
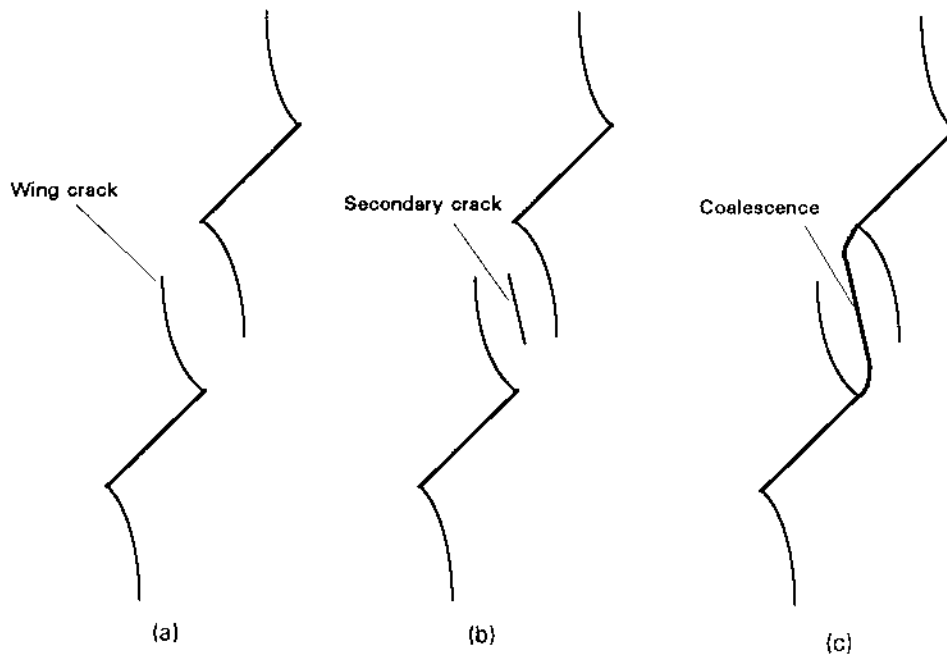
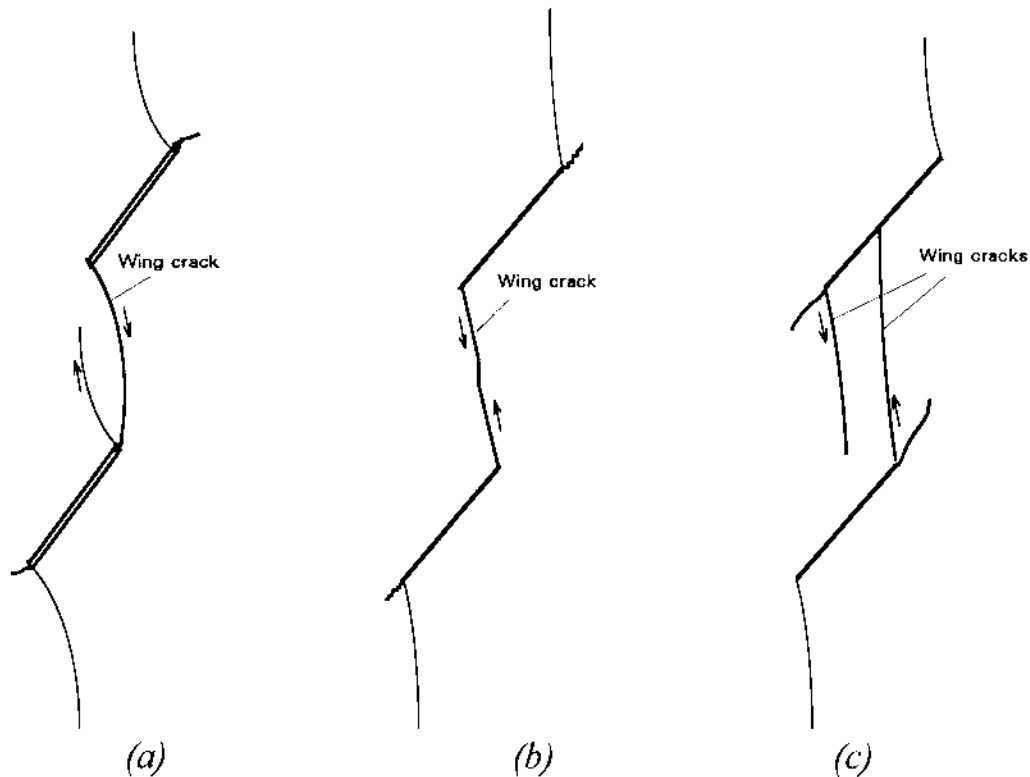


Fig.5.2. Typical sequence of crack initiation, propagation and coalescence when the bridge inclination is  $45^\circ$  and  $60^\circ$ . (a) Wing cracks initiate from the tips of the pre-existing cracks at low uniaxial load; (b) wing cracks propagate with an increasing of load, and secondary cracks appear at the tips of the pre-existing cracks; and (c) secondary cracks propagate quickly and coalesce, while the outer wing cracks extend.

Fig.5.3). When the two pre-existing cracks are overlapping, i.e., the bridge inclination is  $105^\circ$  and  $120^\circ$ , the coalescence is caused by wing cracks (see Fig.5.4). The path of wing cracks is found depending on the type of pre-existing cracks. Open cracks result in strongly curved wing cracks, while closed cracks produce nearly straight wing cracks.



*Fig.5.3. Typical process of coalescence when the bridge inclination is  $75^\circ$  and  $90^\circ$ . (a) Wing crack propagation; (b) a secondary crack appears at the center of the bridge; and (c) secondary crack propagates and forms coalescence.*



*Fig.5.4. Coalescence caused by wing cracks. (a) A wing crack connects to the tip of a pre-existing crack (bridge inclination =  $105^\circ$ , pre-existing crack is an open crack); (b) a wing crack connects with another wing crack (bridge inclination =  $105^\circ$ , pre-existing crack is a closed cracks); (c) a wing crack connects to a pre-existing crack (bridge inclination  $120^\circ$ ).*

### 5.1.2 Failure mode of the bridge

Different processes of coalescence is accompanied by different failure mechanisms. By examining the surface characteristics, different types of failure, i.e., tensile failure, shear failure or mixed tensile and shear failure, are found depending on the bridge inclination (see Table 5.1). Crack inclination and the types of pre-existing cracks (open or closed) have minor influence on the failure mode.

*Table 5.1 Mode of the bridge failure with different bridge inclination*

Bridge inclination	Failure mode	Description
45°, 60°	Shear failure	Failure surface is rough and stepped, and often contains pulverized material. Coalescence starts from the crack tips.
75°, 90°	Tensile failure + Shear failure	Failure surface in central part of the bridge is smooth while it is rough and stepped near the crack tip. Coalescence starts from the center of the bridge.
105°, 120°	Tensile failure	Failure surface is smooth and clean. Coalescence starts from crack tips.

### 5.1.3. Load of coalescence

Open and closed pre-existing cracks coalesce in the different load level, see Fig.5.5. The coalescence of closed cracks requires higher load (about 25% higher) than that of open cracks. When the bridge inclination is about 75°, the failure load is the lowest. Different crack inclination ( $\alpha$ ) shows similar results.

Another difference between the open and closed cracks is reflected by the average stress-strain curve (see Fig.5.6). Closed cracks result in a stronger hysteresis than the closed crack during unloading after the occurrence of coalescence.

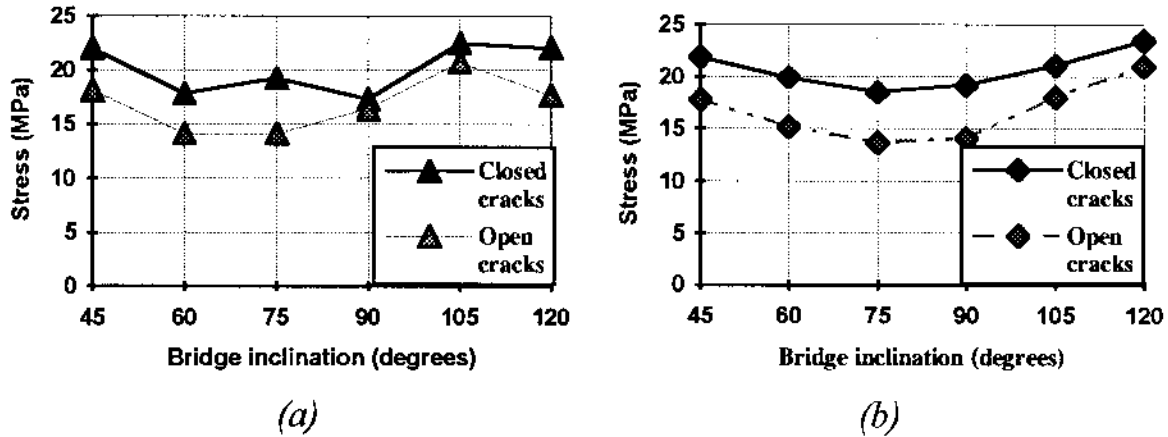


Fig.5.5. The critical uniaxial stress of coalescence for open and closed cracks with different bridge inclination. (a) crack inclination = 45°; (b) crack inclination = 60°.

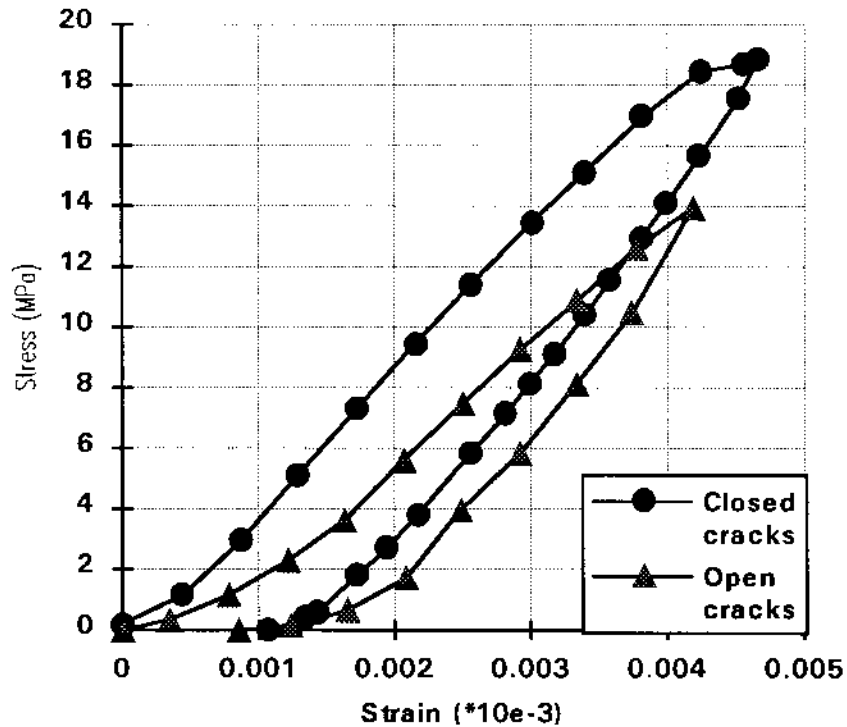


Fig.5.6. Loading and unloading curves of two 60°/75° samples with open cracks and closed cracks, respectively.

## 5.2 Numerical simulation and interpretation

### 5.2.1 Stress analysis

The coalescence caused by tensile failure for overlapping fractures has been well studied by many researchers and it is known that the mode I failure is driven by

tensile stress concentration. The coalescence caused by shearing or mixed shearing and tension for non-overlapping fractures, however, is still not well understood. The reason why non-overlapping cracks can induce shear failure or mixed tensile and shear failure can be found from stress analysis (see Fig.5.7 and Fig.5.8). For the bridge inclination of  $45^\circ$ , there is no tensile stress existing along the path of coalescence after the occurrence of wing cracks. However, high shear stress exists inside the bridge and the maximum shear stress appears at the crack tips and is directing along the path of coalescence. The shear stress results in a shear failure in the bridge. For the bridge inclination of  $90^\circ$ , the extension of wing cracks causes an almost uniformly distributed tensile stress field in the bridge. The maximum tensile stress appears at the center of the bridge and reaches 2.85 MPa when the applied load is 15 MPa. The gypsum mixture was reported to have a tensile strength of about 2.3 MPa (Nilson,1968). Therefore, a tensile failure should occur in the central part of the bridge. Close to the pre-existing crack tip no tensile stress exists but the maximum shear stress reaches a maximum magnitude and follows the direction of the actual path of coalescence observed in the tests. Consequently, the failure near the tips of the pre-existing cracks is caused by shearing.

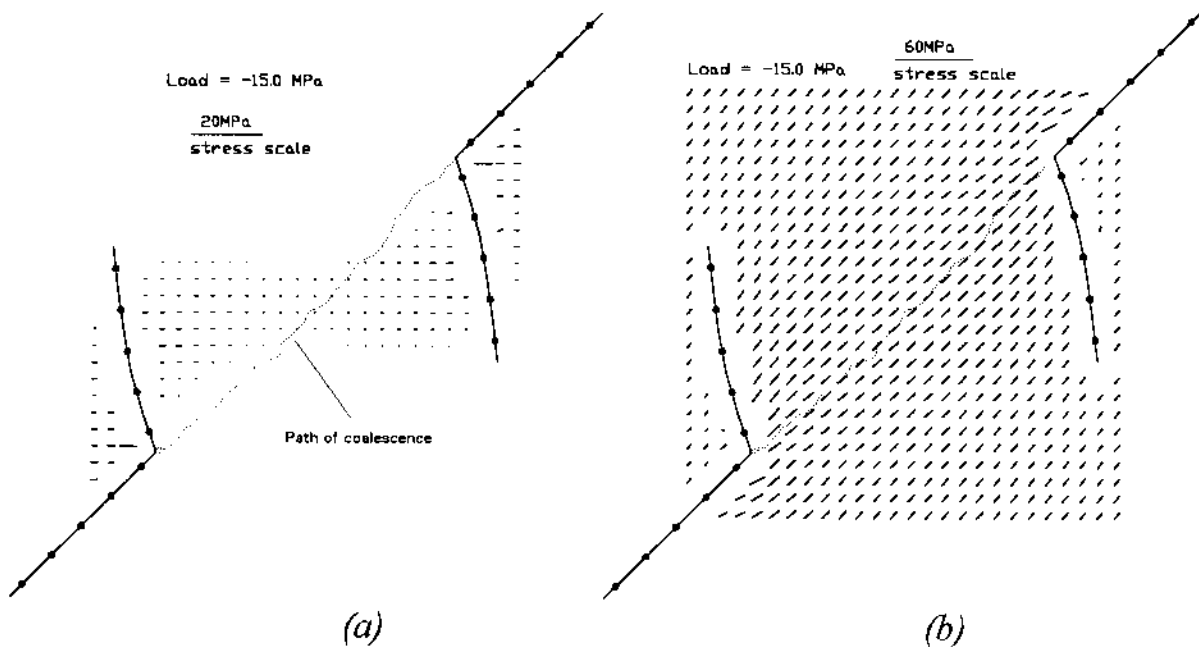


Fig.5.7. Stress distribution in the bridge between two closed  $45^\circ/45^\circ$  cracks (crack inclination =  $45^\circ$ ; bridge inclination =  $45^\circ$ ) after the occurrence of wing cracks. (a) Tensile stress field; (b) maximum shear stress field.

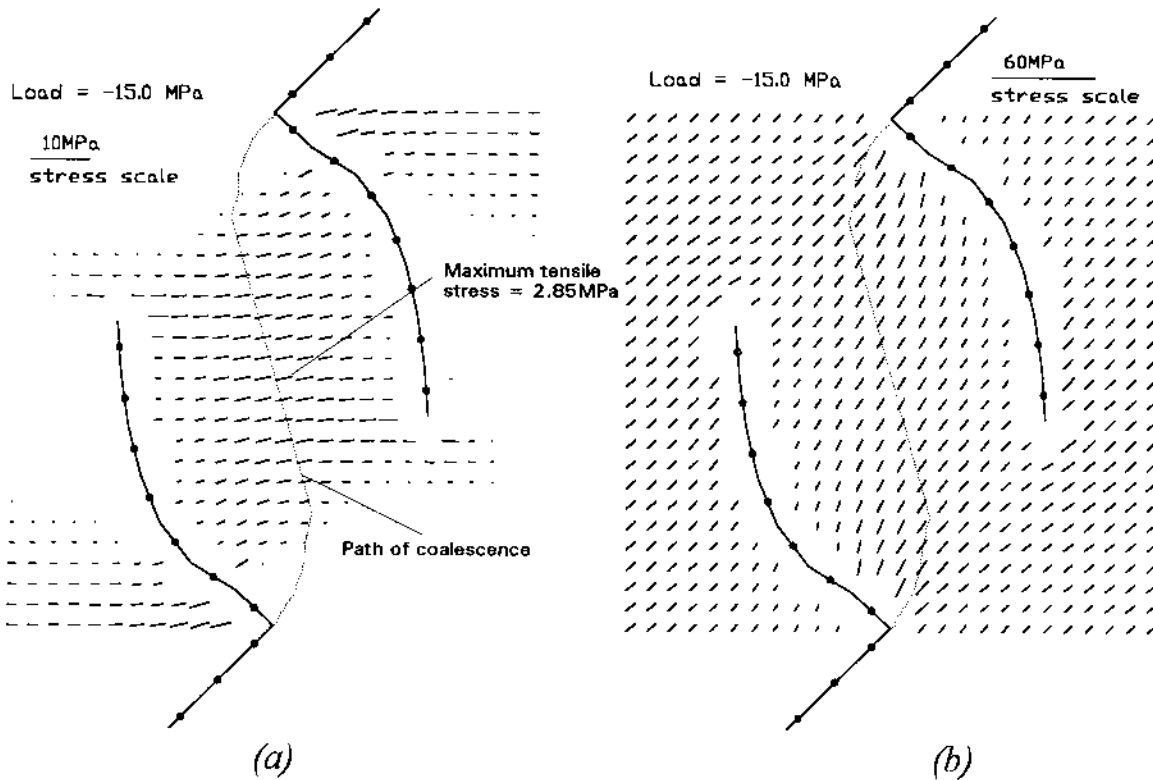


Fig.5.8. Stress distribution in the vicinity of the bridge between two  $45^\circ/90^\circ$  closed cracks after the occurrence of wing cracks, referring to Fig.7. The pre-existing cracks are assigned the stiffness  $K_n=K_s=10 \text{ GPa/m}$ , and the friction angle  $\phi=35^\circ$ . (a) Tensile stress; (b) maximum shear stress.

### 5.2.2. Modelling by using the modified G-criterion and DDM.

The modified G-criterion and the DDM technique are applied to the geometry of the experimental tests. Two cracks with different crack inclination and bridge inclination are in an infinite elastic medium subjected to far-field uniaxial compression. The mechanical parameters of the elastic medium and cracks used in the simulation are listed in Table 5.1.

For different bridge inclinations and crack types, the numerical simulation produces identical processes to those observed in the experiments. The simulated process of coalescence of two  $45^\circ/60^\circ$ ,  $45^\circ/90^\circ$  and  $45^\circ/105^\circ$  closed cracks is shown in Figs.5.9, 5.10 and 5.11, respectively. The comparison between the simulated and experimental coalescence load is shown in Fig.5.12. Closed cracks with an inclination of  $30^\circ$  are found not to coalesce because the cracks are not sliding, which also agrees with the experimental observation.

Table 5.1. Mechanical properties used in numerical simulation.

	Intact material	Pre-existing cracks			New developed cracks
		Closed (A)	Closed (B) <sup>§</sup>	Open	
E (MPa)	6200 *				
$\nu$	0.28 *				
$\sigma_t$ (MPa)	2.3 *				
Kn (GPa/m)		500	50	0	10000
Ks (GPa/m)		500	50	0	10000
$\phi$ (°)		35 #	30	0	30
c (MPa)		2.0 #	1.0	0	0
$G_{Ic}$ (J/m <sup>2</sup> )	5 □				
$G_{IIc}$ (J/m <sup>2</sup> )	100				

\* Values according to test results for gypsum material by Nelson (1968).

# Values according to tests with small samples containing through-going cracks.

□ Value obtained from three-point bending tests of notched gypsum samples.

§ This type of property is only assigned to the closed cracks in the sample 45°/90° where the crack contact is weaker due to longer curing time before the polyethylene sheets were pulled out during sample preparation.

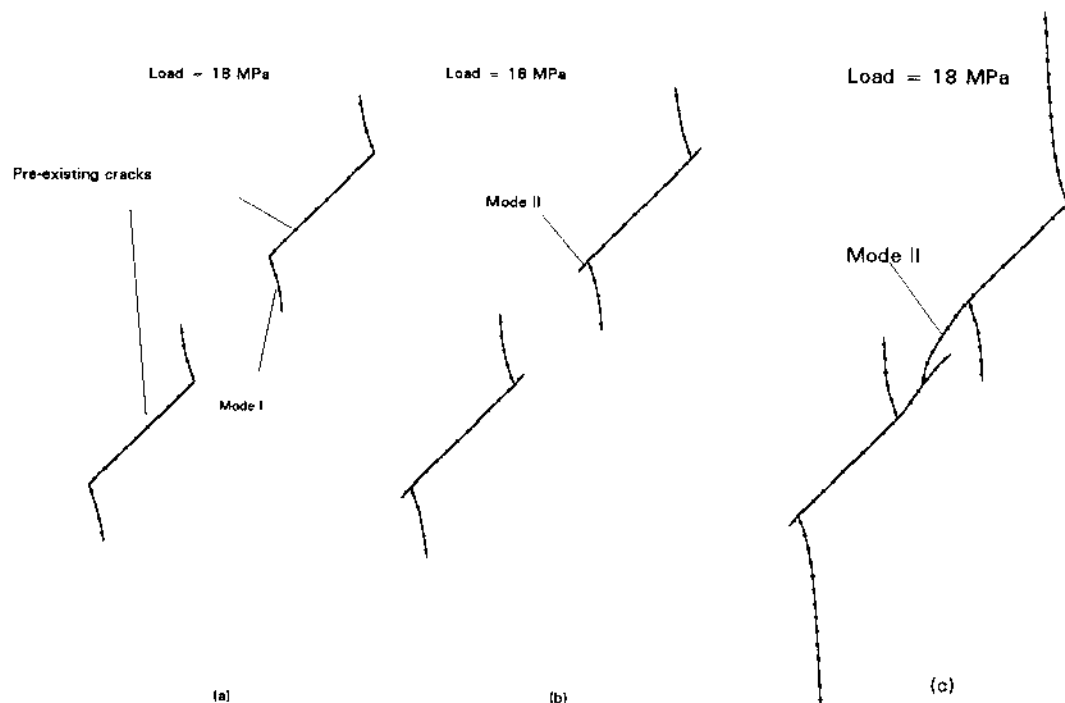
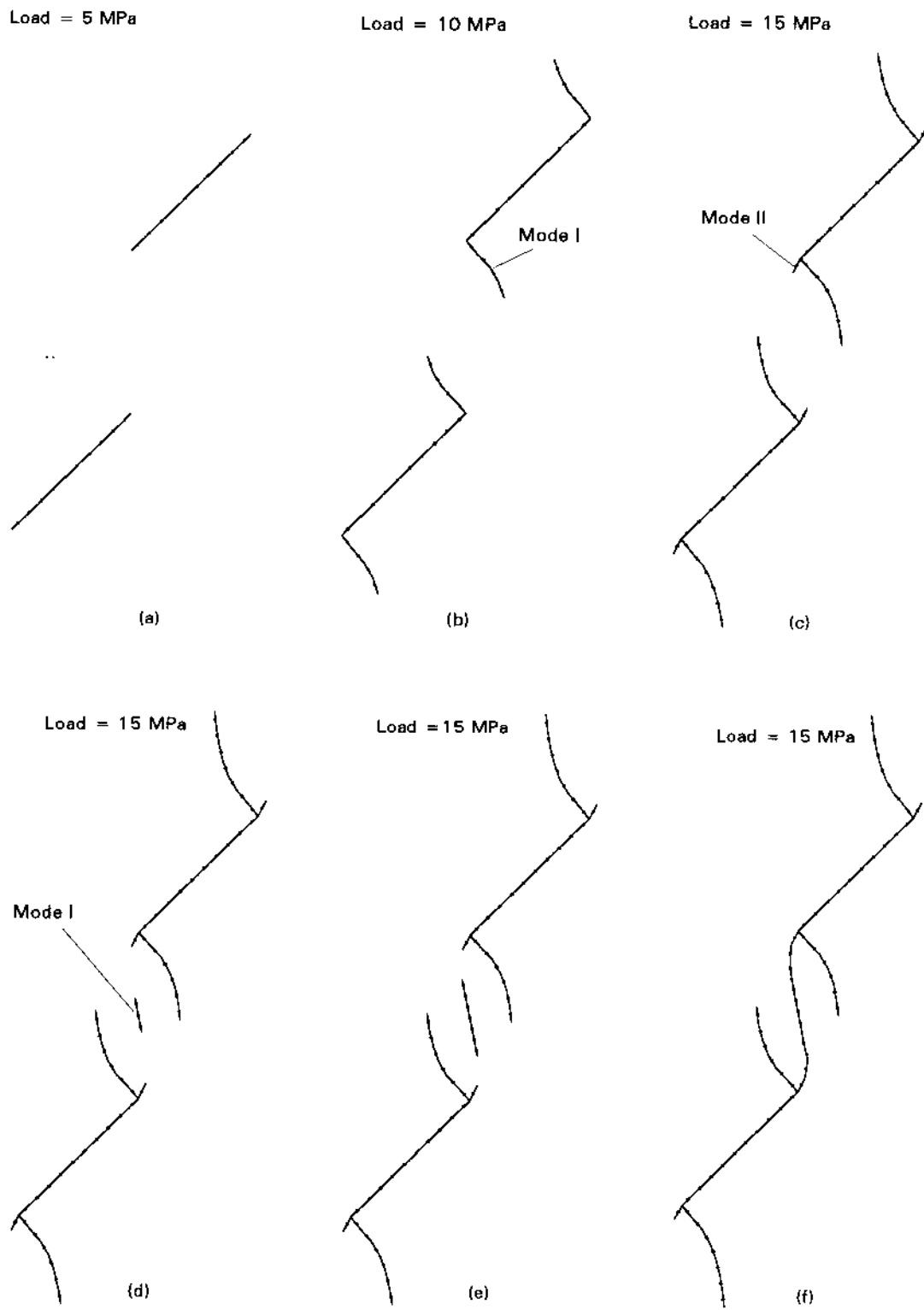


Fig.5.9 Simulated process of coalescence between two 45°/60° closed cracks. (a) Mode I crack initiation and propagation at the uniaxial load of 10 MPa; (b) mode II initiation at the load of 18 MPa; and (c) mode II crack propagation and coalescence at the load of 18 MPa. Compare the experimental results in Fig.5.2.





*Fig.5.10. Simulated process of coalescence of two 45°/90° closed cracks. (a) Initial state; (b) mode I crack initiation and propagation; (c) mode II crack initiation, the tensile stress at the center of the bridge is determined to be larger than tensile strength; (d) introduction of a new crack at the center of the bridge to simulate the tensile failure; (e) growth of the new crack; and (f) final coalescence. Compare the experimental results in Fig.5.3.*

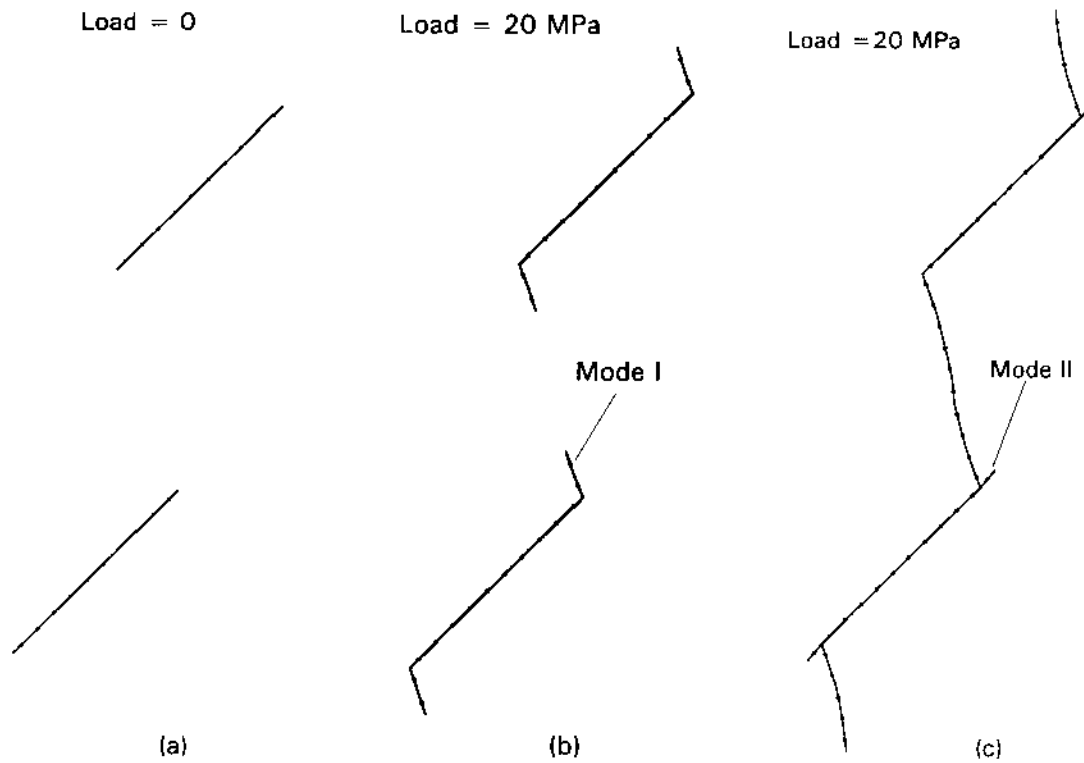


Fig.5.11. Simulated coalescence of two  $45^{\circ}/105^{\circ}$  closed cracks. Compare the experimental results in Fig.5.4b.

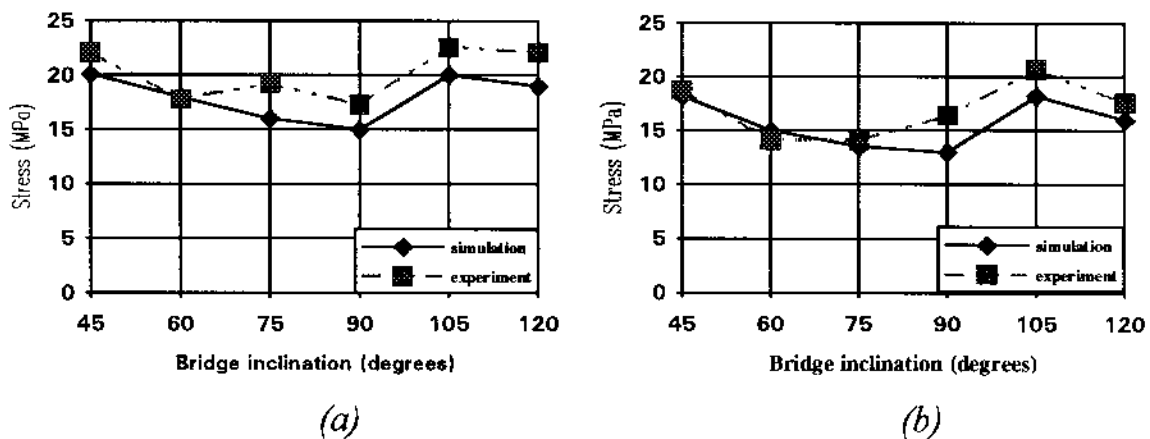


Fig.5.12. Comparison of numerical and experimental load of coalescence. The inclination of the two pre-existing cracks is  $45^{\circ}$ . (a) Closed pre-existing cracks; (b) open pre-existing cracks.

Both experimental and numerical results can be summarized as follows:

- (1) Whether contact fractures can coalesce or not depends upon if the fractures slide or not.

- (2) The failure mode of the bridge between two inclined fractures under uniaxial compression is mainly dependent upon the inclination of the bridge. With low bridge inclination ( $\beta \leq 60^\circ$ ), the coalescence is caused by shear failure; with the bridge inclination around  $75^\circ$  and  $90^\circ$  it is caused by mixed tensile and shear failure; and with high bridge inclination ( $\beta \geq 105^\circ$ ), the coalescence is caused by tensile failure.
- (3) The mixed mode failure occurs at the lowest uniaxial load, and it controls the strength of fractured rock masses. For this reason the mixed mode failure has to be considered in stability analysis of rock excavations.
- (4) The modified G-criterion and the numerical method DDM is proved to be a powerful tool to predict fracture coalescence of geological materials.

## 6. Conclusions and recommendations for future work

### 6.1 Conclusions

The fractured rock mass has non-linear stress-strain response during loading and shows hysteresis during unloading. These characteristics of fractured rock masses have been successfully simulated in this study by considering the interaction between rock fractures and rock bridges. Fracture sliding and fracture propagation at the load level beyond the strength of the fractured rock mass are found to be the main reason causing its nonlinearity and hysteresis. The conceptual model which considers the sliding of the fractures is proved to explain the hysteresis at lower load level, and the tensile failure model which considers both fracture sliding and the mode I fracture propagation has been demonstrated to predict both the nonlinearity and hysteresis at higher load level.

At a substantially high stress level, fractured rock masses are demonstrated to fail along the fractures and bridges. Experimental tests with pre-cracked gypsum samples subjected to uniaxial compressive loading have increased the understanding of the mechanism of fracture coalescence. The failure of the rock bridge depends on the failure (sliding) of rock fractures. The mode of failure is depending upon the fracture-bridge configuration and the loading direction. When the fractures are close to overlapped (i.e., bridge inclination of inclination  $75^\circ$  or  $90^\circ$ ), they are more likely to coalesce and the coalescence is mixed tensile and shear failure.

To predict both tensile failure and shear failure, a new fracture propagation criterion, the F-criterion, has been proposed. The criterion, together with the numerical method DDM, well predict the mixed mode propagation which is common for rock fractures. Applied to the experimental tests, the F-criterion and DDM have produced the path and critical load of fracture coalescence in very good agreement with the experimental results. The numerical simulation has also confirmed the experimental observation of the mechanism of fracture coalescence.

### 6.2 Recommendations for future study

The results presented in this study are mostly for a simple fracture-bridge system under uniaxial compressive loading. In nature, fractured rock masses

contain multiple fractures (often randomly distributed) and are always subjected to three-dimensional loading. Even though the analytical and numerical models presented in this thesis can be directly applied to fracture network under biaxial loading, such applications have not been conducted because of the lack of experimental results. Therefore, experimental study of multi-fractures under biaxial loading is of great importance in the continuation of this study. The future study is proposed as the following:

- (1) Uniaxial compressive loading test of gypsum (or concrete, or rock) samples containing multi-fractures with randomly distribution. The path of multi-fracture coalescence is the main objective of the study and the results are expected to provide further validation of the analytical and numerical models.
- (2) Biaxial compressive loading test of simple fracture-bridge system. According to the numerical prediction, It is expected that the rock bridge will fail in mode II without mode I being involved.
- (3) Biaxial compressive loading test of samples containing randomly distributed multi-fractures. The outcome of this test will provide a more detailed understanding of the failure of fractured rock masses. This study can also be used to check the capacity of the numerical models for various fracture networks and loading conditions.
- (4) Improvement of the various models into an universal computer code for its application to rock engineering problems. The code will have high capacity in the prediction of the strength of fractured rock masses subjected to any loading condition and with any fracture network. Its application can be extended to most of the existing rock engineering problems such as slope stability, mining design, tunnel excavation, borehole stability and performance assessment of underground nuclear waste repository.

## References

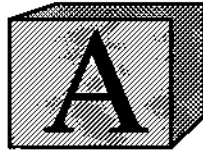
- Aliabadi M.H. and Rooke D.P. *Numerical fracture mechanics*, Kluwer Academic Publishers. (1991)
- Boone T.J., Wawrzynek P.A. and Ingraffea A.R. "Finite element modelling of fracture propagation in orthotropic materials". *Int. J. Engng. Frac. Mech.* **26(2)**, 185-201.(1987)
- Brace W. and Byerlee J. "Recent experimental studies of brittle fracture of rocks". In: *Failure and Breakage of Rock, AIME*, 57-81. (1967)
- Brady B.H.G., Cramer M.L. and Hart R.D. "Preliminary analysis of a loading test on a large basalt block". *Int. J. Rock Mech. Min. Sci.* **22(5)**, 345-348. (1985)
- Brady B.H.G. and Brown E.T. *Rock mechanics for underground mining*, George Allen & Unwin Publication. (1985)
- Chiang W.T. "Fracture criteria for combined mode cracks". *Fracture, ICP4*, Waterloo, Canada, **4**, 135-154. (1977).
- Crouch S.L. "Solution of plane elasticity problems by the displacement discontinuity method". *Int. J. Num. Methods Engng.* **10**, 301-343. (1976)
- Crouch S.L. and Starfield A.M. *Boundary element methods in solid mechanics*. George Allen & Unwin (publisher). (1983)
- Cundall P.A. "UDEC—A general distinct element program for modelling jointed rock". Report PCAR-1-80, U.S.Army. (1980)
- Deng Q. and Zhang P. "Research on the geometry of shear fracture zones". *J. Geophy. Res.* **89**, 5699-5710. (1984)
- Einstein H.H., Veneziano D., Baecher G.B. and O'reilly K.J. "The effect of discontinuity persistence on rock stability". *Int. J. Rock Mech. Min. Sci. & Geomech. Abs.* **20(5)**, 227-237. (1983)
- El-Tahan W.W., Staab G.H., Advani S.H. and J. K. Lee. "A mixed mode local symmetric fracture criterion for geo-materials". *Proc. 32th U.S. Symp. Rock Mechanics.* 455-462 (1990).
- Eordgan F. and Sih G.C. "On the crack extension in plates under plane loading and transverse shear". *ASME J. Bas. Engng* **85**, 519-527. (1963).
- Griffith, A. "The phenomena and rupture flow in solids", *Phil. Trans. R. Soc. London.* **A221**, 163-198. (1921)
- Griffith, A. "The theory of rupture". *Proc. 1st Int. Cong. Appl. Mech., Delft.* 55-63. (1925)

- Hamajima R., Kawai T., Yamashita K. and Kusabuka M. Numerical analysis of cracked and jointed rock mass". *5th Int. Con. Num. Meth. Geomech.* (1985).
- Hellan K. *Introduction to fracture mechanics*. McGraw-Hill Book Company (publisher). (1985).
- Hoek E. and Brown E.T. *Underground excavations in rock*, Institute of Mining and Metallurgy Publication (London). (1982).
- Hoori H. and Nemat-Nasser S. "Compression-induced microcrack growth in brittle solid: axial splitting and shear failure". *J. Geophys. Res.* **90**(B4), 3105-3125. (1985)
- Horri H. and Nemat-Nasser S. "Brittle failure in compression: splitting, faulting and brittle-ductile transition". *Phil. Trans. Roy. Soc.*, **319** (1549), 337-374. (1986)
- Hussain M.A., Pu S.L. and Underwood J. "Strain energy release rate for a crack under combined mode I and mode II". *Fracture Analysis, ASTM-STP.* **560**, 2-28. Am. Soc. Testing Materials, Philadelphia (1974).
- Ingrafea A. "Finite element models for rock fracture mechanics". *Int. J. Num. Ana. Meth. Geomech.* **4**, 24-43. (1987)
- Kachanov, M.L. "A microcrack model of rock inelasticity —Part I and II". *Mech. Mater.* **1**, 19-41. (1982)
- Kemeny, J.M. and Cook, N.G.W. "Micromechanics of deformation in rocks". In: *Toughening Mechanisms in Quasi-Brittle Materials*, S.P. Shaw (ed). Kluwer Academic, The Netherland, 155-188. (1991)
- Kemeny, J.M. "A model for non-linear rock deformation under compression due to subcritical crack growth". *Int. J. Rock Mech. Min. Sci.* **28**, 459-467. (1991)
- Kulatilake P.H.S.W., Ucpirti H., Wang S., Rådberg G. and Stephansson O. "Use of the distinct element method to perform stress analysis in rock with non-persistent joints and to study the effect of joint geometry parameters on the stress and deformability of rock masses". *Rock Mech. Rock Engng.* **25**(4), 253-274. (1992)
- Lajtai E.Z. "Shear strength of weakness planes in rock". *Int. J. Rock Mech. Min. Sci. & Geomech. Abs.* **6**, 299-515. (1969).
- Lajtai E. "Brittle fracture in compression". *Int. J. Fracture*, **10**(4), 525-536. (1974)
- Li, C. "Deformation and failure of brittle rocks under compression". Ph.D Thesis No.1993:118D, Luleå University of Technology, Sweden. (1993)
- Li V.C. "Mechanics of shear rupture applied to earthquake zones". In: *Fracture mechanics of rock*, Atkinson K.B. (ed). Academic Press, London, 351-428.(1991).

- Lockner D., Moore D. and Reches Z. "Microcrack interaction leading to shear fracture". *Proc. 33rd U.S. Symp. Rock Mech.* 807-816. (1992)
- Melin S. "The infinitesimal kink". Report LUTFD2/(TFHF-3022)/1-19/(1985). (Division of Solid Mechanics, Lund Institute of Technology, Lund.)
- Nilson R. "Modelling a jointed rock mass". S.M. Thesis, MIT. (1968)
- Petit J.-P. and Barquins M. "Can natural faults propagate under mode II conditions?" *Tectonics*, **7(6)**, 1243-1256 (1988).
- Reyes O. and Einstein H.H. "Failure mechanism of fractured rock — A fracture coalescence model". *Proc. 7th Int. Con. on Rock Mechanics*, **1**, 333-340. (1991)
- Savilahti T., Nordlund E. and Stephansson O. "Shear box testing and modelling of joint bridges". In: *Rock Joints*, Barton & Stephansson (eds). *Proc. Int. Symp. Rock Joints (Norway)*. 295-300. (1990)
- Schultz R. "Stress intensity factors for curved cracks obtained with the displacement discontinuity method". *Int. J. Fracture*, **37**, R31-34. (1988)
- Segall P. and Pollard D. "Mechanics of discontinuous faults". *J. Geophys. Res.* **85(B8)**, 4337-4350. (1980)
- Segall P. and Pollard D. "Nucleation and growth of strike slip faults in granite". *J. Geophys. Res.* **88(B1)**, 555-568. (1983)
- Shen B. and Stephansson O. "Cyclic loading characteristics of joints and rock bridges in a jointed rock specimen". *Proc. Int. Symp. on Rock Joints, Leon, Norway*, 715-729. (1990)
- Shen B. and Stephansson O. "Rock mass response to glaciation and thermal loading from nuclear waste". *Proc. Int. Symp. GEOVAL-90, Stockholm*, 550-558. (1990)
- Shen B. and Stephansson O. "Deformation and propagation of finite joints in rock masses". *Proc. Int. Conf. on Fractured and Jointed Rock Masses, Lake Tahoe, U.S.A.* **2**, 312-318. (1992) (preprints)
- Shen B. and Stephansson O. "Numerical analysis of Mode I and Mode II propagation of rock fractures". *Int. J. Rock Mech. Min. Sci. (special issue of 34th U.S. Symposium on rock mechanics)*. (1993) (in press)
- Shen B. and Stephansson O. "Modification of the G-criterion for crack propagation subjected to compression". *Int. J. of Engineering Fracture Mechanics*. (1993) (in press)
- Shen B., Stephansson O., Einstein H. and Ghahreman B. "Coalescence of open and closed cracks — A laboratory investigation". *Int. J. Rock Mech. Min. Sci.* (1993) (submitted).
- Shen B. "The mechanism of fracture coalescence in compression— Experimental study and numerical simulation". *Int. J. Eng. Frac. Mech.* (1993) (submitted).



- Sih G.C. "Strain-energy-density factor applied to mixed mode crack problems". *Int. J. Fracture*. **10(3)**, 305-321 (1974).
- Singh, B. "Continuum characterization of jointed rock masses — Part I, The constitutive equations". *Int. J. Rock Mech. Min. Sci.*, **10**, 311-335. (1973)
- Stephansson O. "The Näsliden project — rock mass investigation". In: *Application of Rock Mechanics to Cut and Fill Mining* (eds. Stephansson and Jones) 145-161. (1981)
- Stephansson O., Shen B. and Lemos J. "Modelling of excavation, thermal loading and bentonite swelling pressure of a radioactive waste repository". *Proc. Int. Conf. High-Level Radioactive Waste Management, Las Vegas, U.S.A.*, 1375-1381.(1991)
- Stephansson O. and Shen B. "Modelling of rock mass for site location of a nuclear waste repository". *Proc. 7th Int. Cong. on Rock Mechanics., Aachen, Germany*, 157-162.(1991)
- Stephansson O. and Shen B. "Modelling of faulted rock mass response to glaciation, thermal loading and seismicity". *Quarterly Journal of Engineering Geology*, **24**, 355-262.(1991)
- Wang R., Zhao Y., Chen Y., Yan H., Yin Y., Yao C. and Zhang H. "Experimental and finite element simulation of X-type shear fractures from a crack in marble". *Tectonophysics*. **144**, 141-150. (1987)
- Wong, T-F, "Micromechanics of faulting in Westerly granite". *Int. J. Rock Mech. Min. Sci.* **19**, 49-64. (1982)



# **Cyclic loading characteristics of joints and rock bridges in a jointed rock specimen**

*B. Shen and O. Stephansson*

*Proc. Int. Symp. on Rock Joints, Leon, Norway, pp.715-729. (1990)*

# Cyclic loading characteristics of joints and rock bridges in a jointed rock specimen

B. Shen & O. Stephansson

*Division of Rock Mechanics, Luleå University of Technology, Luleå, Sweden*

**ABSTRACT:** A new conceptual model is developed to analyze the behaviour of a specimen containing a joint and rock bridges during a loading cycle. The model employs the equivalent shear and normal stiffnesses ( $K_s^b$ ,  $K_n^b$ ) to describe the deformation of the rock bridges. For some special cases the equivalent stiffnesses are measured by comparing the analytical results with numerical results.

## 1 INTRODUCTION

Jointed rock masses exhibit a complicated mechanical behaviour. To predict the rock mass response to stress loading, Singh (1971) simplified the joints in a rock mass as a joint system which completely cut the rock mass into regular blocks. Based on this assumption he obtained an analytical solution to describe the elastic behaviour of a jointed rock mass. Generally joints have a limited length and may end inside an intact rock block, therefore the mechanical behaviour of the rock mass should include the effect of the rock bridges and the interaction between joints and rock bridges. Since rock bridges usually cause a very complicated stress distribution in the rock mass, there was no general analytical solution for the stress-strain relations during loading and unloading. To give a general idea about loading and unloading characteristics, Brady et al (1985) presented a conceptual model which concerned a single crack in a rock specimen, see Fig.1(a). Based on the assumption of uniform stress distribution on the crack and its extensions, Brady et al. described the analytical stress-strain relations of the conceptual model during loading and unloading. Brady's model was an interesting contribution for considering the effect of joints and bridges on the mechanical behaviour of jointed rock masses. However, its stress-strain relations are not accurate when the joint is too long compared with the size of the specimen. For such geometry, large stress concentration occurs near the rock bridges

which were not accounted for in his analysis. In a rock mass, the joint lengths are usually larger than the bridges, therefore it is necessary to independently consider the stresses on joints and bridges for studying the effects of joints and bridges.

## 2 THE NEW CONCEPTUAL MODEL AND ITS ANALYTICAL RESULTS

Based on Brady's model, a new conceptual model is developed, see Fig.1(b). The model consists of a joint with inclination  $\theta$ . The joint is completely contained in the specimen, with a rock bridge on each end. The resultant stiffnesses of the joint are  $K_s^j$  and  $K_n^j$  (for the shear and normal components), and the rock bridge is characterized by the resultant equivalent stiffnesses,  $K_s^b$  and  $K_n^b$ . The joint friction angle is  $\phi$ . The intact rock above and below the joint plane is modeled as a spring with stiffness,  $k$ , in axial direction.

Three modes of deformation are developed for this model during loading and unloading, which depend on i) the stiffnesses of the joint, bridges and intact rock; ii) the joint friction angle and joint inclination; iii) the length of the joint and bridges. Simple loading can be purely elastic or exhibit a bilinear response, depending whether the slip is initiated along the joint. The unloading behaviour is related to the loading behaviour and the extent of slip during the loading cycle.

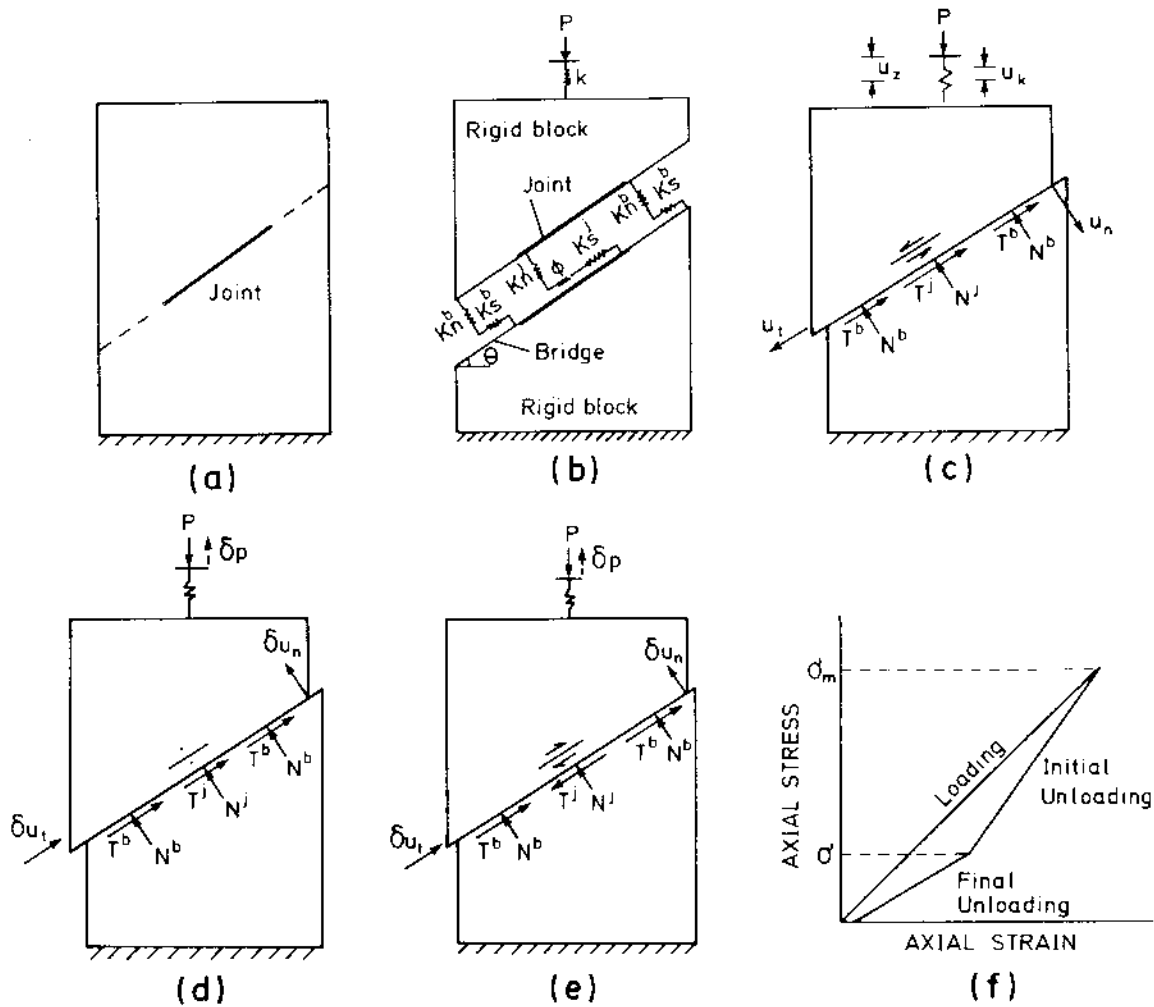


Fig.1 The new conceptual model for a jointed specimen and its development during loading and unloading

### 2.1 Joint slip condition

During loading, when the shear force on the joint satisfies equation (1) the joint will slip.

$$T^j > N^j \cdot \tan\phi \quad (1)$$

Where  $T^j$  and  $N^j$  are the shear force and normal force along the joint. Suppose that the resultant force on the specimen in its axial direction is  $P$ , then  $T^j$  and  $N^j$  can be described by equation (2),

$$T^j = \frac{K_s^j}{K_s^j + 2K_s^b} \cdot P \cdot \sin\theta \quad N^j = \frac{K_n^j}{K_n^j + 2K_n^b} \cdot P \cdot \cos\theta \quad (2)$$

By substituting equation (2) into (1), the critical inclination  $\theta$  at which the joint slips during loading is obtained as:

$$\theta > \tan^{-1} \left[ \frac{K_s^j + 2K_s^b}{K_n^j + 2K_n^b} \cdot \frac{K_n^j}{K_s^j} \cdot \tan\phi \right] \quad (3)$$

If the above condition is not met, then no slip occurs and only elastic loading and unloading ensues. For the purposes of this paper, such elastic loading behaviours is not relevant and thus only the case at which the initial slip occurs is considered. For the jointed specimen, the stress-strain relationship during loading and unloading is analyzed as following:

### 2.2 Loading

Here,  $u_k, u_n$  and  $u_t$  are used to represent the axial displacement of intact rock and the shear and normal displacement along the joint plane.  $u_z$  is used to represent the resultant axial displacement of the specimen, see Fig.1(c). When the compressive load,  $P$ , increases  $\delta P$ , the increase of  $u_k$  and  $u_n$  can be described as:

$$\delta u_k = \frac{\delta P}{k} \quad \delta u_n = \frac{\delta P \cdot \cos\theta}{K_n^j + 2K_n^b} \quad (4)$$

The shear displacement increment  $u_t$  along the

joint plane,  $\delta u_t$ , is related to the joint slip. Due to joint slip, the shear force increment on the joint depends on the increase of normal force on the joint:

$$\delta T^j = \delta N^j \cdot \tan\phi = \delta P \cdot \sin\theta \cdot \frac{K_n^j}{K_n^j + 2K_s^b} \cdot \tan\phi \quad (5)$$

and the shear force increment on the rock bridges is:

$$\delta T^b = 2K_s^b \cdot \delta u_t \quad (6)$$

Shear force equilibrium along the joint plane dictates that:

$$\delta T^j + \delta T^b = \delta P \cdot \sin\theta \quad (7)$$

Combining equation (5), (6) and (7), an expression for  $\delta u_t$  can be developed:

$$\delta u_t = \frac{\delta P \cdot \sin\theta}{2K_s^b} \cdot \left[ 1 - \frac{K_n^j}{K_n^j + 2K_n^b} \cdot \tan\theta \right] \quad (8)$$

The increase of  $u_z$  is described by:

$$\delta u_z = \delta u_k + \delta u_n \cdot \cos\theta + \delta u_t \cdot \sin\theta \quad (9)$$

Substituting equations (4) (8) into (9) yield:

$$\delta u_z = \frac{1}{k} \cdot \delta P + \frac{\cos^2\theta}{K_n^j + 2K_n^b} \cdot \delta P + \frac{\sin\theta}{2K_s^b} \cdot \left[ 1 - \frac{K_n^j}{K_n^j + 2K_n^b} \cdot \tan\theta \right] \cdot \delta P \quad (10)$$

Dividing both sides of equation (10) by  $\delta P$ , and converting the force-displacement ratio ( $\delta P/\delta u_z$ ) to a stress-strain ratio ( $d\sigma/d\varepsilon$ ) by assuming the specimen with height,  $H$ , and width,  $W$ , the following equation is obtained:

$$\frac{d\sigma}{d\varepsilon} = L \left[ \frac{L}{E'} + \frac{\cos^2\theta}{K_n^j + 2K_n^b} + \frac{\sin\theta}{2K_s^b} \left( \sin\theta - \frac{K_n^j}{K_n^j + 2K_n^b} \cdot \tan\phi \cdot \cos\theta \right) \right]^{-1} \quad (11)$$

Where  $E'$  is Young's modulus of the intact rock for the plane stress condition, and  $L$  is height/width ratio,  $L=H/W$ .

Equation (11) defines the slope of the stress-strain curve during loading.

### 2.3 Initial unloading

When the compressive loading force  $P$  decreases by  $\delta P$ , the shear displacement along the fictitious joint plane also decreases. Initially, the joint is locked and only elastic deformation occurs along the

joint. Considering these characteristics, the decrease of the displacement of the intact rock and the fictitious joint plane becomes:

$$\delta u_k = \delta P/k \quad (12)$$

$$\delta u_t = \frac{1}{K_s^j + 2K_s^b} \cdot \delta P \cdot \sin\theta \quad (13)$$

$$\delta u_n = \frac{1}{K_n^j + 2K_n^b} \cdot \delta P \cdot \cos\theta \quad (14)$$

Notice that  $\delta u_k$ ,  $\delta u_t$  and  $\delta u_n$  have opposite direction to that during loading, see Fig.1(d). Substituting equations (12), (13) and (14) into equation (9) and converting force-displacement ratio to stress-strain ratio, the slope of  $\sigma$ - $\varepsilon$  curve becomes:

$$\frac{d\sigma}{d\varepsilon} = L \cdot \left[ \frac{L}{E'} + \frac{\cos^2\theta}{K_n^j + 2K_n^b} + \frac{\sin^2\theta}{K_s^j + 2K_s^b} \right]^{-1} \quad (15)$$

Although the unloading stage is completely elastic, the modulus of the jointed system is less than the Young's modulus of the intact rock.

### 2.4 Final unloading

As the shear displacement decreases, the shear force along the joint decreases and finally becomes negative, see Fig.1(e). When the shear force along the joint exceeds joint's shear strength, the direction of sliding reverses. Suppose that the maximum loading force is  $P_m$  and the maximum elastic displacement along the joint is  $u_m$  when the maximum force is loaded,  $u_m$  is given by:

$$u_m = \frac{1}{K_s^j} \cdot \frac{K_n^j}{K_n^j + 2K_n^b} \cdot P_m \cdot \cos\theta \cdot \tan\phi \quad (16)$$

Since the shear force on the joint must equal its frictional resistance when the joint is slipping, there is:

$$(\delta u_t - u_m) \cdot K_s^j = P \cdot \cos\theta \cdot \frac{K_n^j}{K_n^j + 2K_n^b} \cdot \tan\phi \quad (17)$$

Substituting  $\delta u_t$  from equation (13) and  $u_m$  from equation (16) into equation (17) and setting  $\alpha_1 = \frac{K_s^j}{K_s^j + 2K_s^b}$ ,  $\alpha_2 = \frac{K_n^j}{K_n^j + 2K_n^b}$  produced:

$$\frac{\sigma}{\sigma_m} = \frac{P}{P_m} = \frac{\alpha_1 \cdot \sin\theta - \alpha_2 \cdot \cos\theta \cdot \tan\phi}{\alpha_1 \cdot \sin\theta + \alpha_2 \cdot \cos\theta \cdot \tan\phi} \quad (18)$$

Where  $\sigma$  and  $\sigma_m$  are the axial stresses co-

responding to the axial forces P and P<sub>m</sub>. Equation (18) describes the critical ratio of stress to maximum stress at which the joint slips back during unloading.

During final unloading, the slope of σ-ε curve can be obtained by using the same method as during loading:

$$\frac{d\sigma}{d\varepsilon} = L \cdot \left[ \frac{L}{E'} + \frac{\cos^2 \theta}{K_n^j + 2K_n^b} + \frac{\sin \theta}{2K_s^b} \cdot \left( \sin \theta + \frac{K_n^j}{K_n^j + 2K_n^b} \cdot \tan \phi \cdot \cos \theta \right) \right]^{-1} \quad (19)$$

Equations (11), (15), (18) and (19) create a complete σ-ε curve for a loading cycle as shown in Fig.1(f).

### 3 NUMERICAL MEASUREMENT FOR SHEAR AND NORMAL STIFFNESSES OF THE ROCK BRIDGES

Because the stress distribution near the rock bridges is very complicated, the equivalent stiffnesses of rock bridges, which represents their deformability, is difficult to determine mathematically. Therefore back-analysis is used in this paper, i.e. the numerically tested slopes of σ-ε curve are used to induce the bridge stiffnesses K<sub>s</sub><sup>b</sup>, K<sub>n</sub><sup>b</sup> by using two of the three equations (11), (15) and (19).

UDEC is a powerful tool to calculate the mechanical behaviour of jointed rock masses. For the rock specimen containing a joint with limited length, UDEC assumes that a joint completely passes through the specimen with independent stiffnesses on the joint and the rock bridges. Since the intact rock is treated as deformable medium in UDEC, the deformation of the bridges has been modelled by the rock deformation, therefore the introduction of the bridge's stiffnesses in UDEC are just because of the requirement of the UDEC, and only when the bridge's stiffnesses are very high the accurate solution can be obtained. However, the intact rock in the new conceptual model is considered as uniformly deformable blocks, with the deformability of rock bridges represented by bridge's stiffnesses. Therefore the bridge's stiffnesses in the new conceptual model and in UDEC are by no means same if uneven rock deformation is considered in UDEC.

Before using the UDEC test results to back-analyze the bridge's stiffnesses in the conceptual model, it is necessary to make sure that the UDEC can produce the same results as the new conceptual model when only uniform rock deformation is considered. A specimen (Fig.2) is tested

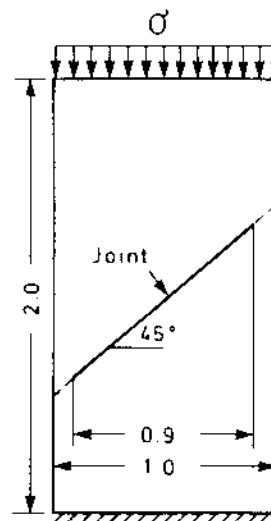


Fig.2 Jointed specimen used for the numerical test

by UDEC with a lower stiffnesses on the bridges. Since the lower stiffnesses make the rock deformation along the joint plane almost uniform in UDEC calculation, the same bridge's stiffnesses can be used in UDEC and the conceptual model. The mechanical properties of intact rock, joint and bridges are listed below:

Intact rock properties:

the new model: E' = 95.2 GPa ν' = 0.35

UDEC: E = 88.8 GPa ν = 0.26

Average stiffnesses per unit length:

joint JK<sub>n</sub><sup>j</sup> = 55 GPa/m JK<sub>s</sub><sup>j</sup> = 55 GPa/m

bridges JK<sub>n</sub><sup>b</sup> = 55 GPa/m JK<sub>s</sub><sup>b</sup> = 55 GPa/m

Joint friction angle φ = 30°

Note: 1. The new conceptual model and UDEC were based on the plane stress and plane strain conditions respectively, therefore E', ν' for plane stress condition and E, ν for plane strain condition were used.

2. The stiffnesses presented in equations (11), (15) and (19) are resultant stiffnesses on the total length of the joint or bridges. When average stiffnesses on per unit length are used here, transformation is needed.

Fig.3 shows the numerical results of UDEC and the analytical results of the new conceptual model. Excellent agreement is obtained.

For testing the equivalent bridge's stiffnesses, K<sub>s</sub><sup>b</sup> and K<sub>n</sub><sup>b</sup>, in the new conceptual model, high bridge's stiffnesses are used in UDEC for loading and unloading of the same specimen shown in Fig.2, which are:

(JK<sub>n</sub><sup>b</sup>)<sub>UDEC</sub> = 550 GPa/m

(JK<sub>s</sub><sup>b</sup>)<sub>UDEC</sub> = 550 GPa/m

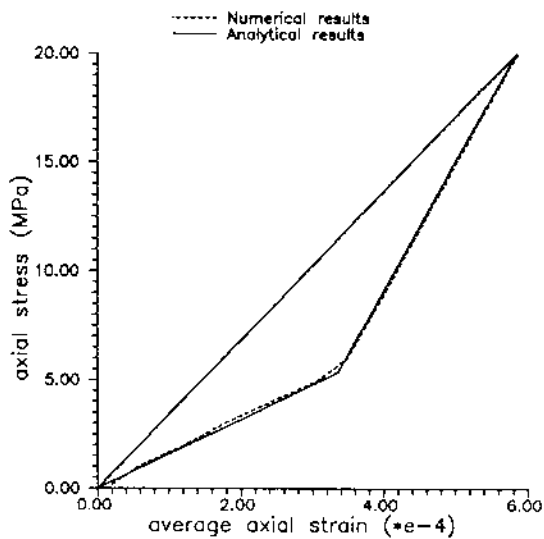


Fig.3 Comparison between the results of numerical test and the new model

In this UDEC analysis, the rock deformation in the rock of bridge zone is much larger than the deformation along the joint plane. Therefore, when the new conceptual model produces the same results as UDEC, its equivalent stiffnesses must represent the real deformability of the rock bridges.

The numerical loading and unloading test for the same specimen shown in Fig.2 using the high bridge's stiffnesses results in the following slopes of the  $\sigma$ - $\epsilon$  curve:

$$\left( \frac{d\sigma}{d\epsilon} \right)_{\text{loading}} = 50.89 \text{ GPa}$$

$$\left( \frac{d\sigma}{d\epsilon} \right)_{\text{initial unloading}} = 64.10 \text{ GPa}$$

Since the slope of  $\sigma$ - $\epsilon$  curve during final unloading sometimes is not accurate in UDEC calculation for the numerical reason, it is not used here.

Substituting these two results into equations (11) and (15) respectively and giving values to other known variables for our specimen result in:

$$\begin{cases} \frac{1}{35+K_n^b} + \frac{1}{K_s^b} \left[ 1 - \frac{20.2}{35+K_n^b} \right] - 0.073 = 0 \\ \frac{1}{35+K_n^b} + \frac{1}{35+K_s^b} - 0.041 = 0 \end{cases}$$

The solution of the above simultaneous equations yields:

$$K_n^b = 16.42 \text{ GPa/m} \quad K_s^b = 11.40 \text{ GPa/m}$$

Converting the resultant stiffnesses,  $K_n^b$  and  $K_s^b$ , to stiffnesses per length, the average equivalent stiffnesses of the

bridges in the conceptual model are obtained as:

$$\begin{aligned} (JK_n^b)_{\text{model}} &= 232 \text{ GPa/m} \\ (JK_s^b)_{\text{model}} &= 161 \text{ GPa/m} \end{aligned}$$

The average equivalent stiffnesses of the rock bridge are different with different bridge length and different joint and rock properties. For example, when the total bridge length in the same specimen is tripled, i.e. it takes 30% parts in the fictitious joint plane, the average equivalent stiffnesses become:

$$\begin{aligned} (JK_n^b)_{\text{model}} &= 318 \text{ GPa/m} \\ (JK_s^b)_{\text{model}} &= 184 \text{ GPa/m} \end{aligned}$$

#### 4 CONCLUSION

The new conceptual model introduces the equivalent normal and shear stiffnesses of rock bridges which are independent of the joint properties. This joint/rock bridge system is used to predict stress-strain relations of a jointed rock mass during a loading and unloading cycle. Since the stress concentrations near the bridges are considered, the new model can give a realistic  $\sigma$ - $\epsilon$  relationship even when the rock bridges are relatively short.

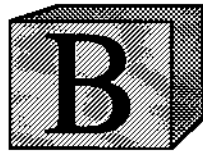
The results of the new model indicate that the initial unloading is completely elastic. The slope of the  $\sigma$ - $\epsilon$  curve during this stage is related to the properties of rock mass and the shear and normal stiffnesses of the joint and bridges. The  $\sigma$ - $\epsilon$  relationship during the loading stage reflects the elastic deformation of the specimen together with joint slip.

For measuring the equivalent stiffnesses of the rock bridges in the new conceptual model, UDEC is used with very high stiffnesses in the rock bridge zones.

ACKNOWLEDGEMENT: The authors thank Anders Bro for his benefited discussion and his help for correcting the English.

#### REFERENCE

- Singh, B. Continuum Characterization of Jointed Rock Masses. Int. J. Rock Mech. Min. Sci. & Geomech. Abstr. 10, 311-355 (1973).
- Brady, B.H.G., Cramer, M.L. and Hart, R.D. Technical Note: Preliminary Analysis of a Loading Test on a Large Basalt Block. Int. J. Rock Mech. Min. Sci. & Geomech. Abstr. 22, 345-348 (1985).
- Cundall, P.A., UDEC—A Generalized Distinct Element Program for Modelling Jointed Rock. Report PCAR-1-80, U.S. Army. (1980)



# **Deformation and propagation of finite joints in rock masses**

*B. Shen and O. Stephansson*

*Proc. Int. Conf. on Fractured and Jointed Rock Masses, Lake Tahoe, U.S.A.,  
Vol.2, pp.312-318.(preprints) (1992)*



# Deformation and Propagation of Finite Joints in Rock Masses

B. Shen and O. Stephansson

Engineering Geology, Royal Institute of Technology, Stockholm, Sweden

## Abstract

A DDM model is developed to simulate the load-displacement characteristics of rock masses containing joints with finite length. The model can handle joint surface contact and friction during loading and unloading and joint tip propagation under mixed modes (Mode I and II). Joint tip propagation is found to cause non-linear stress-strain behaviour during loading while reverse joint slip induces non-linearity during unloading. The load-displacement curves obtained by applying the DDM model to some jointed rock blocks are discussed and compared with experimental results from large block tests.

## 1. Introduction

In principle, two approaches exist for analyzing the deformability of jointed rock masses: the continuous approach and the discontinuous approach. In the continuous approach the jointed rock mass is treated as an elastic and continuous body with equivalent elastic properties [1]; in the discontinuous approach the rock mass is considered as an assembly of rock blocks [2][3], and the interaction of the blocks controls the rock mass behaviour. In both of the two approaches, the joints are mostly assumed to be persistent in the rock mass. However, joints and sets of joints have finite persistence and rock bridges of intact rock will exist between the ends of joints. The existence of rock bridges stiffens the rock mass. Joints may extend and coalesce at higher stress levels [4], which weakens the rock mass and causes failure of rock bridges. Therefore, new approaches which can handle joint tip propagation are needed for the analysis of jointed rock masses.

A conceptual model and an analytical solution of a simple rock mass were used to study the cyclic loading characteristics of the joint-rock bridge system in a study by Shen and Stephansson [5]. To be able to analyse more complicated

joint-rock bridge systems, where the joint tip propagation is involved, numerical techniques have to be applied. Among the existing numerical methods, the Boundary Element Method (BEM) has been of interest for the solution of elastic problems. In comparison with the Finite Element Method (FEM), BEM offers less computation time, no requirement to remesh when joint tips are propagating and the final results are more accurate. There are two key issues to be considered when BEM is applied to the rock masses with finite joints. One is to represent the joints in such a way that they can make proper contact, open, slip and change slip directions during loading cycles. Another issue is to predict the initiation of joint tip propagation and simulate the propagation path for mixed modes (Mode I and II). BEM and its applications to rock mechanics and fracture mechanics offer methods to solve the problems. Crouch and Starfield [6] suggested a load incremental method to simulate joint slip and presented the idea of using 'crack tip element' to model stresses and displacements near crack tips by means of BEM. This idea was further developed to calculate the stress intensity factors for the mixed-mode problems by Guo et al [7]. Schultz [8] used non-uniformly distributed crack elements to calculate the stress intensity factors at crack tips. By using constant discontinuity displacement elements it gives a convenient way of estimating stress intensity factors. In modelling the propagation of open cracks under combined stress condition, Ghorbanpoor and Zhang [9] introduced a criterion of crack propagation for mixed modes.

The studies mentioned above are limited to special cases, i.e. either closed joints without joint tip propagation or joint (crack) tip propagation without joint (crack) surface contact. In attempting to model rock masses with finite joints and sets of non-persistent joints, however, both joint surface contact and joint tip propagation need to be considered. This requires further developments of the modelling techniques. In the model to be discussed in this paper, the Displacement Discontinuity Method (DDM), one of the indirect methods of BEM, is employed due to its convenience in directly calculating joint displacement. The non-uniformly distributed elements with constant displacements are used for joints to improve the accuracy of calculated stress intensity factors at joint tips. A mixed-mode (Mode I and II) joint tip propagation is introduced, and the load incremental method is employed to study joint deformability during cyclic loading.

## 2. Displacement Discontinuity Method

The Displacement Discontinuity Method (DDM) was developed by Crouch [10] and later widely used in modelling problems containing discontinuities. The

displacement discontinuities,  $D_s$  and  $D_n$ , across a joint are directly presented as unknowns. For the problem geometry shown in Fig.1 the governing equations can be written in the matrix form:

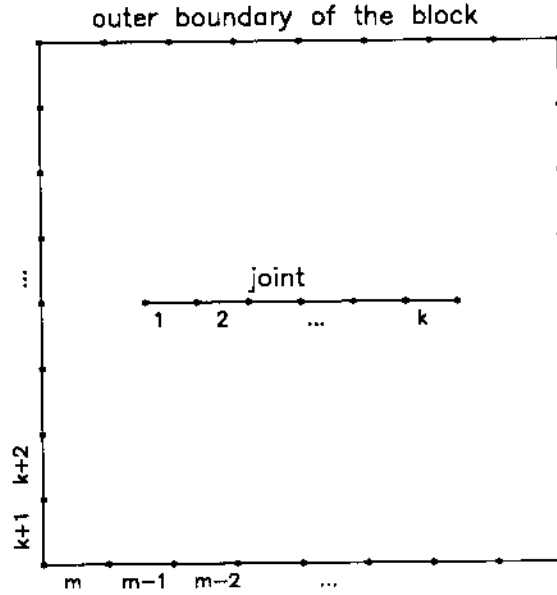


Fig.1. Displacement discontinuity elements along the boundary of a rock block and an enclosed joint.

$$\begin{bmatrix}
 A_{ss}^{11} & A_{sn}^{11} & \dots & A_{ss}^{1k} & A_{sn}^{1k} & \dots & A_{ss}^{1m} & A_{sn}^{1m} \\
 A_{ns}^{11} & A_{nn}^{11} & \dots & A_{ns}^{1k} & A_{nn}^{1k} & \dots & A_{ns}^{1m} & A_{nn}^{1m} \\
 \vdots & \vdots & \ddots & \vdots & \vdots & \ddots & \vdots & \vdots \\
 A_{ss}^{k1} & A_{sn}^{k1} & \dots & A_{ss}^{kk} & A_{sn}^{kk} & \dots & A_{ss}^{km} & A_{sn}^{km} \\
 A_{ns}^{k1} & A_{nn}^{k1} & \dots & A_{ns}^{kk} & A_{nn}^{kk} & \dots & A_{ns}^{km} & A_{nn}^{km} \\
 \vdots & \vdots & \ddots & \vdots & \vdots & \ddots & \vdots & \vdots \\
 A_{ss}^{m1} & A_{sn}^{m1} & \dots & A_{ss}^{mk} & A_{sn}^{mk} & \dots & A_{ss}^{mm} & A_{sn}^{mm} \\
 A_{ns}^{m1} & A_{nn}^{m1} & \dots & A_{ns}^{mk} & A_{nn}^{mk} & \dots & A_{ns}^{mm} & A_{nn}^{mm}
 \end{bmatrix}
 \times
 \begin{bmatrix}
 D_s^1 \\
 D_n^1 \\
 \vdots \\
 D_s^k \\
 D_n^k \\
 \vdots \\
 D_s^m \\
 D_n^m
 \end{bmatrix}
 =
 \begin{bmatrix}
 \sigma_s^1 \\
 \sigma_n^1 \\
 \vdots \\
 \sigma_s^k \\
 \sigma_n^k \\
 \vdots \\
 \sigma_s^m \\
 \sigma_n^m
 \end{bmatrix}
 \quad (1)$$

where  $A_{ss}^{ij}, A_{sn}^{ij}, A_{ns}^{ij}, A_{nn}^{ij}$  ( $i, j = 1, m$ ) are influence coefficients from the shear and normal stresses of the  $i$ th element caused by unit shear and normal displacement discontinuities on the  $j$ th element;  $D_s^i, D_n^i$  are the shear and normal displacement discontinuities of the  $i$ th element; and  $\sigma_s^i, \sigma_n^i$  are the shear and normal stresses on the  $i$ th element. In simplified form eq. (1) can also be written as

$$[\mathbf{K}][\mathbf{D}] = [\boldsymbol{\sigma}] \quad (2)$$

where  $[K]$  is the matrix of influence coefficients which can be calculated based on Crouch's solution for unit displacement discontinuities in an infinite elastic body [10];  $[D]$  is the unknown displacement discontinuity matrix; and  $[\sigma]$  is the matrix of boundary stresses and joint stresses. When the joint is open, the joint stresses are zero, and  $[\sigma]$  is written as

$$[\sigma] = [0, 0, \dots, 0, 0, \sigma_s^{k+1}, \sigma_n^{k+1}, \dots, \sigma_s^m, \sigma_n^m]^T \quad (3)$$

where  $\sigma_s^i, \sigma_n^i$  ( $k+1 \leq i \leq m$ ) are boundary stresses. The displacement discontinuity matrix  $[D]$  can be determined by solving equation (2) with conventional numerical techniques, e.g. Gauss Elimination Method.

For most situations in rock masses, joints are closed. If joint surfaces are in contact and deform elastically without slip, the shear and normal stresses of the joint are proportional to its displacement discontinuities. For the  $i$ th element of the joint ( $i \leq k$ ),

$$\begin{aligned} \sigma_s^i &= K_s D_s^i \\ \sigma_n^i &= K_n D_n^i \end{aligned} \quad (4)$$

Substituting the stresses of joint elements in equation (1) by eq.(4) and after simple manipulation we obtain

$$([K] - [K]^e)[D] = [\sigma] \quad (5)$$

where  $[K]^e$  is the matrix of influence coefficients from the elastic response of the joint, and  $[\sigma]$  is presented by eq.(3).

$$[K]^e = \begin{bmatrix} K_s & 0 & & & & \\ 0 & K_n & & & & \\ & & \ddots & & & \\ & & & K_s & 0 & \\ & & & 0 & K_n & \\ & & & & & \ddots \\ & & & & & & 0 & 0 \\ & & & & & & 0 & 0 \end{bmatrix} \begin{matrix} i=1 \\ i=1 \\ \vdots \\ i=k \\ i=k \\ \vdots \\ i=m \\ i=m \end{matrix}$$

If the joint slips, the shear stress can be determined by the normal stress and its friction angle ( $\phi$ ). For the  $i$ th element of joint,

$$\begin{aligned}\sigma_n^i &= K_n D_n^i \\ \sigma_s^i &= \pm \sigma_n^i \tan \phi = \pm K_n D_n^i \tan \phi\end{aligned}\tag{6}$$

The sign of  $\sigma_s^i$  depends on the direction of slip. The governing equation is written:

$$([\mathbf{K}] - [\mathbf{K}]\mathbf{P})[\mathbf{D}] = [\boldsymbol{\sigma}]\tag{7}$$

where  $[\mathbf{K}]\mathbf{P}$  is the matrix of influence coefficients from the inelastic response of the joint, and  $[\boldsymbol{\sigma}]$  follows eq.(3).

$$[\mathbf{K}]^p = \begin{bmatrix} K_s \pm K_n \tan \phi & & & & & & & \\ 0 & K_n & & & & & & \\ & & \dots & & & & & \\ & & & K_s \pm K_n \tan \phi & & & & \\ & & & 0 & K_n & & & \\ & & & & & \dots & & \\ & & & & & & 0 & 0 \\ & & & & & & 0 & 0 \end{bmatrix} \begin{matrix} i=1 \\ i=1 \\ \vdots \\ i=k \\ i=k \\ \vdots \\ i=m \\ i=m \end{matrix}$$

### 3. Load incremental method

When a joint has experienced slip, its shear displacement can not be directly determined by eqs. (2), (5) and (7). The shear displacement which the joint has undergone must be remembered and included in the total displacement at any loading level. One way to fulfil this requirement in DDM is by using the load incremental method.

For a small increment of boundary stresses  $[\Delta\boldsymbol{\sigma}]$ , the increment of displacement discontinuities  $[\Delta\mathbf{D}]$  of the joint can be calculated by using one of the eqs. (2), (5) and (7), depending on the state of the joint prior to the load increment. The increment of shear and normal stress of each joint element, therefore, is known from the increment of displacement discontinuities  $[\Delta\mathbf{D}]$ . The

total shear and normal stress of each joint element are obtained by adding the increments to the previous value prior to the boundary stress increment. The total shear and normal stress of each joint element are then used to determine the state of the joint for the next load increment. When the Mohr-Coulomb failure criterion is applied to joints the states are as follow:

- (1) open joint:  $\sigma_n > 0$
- (2) elastic joint:  $\sigma_n < 0, |\sigma_s| < c + |\sigma_n|\tan\phi$
- (3) slip of joint:  $\sigma_n < 0, |\sigma_s| \geq c + |\sigma_n|\tan\phi$

where compressive stress is taken to be negative and  $c$  is cohesion. If the joint has experienced slips,  $c = 0$ .

The reverse of the slip direction of the joint during unloading can also be determined by checking whether the sign of total shear stress  $\sigma_s$  has changed.

#### 4. Non-uniformly distributed elements

Constant displacement elements have the advantage of simplicity and they suit all kinds of boundary geometries and loading conditions. The equal-length, constant elements along joints give less accurate results at joint tips. Using the 'crack tip element' and the 'non-uniformly distributed element' are two ways to improve the accuracy in calculating the stress intensity factors. In this study the non-uniformly distributed element is employed.

An elliptical crack in an infinite body under uniaxial tensile stress has a normal displacement curve similar to a circle (Fig.2a). The best way to simulate the displacement values is by arranging the elements along the crack in such a way that the projections of all the elements on the displacement curve have the same length, Fig.2b. Provided the displacement curve is circular, the length of the elements along the crack is given by

$$L_i = 2a \sin\left(\frac{\pi}{2n}\right) \sin\left(\frac{(2i-1)\pi}{2n}\right) \quad (8)$$

where  $L_i$  = the length of the  $i$ th element;  
 $n$  = total number of elements along the crack;  
 $a$  = half length of the crack.

If the discontinuity is a joint with only one tip inside a rock block, the joint will be considered as a half-crack.

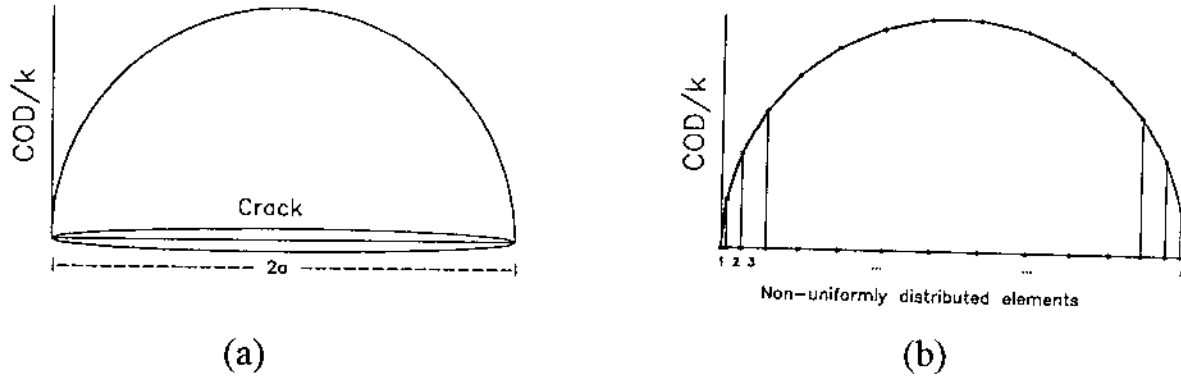


Fig.2. Non-uniformly distributed element approach in DDM. (a) Crack Opening Displacement (COD) versus crack length along an elliptical tensile crack in an infinite body; (b) arrangement of non-uniformly distributed elements along the crack.  $k$  is a factor.

The stress intensity factors ( $K_I$  and  $K_{II}$ ) can be estimated from the displacement discontinuities of the tip element. According to Schultz [8] they are written as:

$$K_I = \frac{E}{8\pi(1-\nu^2)} \sqrt{\frac{2\pi}{d}} D_n$$

$$K_{II} = \frac{E}{8\pi(1-\nu^2)} \sqrt{\frac{2\pi}{d}} D_s$$
(9)

where  $D_n$  and  $D_s$  are normal and shear displacement discontinuities of tip elements;  $E$  and  $\nu$  are Young's modulus and Poisson's ratio,  $d$  is the half-length of the tip element. The displacement discontinuities at the mid-point of the tip element with constant displacements exceeds the analytical value by a factor of  $\pi/2$  [11]. Therefore a reduction of  $K_I$  and  $K_{II}$  by  $\pi/2$  is included in eq. (9).

By using the non-uniformly distributed elements described by eq. (8), the stress intensity factors are estimated with sufficient accuracy by eq. (9). Results from analyses of a horizontal crack in an infinite plate with unit vertical tensile stress demonstrate that 15 elements along the crack will produce a ratio of stress intensity factor with an accuracy of 93%, see Fig.3.

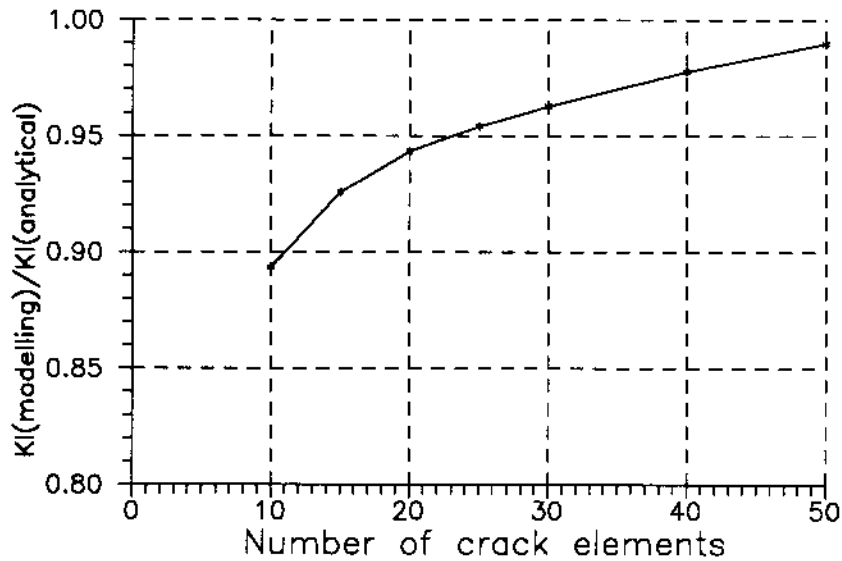


Fig.3. Ratio of stress intensity factor for an uniaxial tensile crack in an infinite elastic plate calculated by non-uniformly distributed elements versus the number of crack elements.

## 5. Joint tip propagation under mixed modes

Joints in rock masses are seldom oriented parallel or perpendicular to the applied principal stresses. Therefore, compression, tension and shearing prevail and mixed-mode conditions have to be considered in studying joint tip propagation. There are several theories which may be used to describe the joint tip propagation for mixed mode problems. These theories are minimum strain energy density [12], maximum energy release rate [13] and maximum principal stress [14]. In this study the maximum principal stress theory is used because of its simplicity and its relatively easy coupling with DDM.

The maximum principal stress theory postulates that joint tip propagation will occur in the direction of the maximum compressive principal stress. For the problem of an open, sharp crack in a polar co-ordinate system, the stresses near a crack tip (Fig.4) can be written as[15]:

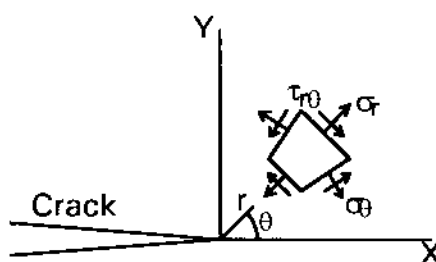


Fig.4. Stresses in polar co-ordinate system near a sharp, open crack tip.



$$\sigma_r = \frac{K_I}{4\sqrt{2\pi r}} \left[ 5\cos\frac{\theta}{2} - \cos\frac{3\theta}{2} \right] + \frac{K_{II}}{4\sqrt{2\pi r}} \left[ -5\sin\frac{\theta}{2} + 3\sin\frac{3\theta}{2} \right] + O(r^0) \quad (10)$$

$$\sigma_\theta = \frac{K_I}{4\sqrt{2\pi r}} \left[ 3\cos\frac{\theta}{2} + \cos\frac{3\theta}{2} \right] + \frac{K_{II}}{4\sqrt{2\pi r}} \left[ -3\sin\frac{\theta}{2} - 3\sin\frac{3\theta}{2} \right] + O(r^0) \quad (11)$$

$$\tau_{r\theta} = \frac{K_I}{4\sqrt{2\pi r}} \left[ \sin\frac{\theta}{2} + \sin\frac{3\theta}{2} \right] + \frac{K_{II}}{4\sqrt{2\pi r}} \left[ \cos\frac{\theta}{2} + 3\cos\frac{3\theta}{2} \right] + O(r^0) \quad (12)$$

$O(r^0)$  is a non-singularity term and it will be omitted in later discussions. The direction of joint tip propagation, i.e. the maximum compressive principal stress direction ( $\theta_m$ ) can be obtained by setting stress  $\tau_{r\theta} = 0$  in eq. (12) and solving for  $\theta_m$  as:

$$\left[ \tan\left(\frac{\theta_m}{2}\right) \right]_{1,2} = \frac{1}{4} \frac{K_I}{K_{II}} \pm \frac{1}{4} \sqrt{\left(\frac{K_I}{K_{II}}\right)^2 + 8} \quad (13)$$

where the subscript 1,2 denotes the directions of the principal stress  $\sigma_1$  and  $\sigma_2$ . Since tensile stress causes fracturing, the fracture toughness for Mode I ( $K_{Ic}$ ) can be used as the critical condition for joint tip propagation and the tangential stress  $\sigma_\theta$  in eq. (11) becomes

$$\sigma_\theta = \frac{K_{Ic}}{\sqrt{2\pi r}} \quad \text{for } \theta=0 \quad (14)$$

Inserting eq. (14) into the left side of eq. (11) and substituting  $\theta_m$  in the right side of eq. (11) we obtain the criterion for mixed mode propagation as:

$$K_{Ic} = K_I \cos^3 \frac{\theta_m}{2} - 3K_{II} \cos^2 \frac{\theta_m}{2} \sin \frac{\theta_m}{2} \quad (15)$$

In this study eqs. (9), (13) and (15) are the governing equations in modelling joint tip propagation by DDM. The direction of propagation( $\theta_m$ ) is the most important factor in a continuous process of fracture propagation. The fact that eq. (13) is valid for open, straight cracks while the joints in this study are often closed and the propagation will be curved calls for corrections to be made.

## 6. Numerical simulation procedure

A rock block containing an internal joint and subjected to vertical uniaxial compressive loading (Fig. 5a) is taken as an example to illustrate the DDM modelling procedure. The modelling procedure is performed in six steps.

(1) Discretize the outer boundary of the block into equal length boundary elements and divide the joint into non-uniformly distributed elements. The length of the elements at the joint tips should be small enough to yield results with satisfactory accuracy.

(2) Load the block by using the load incremental method. The state of the joint is determined and the joint surface displacements ( $D_s$  and  $D_n$ ) are obtained at each and every stress level.

(3) Calculate the stress intensity factors ( $K_I$  and  $K_{II}$ ) at the joint tips by eq. (9) for a given stress level prior to a new loading step.

(4) Use eq. (13) to initially estimate the direction of the maximum principal stress ( $\theta_m$ ). The calculated value of  $\theta_m$  for an open straight crack differs from that of a closed joint. After the joint tips have propagated in a direction that deviates from the strike of the original joint, the prevailing joint has a strong influence on the stress field at new tips. The application of eq. (13) introduces errors in estimating  $\theta_m$ . In our DDM model, therefore, the angle  $\theta_m$  estimated by eq. (13) is only taken as the initial value. Then an arc with a radius equal to the length of tip element and the angle from  $\theta_m - 30^\circ$  to  $\theta_m + 30^\circ$  (Fig. 5b) is defined in front of the joint tip. The principal stresses ( $\sigma_1$  and  $\sigma_2$ ) at 30 points equally spread along this arc are calculated in order to determine the true direction of the maximum principal stress. Fig. 5c demonstrates the efficiency of this correction by comparing the propagation path both prior to and after the correction.

(5) When the direction of the maximum principal stress at the joint tip is determined, eq. (15) is applied to calculate whether the joint tip will propagate or remain. If the joint tip is found to propagate, a new tip element is added to the original tip element in the direction of the propagation. Then step (3), (4) and (5) is repeated until no further propagation is obtained for a given stress level.

(6) Increase the loading in the next sequence and repeat steps (2), (3), (4) and (5) until the expected level of loading is achieved and then unload the block step by step. At each and every loading level, the displacement of the block is

recorded. A complete stress-displacement curve of the top surface of the block during loading and unloading can be determined (Fig.5d).

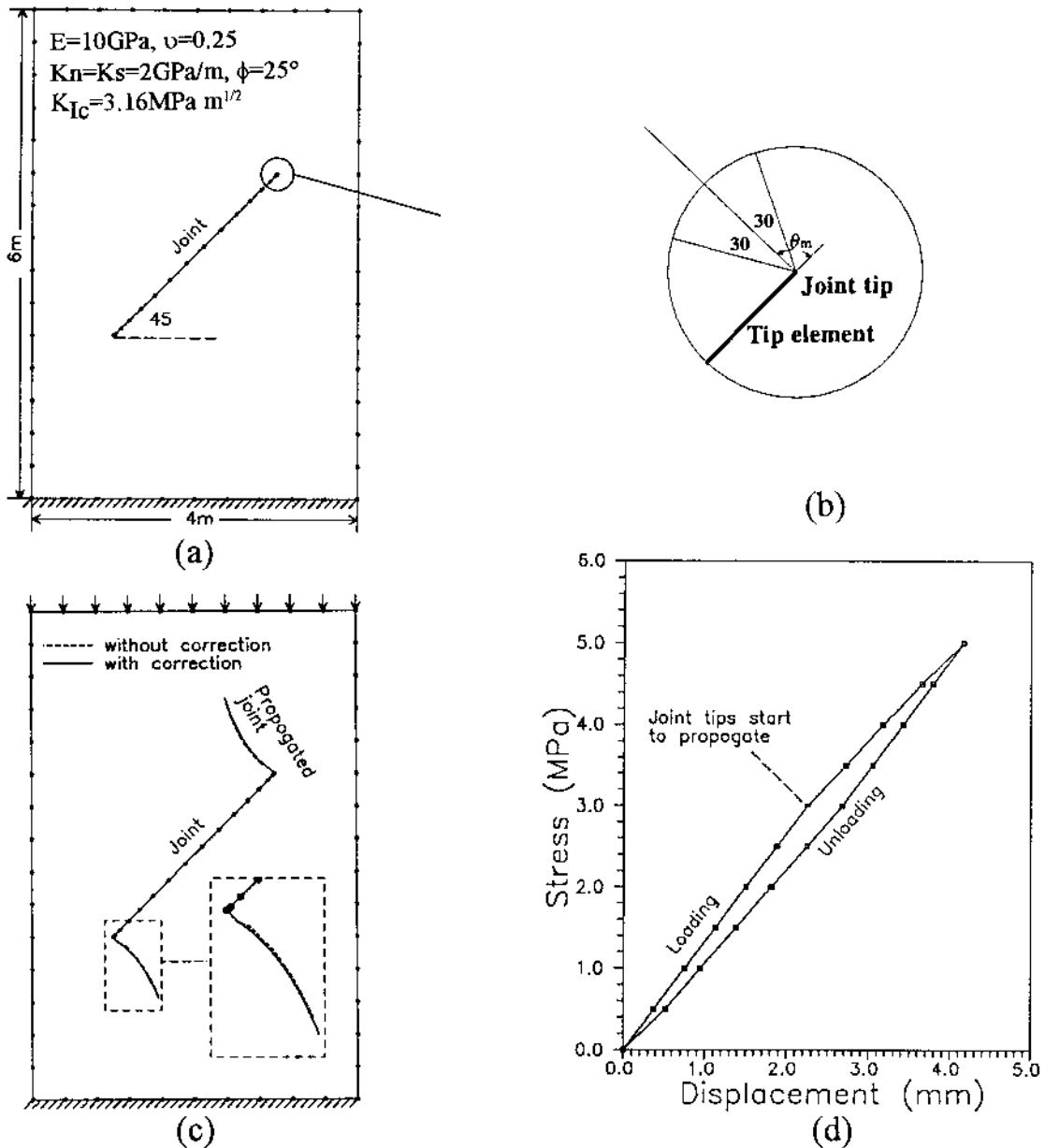


Fig.5. Numerical procedure in modelling the stress-displacement characteristics of a rock block containing a single joint. (a) Geometry of the block and joint; (b) the arc around the joint tip for searching the direction of the maximum principal stress; (c) propagation of joint tips due to the vertical loading of the block; and (d) stress-displacement curve during a loading cycle.

## 7. Results

The DDM model from this study can be applied to the deformability of rock masses with single joint, joint sets and any joint system. The results for a rock

block containing a single joint demonstrate the onset of non-linearity of the stress-displacement curve when joint propagation starts during loading and thereafter remains during unloading, Fig.5d. The non-linearity during loading is caused by the stable propagation of the two joint tips, while it is caused by the reverse slip of the joint during unloading.

In the second numerical test a block with two joints is modelled (Fig.6). Each joint has one tip inside the block and the other tip at the boundary of the block, and a rock bridge exists between the two joint tips inside the block. The loading is performed by increasing the boundary displacement of the top surface. Loading performed by displacement control has the advantages of stable joint tip propagation. The extension of joints at peak displacement is shown in Fig.6a. The first propagation of the joint tips strongly weakens the block and causes a stress drop, but later when the direction of joint propagation becomes parallel to the direction of the maximum principal stress, further propagation does not significantly influence the stiffness of the block, Fig.6b. The non-linearity of the stress-displacement curve during unloading is caused by the reverse slip of the joints.

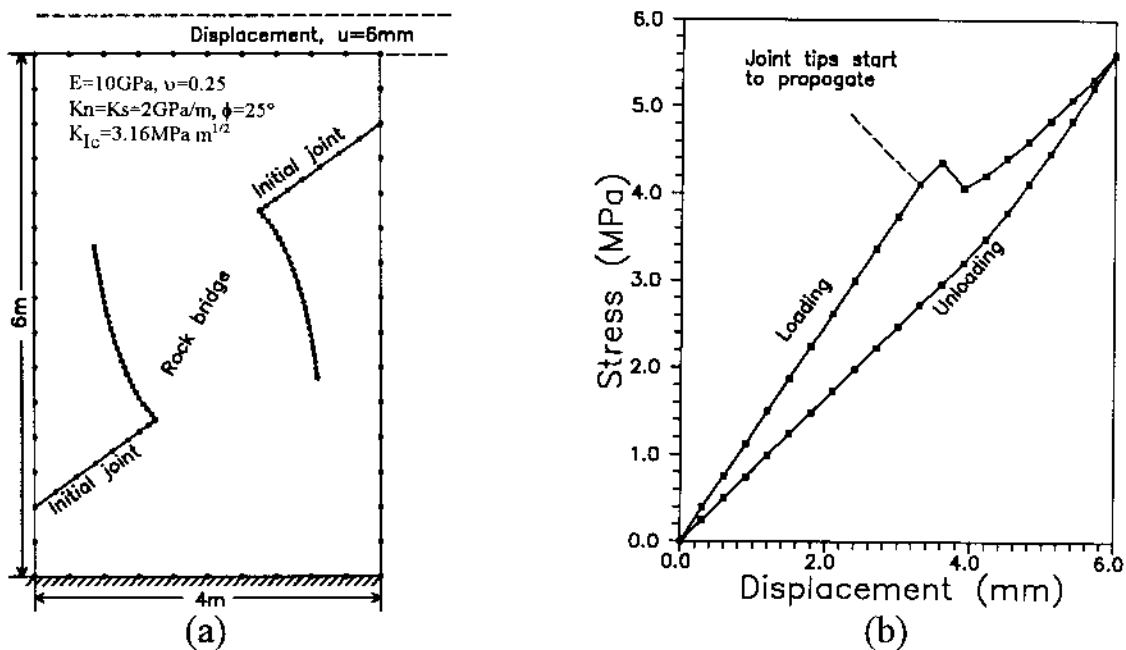


Fig.6. A rock block with two joints and one rock bridge loaded by a control displacement on the top surface. (a) Geometry of the block with initial joints and joint propagation after peak displacement; (b) uni-axial stress versus displacement.

The last example demonstrates stress versus displacement of a rock block containing a set of four joints and several rock bridges (Fig.7a). The propagation of joint tips starts from the two central joints (Fig.7b), later followed by the tips of the more peripheral joints (Fig.7c). Continuous propagation causes the failure

of two rock bridges (Fig.7d). The coalescence of joint tips (or the failure of rock bridges) significantly weakens the rock block and this feature is observed as a stress drop in the stress-displacement curve (Fig.7f).

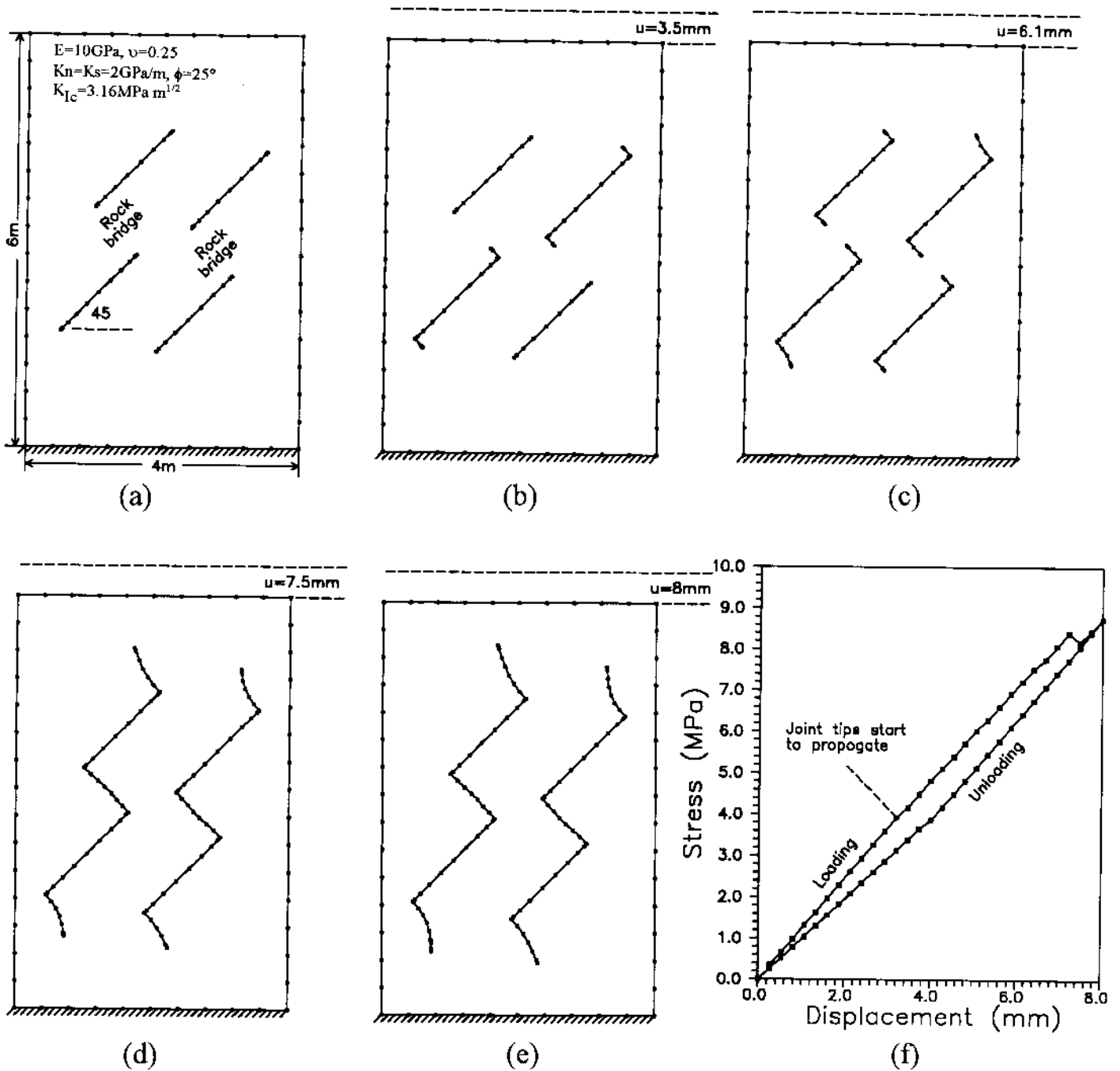


Fig.7. A rock block with a set of four joints and several rock bridges under progressive displacement. (a) Geometry of the block with initial joints; (b) - (e) propagation of joint tips during loading; (f) stress-displacement curve during loading and unloading.

## 8. Discussion

Two common features can be observed from the three examples above. First, joint tips start to propagate at a stress level much lower than the strength of the block. This means that joint tips might propagate prior to the failure of the rock mass. Secondly, although the intact rock is treated as a linearly elastic medium in our examples, a jointed rock block has a non-linear stress-displacement relationship due to joint tip propagation.

From the two features mentioned above we can expect highly non-linear stress-displacement behaviour of a heavily jointed rock mass when it is affected by underground excavation, mining, etc. The non-linear response of jointed rock masses has been observed in many experimental tests, e.g. the Basalt Block Test at the Hanford Test Site[16], see Fig. 8. Although there were no direct observations of joint tip propagation and joint slip in this test, the generic stress-displacement relationship demonstrated in Figs.5d,6b,7f and 8 suggests the joint tip propagation and joint slip had occurred and dominated the non-linearity.

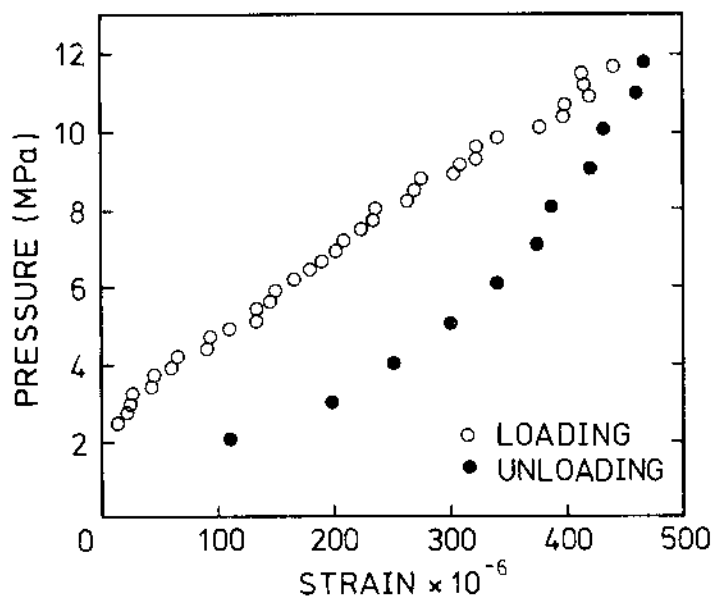


Fig.8. Experimental pressure versus strain of a large basalt block ( $2.2 \times 2.2 \times 2.0$  m) at Hanford Test Site during loading and unloading. After Brady et al. [16].

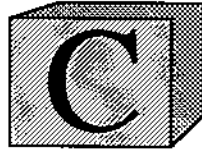
## 9. References

- [1] B. Singh, "Continuum characterization of jointed rock masses: Part I - The constitutive equations," *Int. J. Rock Mech. Min. Sci. & Geomech. Abst.*, Vol. 10, pp.311-335, 1973.

- [2] P.A. Cundall, "UDEC - A generalized distinct element program for modelling jointed rock," Report PCAR- 1-80, Peter Cundall Associates, European Research Office, U.S. Army, 1980.
- [3] G-h. Shi, "Discontinuous deformation analysis - A new numerical model for the statics and dynamics of block systems", Ph D. Thesis, Department of Civil Engineering, University of California, Berkeley, 1989.
- [4] O. Reyes and H.H. Einstein, "Failure mechanisms of fractured rock - A fracture coalescence model", *Proc. 7th Int. Congr. on Rock Mechanics*, Vol.1, pp.333-340, 1991.
- [5] B. Shen and O. Stephansson, "Cyclic loading characteristics of joints and rock bridges in a jointed rock specimen," *Proc. Int. Symp. on Rock Joints*, Loen, Norway, pp. 725-729, 1990.
- [6] S.L. Crouch and A.M. Starfield, *Boundary Element Methods in Solid Mechanics*, London: George Allen & Unwin Publishers Ltd, 1983.
- [7] H. Guo, N.I. Aziz and L.C. Schmidt, "Linear elastic crack tip modelling by the displacement discontinuity method," *Engineering Fracture Mechanics*, Vol. 36, No. 6, pp. 933-943, 1990.
- [8] R.A. Schultz, "Stress intensity factor for curved cracks obtained with the displacement discontinuity method," *Int. J. Fracture*, Vol. 37, pp. R31-R34, 1988.
- [9] A. Ghorbanpoor and J. Zhang, "Boundary element analysis of crack growth for mixed-mode center slant crack problems." *Engineering Fracture Mechanics*, Vol. 36, No. 5, pp. 661-668, 1990.
- [10] S.L. Crouch, "Solution of plane elasticity problems by the displacement discontinuity method." *Int. J. Num. Methods Engng.*, Vol.10, pp.301-343, 1976.
- [11] S.L. Crouch, "Analysis of stresses and displacement around underground excavation: An application of the displacement discontinuity method," Geomechanics report to the National Science Foundation, University of Minnesota, Minneapolis, 1976.
- [12] G.C. Sih, Strain energy density factor applied to mixed mode crack problems," *Int. J. Fracture*, Vol. 11, pp.305-321, 1974.
- [13] M.A. Hussain, S.L. Pu and J.U. Underwood, "Strain energy release rate for a crack under combined mode I and mode II," *Fract. Anal., ASTM, STP*, Vol. 560, pp. 2-28, 1974.
- [14] F. Erdogan and G.C. Sih, "On the crack extension in plates under plane loading and transverse shear." *J. Basic Engng.*, Vol. 85, pp. 519-527, 1963.
- [15] K. Hellan, *Introduction to Fracture Mechanics*, Singapore: McGraw-Hill Book Company, 1984.
- [16] B.H.G. Brady, M.L. Cramer and R.D. Hart, "Technical note: Preliminary analysis of a loading test on a large basalt block," *Int. J. Rock Min. Sci. & Geomech. Abst.* Vol. 22, No. 5, pp. 345-348, 1985.







# **Modification of the G-criterion for crack propagation subjected to compression.**

*B. Shen and O. Stephansson*

*Int. J. of Engineering Fracture Mechanics (in press) (1993).*

# Modification of the G-criterion for Crack Propagation Subjected to Compression

B. Shen & O. Stephansson

Engineering Geology, Royal Institute of Technology, Stockholm, Sweden

## Abstract

Brittle materials subjected to compression can fail and the resulting cracks can propagate in Mode I and Mode II in 2-D. The Maximum Strain Energy Release Rate Criterion (G-criterion) is examined for its capacity of predicting the mixed modes crack propagation. When this criterion is applied to an inclined crack subjected to compression, it predicts the shear failure but not the tensile failure. The reason for this phenomenon is discussed and a new form of this criterion, namely F-criterion, is proposed. The F-criterion uses the sum of normalized  $G_I$  and  $G_{II}$  ( $F = G_I/G_{Ic} + G_{II}/G_{IIc}$ ) as the factor which represents the crack propagation and its direction. Implemented into the numerical method DDM, the F-criterion can predict both Mode I and Mode II propagation of a crack system. The capacity of the F-criterion in predicting both Mode I and Mode II propagation is demonstrated for two models subjected to uniaxial compression for a single crack and a set of two cracks. The numerical simulations show good agreement with the results of laboratory experiments conducted on rocks and gypsum.

## INTRODUCTION

Fracture mechanics has at present increasing applications in the study of fractured rock masses. Unlike many engineering materials, the fracturing at in-site rock masses is mostly controlled by far-field compressive stresses. The study of the crack initiation and propagation when subjected to compression is important in order to understand the behaviour of fractured rock masses. There are three characteristics which are unique for crack propagation in two dimensional problems subjected to compression compared to that subjected to tension:

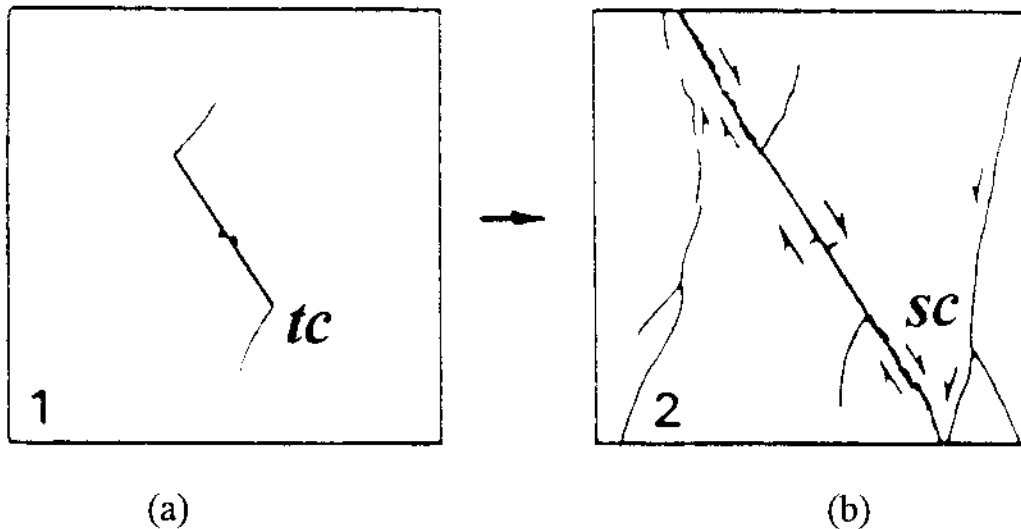


Fig.1. Crack propagation from a single-inclined flaw in high porosity sandstone specimens under uniaxial compression. *tc* — tensile crack; *sc* — secondary crack. From Petit and Barquins [2].

1. A tensile crack, namely *tc* (Fig.1a), appears first near a crack tip and is directed approximately  $90^\circ$  away from the original crack plane and propagates in a curved fashion toward the direction of maximum compressive stress. This process is usually stable and an increasing load is needed to maintain the propagation.

2. In brittle materials, such as rocks, a secondary crack (*sc*, see Fig.1b) occurs when the load reaches a substantially high level [1][2][3]. The *sc* is often initiated in the direction parallel or at a small angle to the original crack plane. The *sc* seems to be formed by shearing.

3. The surfaces of both the original crack and the *sc* are often in contact. Sliding along them may occur during the propagation process for both *tc* and *sc*.

In fracture mechanics there are three criteria commonly used for predicting crack propagation: the maximum tensile stress criterion [4], the minimum strain energy density criterion (S-criterion)[5] and the maximum strain energy release rate criterion (G-criterion)[6]. The maximum tensile stress criterion is based on concentration of tensile stress at crack tips. It is a conventional method to predict Mode I crack propagation [7] but can not be used to simulate the *sc* caused primarily by shearing. The G-criterion and the S-criterion, which are conceptually based on the strain energy in a crack system, seem applicable to predict the *tc* and *sc* since the strain energy is related to all the three stress components in two dimensions. However, for an inclined crack subjected to compression, the S-criterion only predicts two minimum S-values, one

approximately in the direction of maximum tensile stress and the other in the direction of maximum compressive stress. Neither of the minimum  $S$ -values are in the direction of the  $sc$ . The study in this paper is therefore focused on the  $G$ -criterion.

The  $G$ -criterion has many mathematical difficulties in application because the  $G$ -value, in an arbitrary direction, is difficult to present analytically. Hussain et al. [8] and Melin [9] have successfully presented the  $G$ -value, using the stress intensity factors ( $K_I$  and  $K_{II}$ ). However, Hussain's formula has been shown to be inaccurate to predict compressive crack propagation [10][11], and Melin's results are only for tensile crack propagation. In this study we use the Displacement Discontinuity Method (DDM), a boundary element technique, as a numerical tool to calculate the  $G$ -value. The results indicate a maximum  $G$ -value in the direction of maximum shearing whereas there is no obvious maximum in the direction of tensile crack. Therefore, the  $G$ -criterion is in need of modification in order to be applicable to the problem of the mixed mode crack propagation when cracks in brittle material are subjected to compression.

In this paper we first briefly describe the concept and theory of the DDM. This method is then used to calculate the  $G$ -value for an inclined crack subjected to compression and the  $F$ -criterion is proposed. This  $F$ -criterion is subsequently used in DDM to perform the modelling of the crack propagation process. Finally the DDM with the  $F$ -criterion is applied to simulate experimental results of crack propagation in rock and gypsum models which were subjected to uniaxial compression.

## **DISPLACEMENT DISCONTINUITY METHOD (DDM)**

The Displacement Discontinuity Method (DDM) was initially developed by Crouch [12] and later widely used in fracture mechanics [13][14][15]. The advantage of DDM in simulating crack propagation is that it can directly present the crack as crack elements and it needs no remeshing when the crack is propagating. The displacement discontinuities,  $D_s$  and  $D_n$ , across a crack are directly presented as unknowns. For the problem with one crack in an infinite elastic body (Fig.2), the system of governing equations of DDM can be written as:

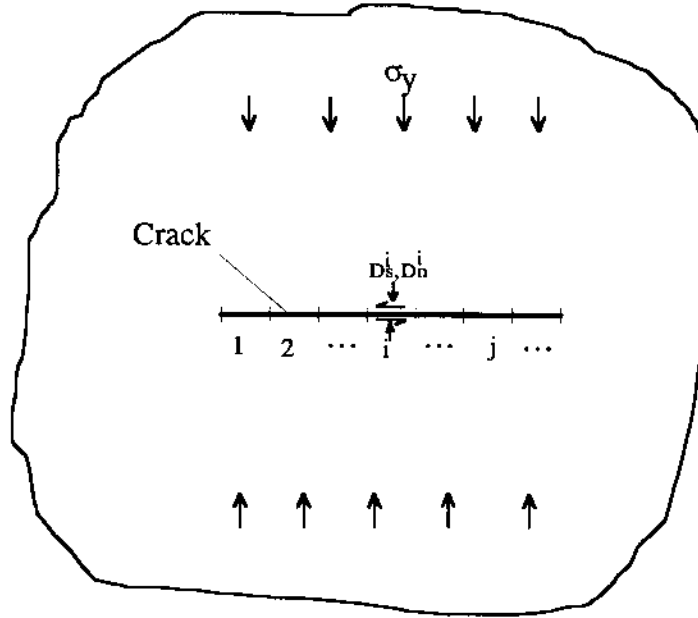


Fig.2. A crack in an infinite elastic body and its discretization by the displacement discontinuity elements.

$$\sigma_s^i = \sum_j (A_{ss}^{ij} D_s^j + A_{sn}^{ij} D_n^j) - (\sigma_s^i)_0 \quad (1)$$

$$\sigma_n^i = \sum_j (A_{ns}^{ij} D_s^j + A_{nn}^{ij} D_n^j) - (\sigma_n^i)_0 \quad (2)$$

where  $\sigma_s^i$  and  $\sigma_n^i$  represent the shear and normal stresses of the  $i$ th element respectively;  $(\sigma_s^i)_0, (\sigma_n^i)_0$  are the far-field stresses transformed in the crack shear and normal directions.  $A_{ss}^{ij}, \dots, A_{nn}^{ij}$  are the influence coefficients, and  $D_s^j, D_n^j$  represent displacement discontinuities of  $j$ th element which are unknowns in the system of equations.

A crack has three states: open, in contact or sliding. Although the DDM was initially developed for an open crack, it can be easily extended to the crack in contact and sliding. For different states the system of governing equations can be represented in the following ways, depending on the shear and normal stresses ( $\sigma_s^i$  and  $\sigma_n^i$ ) of the crack.

1. For an open crack  $\sigma_s^i = \sigma_n^i = 0$ , therefore the system of governing equations (1) (2) can be rewritten as:

$$\sigma_s^i = 0 = \sum_j (A_{ss}^{ij} D_s^j + A_{sn}^{ij} D_n^j) - (\sigma_s^i)_0 \quad (3)$$

$$\sigma_n^i = 0 = \sum_j (A_{ns}^{ij} D_s^j + A_{nn}^{ij} D_n^j) - (\sigma_n^i)_0 \quad (4)$$

2. When the two crack surfaces are in contact,  $\sigma_s^i$  and  $\sigma_n^i$  depend on the crack stiffness ( $K_s, K_n$ ) and the displacement discontinuities ( $D_s^i, D_n^i$ )

$$\sigma_s^i = K_s D_s^i \quad (5)$$

$$\sigma_n^i = K_n D_n^i \quad (6)$$

where  $K_s, K_n$  are the crack shear and normal stiffnesses [16], respectively. Substituting eqs. (5) and (6) into eqs. (1) and (2) and carrying out the simple mathematical manipulation, then, the system of governing equations becomes:

$$0 = \sum_j (A_{ss}^{ij} D_s^j + A_{sn}^{ij} D_n^j) - (\sigma_s^i)_0 - K_s D_s^i \quad (7)$$

$$0 = \sum_j (A_{ns}^{ij} D_s^j + A_{nn}^{ij} D_n^j) - (\sigma_n^i)_0 - K_n D_n^i \quad (8)$$

3. For a crack with its surfaces sliding (or slipping)

$$\sigma_n^i = K_n D_n^i$$

$$\sigma_s^i = \pm \sigma_n^i \tan \phi = \pm K_n D_n^i \tan \phi \quad (9)$$

where  $\phi$  is the friction angle of the crack. The sign of  $\sigma_s^i$  depends on the sliding direction. Consequently, the system of equations (1) and (2) can be presented as:

$$0 = \sum_j (A_{ss}^{ij} D_s^j + A_{sn}^{ij} D_n^j) - (\sigma_s^i)_0 \pm K_n D_n^i \tan \phi \quad (10)$$

$$0 = \sum_j (A_{ns}^{ij} D_s^j + A_{nn}^{ij} D_n^j) - (\sigma_n^i)_0 - K_n D_n^i \quad (11)$$

The displacement discontinuities ( $D_s^i, D_n^i$ ) of the crack are obtained by solving the system of governing equations using conventional numerical

techniques, e.g. Gauss elimination method. If the crack is open the stresses  $(\sigma_s^i, \sigma_n^i)$  are zero, otherwise if the crack is in contact or sliding, they can be calculated by eqs. (5), (6) or (9).

### CALCULATION OF G-VALUE BY USING DDM

The G-value is, by definition, the change of the strain energy in an linear elastic body when the crack has grown one unit of length. Therefore, to obtain the G-value the strain energy must first be estimated.

By definition, the strain energy,  $W$ , in a linear elastic body is

$$W = \iiint_V \frac{1}{2} \sigma_{ij} \varepsilon_{ij} dV . \quad (12)$$

where  $\sigma_{ij}$  and  $\varepsilon_{ij}$  are the stress and strain tensors, and  $V$  is the volume of the body. The strain energy can also be calculated from the stresses and displacements along its boundary

$$W = \frac{1}{2} \int_S (\sigma_s u_s + \sigma_n u_n) ds \quad (13)$$

where  $\sigma_s, \sigma_n, u_s, u_n$  are the stress and displacement in tangential and normal direction along the boundary of the elastic body. Applying eq.(13) to the crack system with far-field stresses  $(\sigma_s)_0$  and  $(\sigma_n)_0$  in the shear and normal direction of the crack, the strain energy,  $W$ , in the infinite elastic body is

$$W = \frac{1}{2} \int_0^a [(\sigma_s - (\sigma_s)_0) D_s + (\sigma_n - (\sigma_n)_0) D_n] da \quad (14)$$

where  $a$  is the crack length,  $D_s$  is the shear displacement discontinuity and  $D_n$  is the normal displacement discontinuity of the crack. When DDM is used to calculate the stresses and displacement discontinuities of the crack, the strain energy can also be written in terms of the element length ( $a^i$ ) and the stresses and displacement discontinuities of the  $i$ th element of the crack

$$W \approx \frac{1}{2} \sum_i (a^i (\sigma_s^i - (\sigma_s^i)_0) D_s^i + a^i (\sigma_n^i - (\sigma_n^i)_0) D_n^i) \quad (15)$$

The G-value can be estimated by

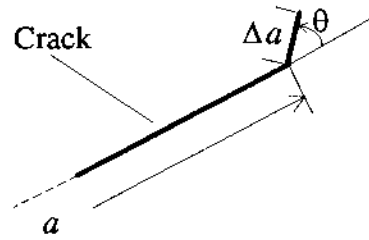


Fig.3. Fictitious crack increment  $\Delta a$  in direction  $\theta$  with respect to the initial crack orientation.

$$G(\theta) = \frac{\partial W}{\partial a} \approx \frac{[W(a + \Delta a) - W(a)]}{\Delta a} \quad (16)$$

where  $W(a)$  is the strain energy governed by the original crack while  $W(a + \Delta a)$  is the strain energy governed by both the original crack,  $a$ , and its small extension,  $\Delta a$ . Both  $W(a)$  and  $W(a + \Delta a)$  can be determined easily by directly using DDM and eq.(15). To calculate  $W(a + \Delta a)$  we need to introduce a 'fictitious' element to the tip of the original crack with the length  $\Delta a$  in the direction  $\theta$ , see Fig.3.

### MODIFICATION OF THE G-CRITERION

The original Maximum Strain Energy Release Rate Criterion (G-criterion) states that: (1). The propagation of a crack tip is in the direction which maximizes the strain energy release rate (G-value), i.e.,  $G(\theta = \theta_0) = G_{max}$ , (2). When the maximum strain energy release rate ( $G_{max}$ ) is equal to or greater than the critical value ( $G_c$ ), i.e.,  $G_{max} \geq G_c$ , the crack tip starts to propagate.

If we define the strain energy release rate due to Mode I deformation at a crack tip as  $G_I$  and that due to Mode II deformation as  $G_{II}$ , the resultant strain energy release rate is then equal to the sum of two parts,  $G = G_I + G_{II}$ .  $G_I$  and  $G_{II}$  can be easily obtained by using the DDM if we restrict the normal or shear displacement of the "fictitious" element to zero. The G-criterion is applicable for predicting crack propagation subjected to tension but not applicable when the crack is subjected to compression. This is demonstrated by the following two cases.

#### 1. An inclined crack subjected to tension.

The geometry of the crack is shown in Fig.4a. The crack is evenly divided into 20 constant displacement discontinuity elements. A 'fictitious' element



(Fig.4a) is added to one tip of the crack to simulate its propagation. The 'fictitious' element can be rotated and therefore at any direction the G-value can be calculated. In the numerical calculations a very high normal stiffness ( $K_n = 10^{18} \text{Pa/m}$ ) is applied to the 'fictitious' element to prevent a numerical overlap of the crack surfaces. The G-value varies with the angle  $\theta$  (Fig.4b). Comparing the results from different methods, the maximum G-value ( $G_{\max}$ ) and its direction ( $\theta_0$ ) vary slightly:

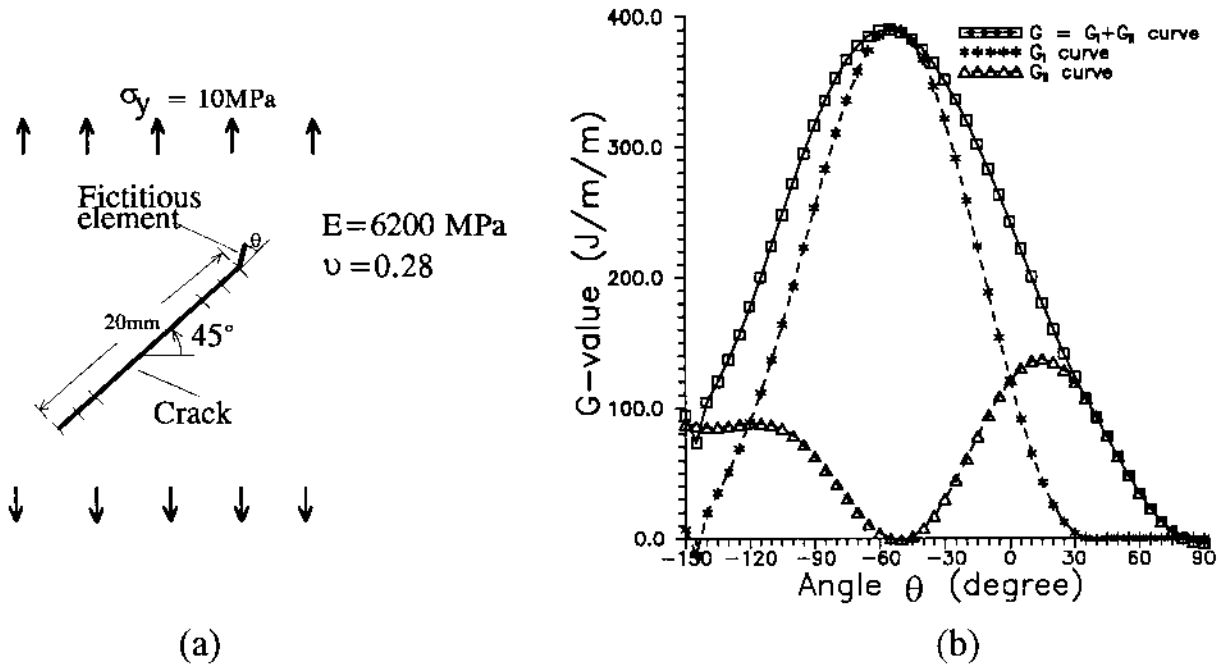


Fig.4. Calculation of strain energy release rate,  $G$ , of an inclined crack subjected to tension. (a) Geometry of the crack and the loading condition; (b)  $G$ -value versus direction  $\theta$  calculated by DDM.

DDM (this study)	$G_{\max} = 390 \text{J/m}^2$	$\theta_0 = -55^\circ$
Maximum Tensile Stress Criterion[7] <sup>§</sup>	$G_{\max} = 390 \text{J/m}^2$	$\theta_0 = -57^\circ$
Hussain's formula[8]	$G_{\max} = 475 \text{J/m}^2$	$\theta_0 = -60^\circ$
Melin's results crack kink [9]	$G_{\max} = 384 \text{J/m}^2$	$\theta_0 = -55^\circ$

The results obtained by using the DDM are in a good agreement with those predict by the Maximum Tensile Stress Criterion and Melin's results but in somewhat less agreement compared with Hussian's formula.

<sup>§</sup> [7] gives the equivalent stress intensity factor  $K_{Ie} : K_u = K_I \cos^3(\theta/2) - 3K_{II} \cos^2(\theta/2) \sin(\theta/2)$

The G-value then can be obtained by using the relation  $G = \frac{(1-\nu^2)}{E} K_u^2$

When a crack is subjected to tension, the  $G_I$ -curve is dominant in the resultant  $G$ -curve, and therefore the peak  $G$ -value will coincide with the peak  $G_I$  value (Fig.4b). In this case the  $G$ -criterion will give a good prediction of the crack propagation.

2. An inclined crack subjected to compression.

The same geometry is used but a compressive far-field stress is applied (Fig.5a). We assume that the crack is a flaw without surface contact. The  $G(\theta)$  is calculated using the same method as described above. The  $G$ -value varies with direction (Fig.5b). The  $G$ -value does not have a peak for the expected propagation of the tensile crack (direction  $\theta \approx 90^\circ$ ) but has a maximum value in a direction which corresponds to the maximum shearing ( $\theta \approx 15^\circ$ ). The dominant  $G_{II}$ -curve predicts that Mode II propagation will occur first. Normally, Mode I propagation always occurred first in laboratory experiments. The explanation for this contradiction is thought to be due to the difference between the Mode I and Mode II toughness for energy ( $G_{IC}$  and  $G_{IIC}$ )

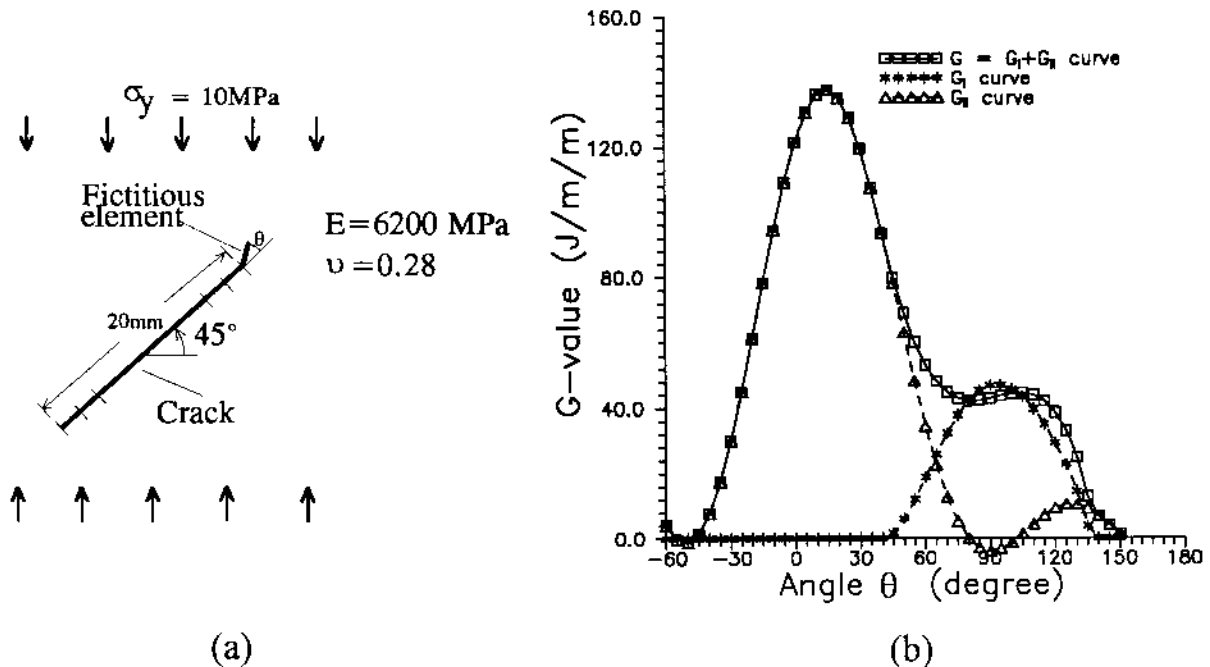


Fig.5. Calculation of strain energy release rate,  $G$ , of an inclined crack subjected to compression. (a) Geometry of the crack and the loading condition; (b)  $G$ -value versus direction  $\theta$  calculated by DDM.

It has been recognized that  $G_{IIC}$  is normally much higher than  $G_{IC}$  due to the difference of failure mechanism[17], e.g. for rocks  $G_{IIC} > 10^2 G_{IC}$ . The

difference between  $G_{IC}$  and  $G_{IIc}$  implies that, even though the G-value has a maximum value in Mode II failure direction, the real propagation may not take place in Mode II but in Mode I, because the Mode I failure condition may be satisfied earlier than that of Mode II. However, due to the equal-weight given to  $G_I$  and  $G_{II}$  in the resultant G-value, Mode I failure can not be determined from the G-curve. This shortcoming has led us to modify the original G-criterion.

We consider a new parameter  $F(\theta)$ ,

$$F(\theta) = \frac{G_I(\theta)}{G_{Ic}} + \frac{G_{II}(\theta)}{G_{IIc}} \quad (17)$$

as the factor that controls the propagation of a crack tip. When the following conditions are satisfied:

$$F(\theta = \theta_0) = \text{maximum, and} \quad (18)$$

$$F(\theta_0) \geq 1 \quad (19)$$

the crack starts to propagation in the direction  $\theta = \theta_0$ . We name the above criterion based on the factor  $F$  as  $F$ -criterion. When  $G_{IC}$  is equal to  $G_{IIc}$ , the  $F$ -criterion is equivalent to the original G-criterion.

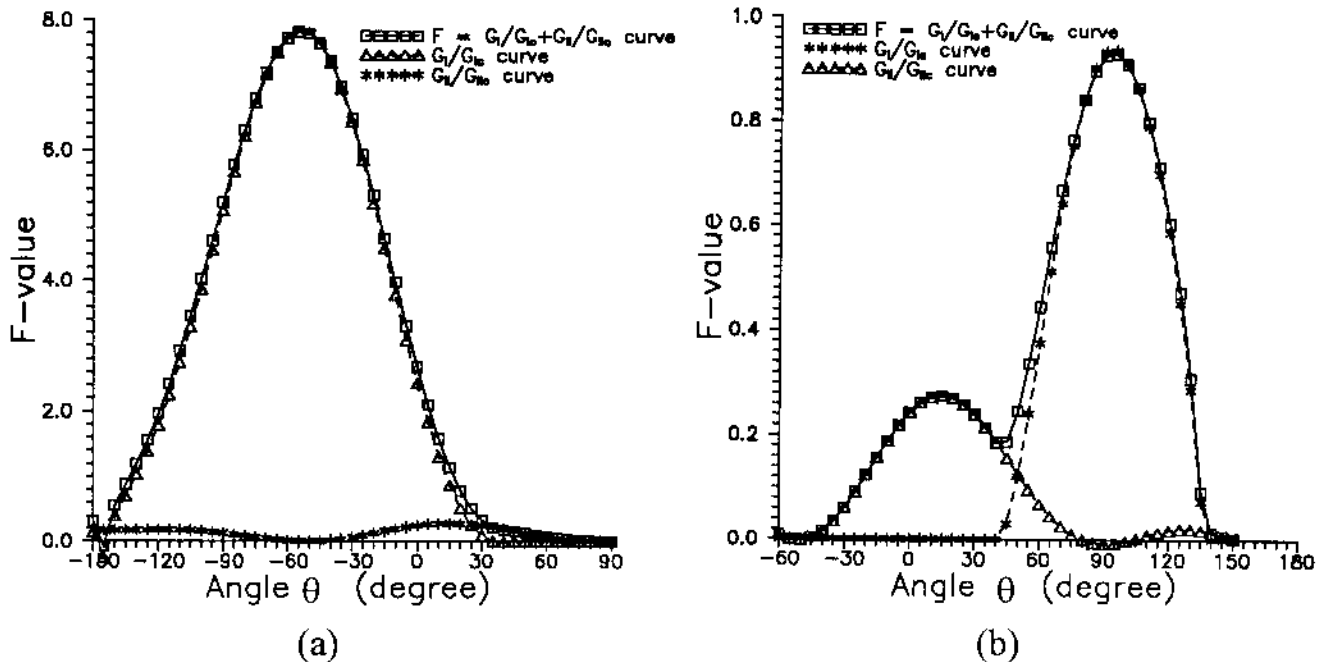


Fig.6.  $F$ -value ( $F = G_I/G_{Ic} + G_{II}/G_{IIc}$ ) versus direction  $\theta$  at the crack tip with the geometry shown in Fig.5a and the assumption that  $G_{Ic} = 50 \text{ J/m}^2$  and  $G_{IIc} = 500 \text{ J/m}^2$ . (a) Uniaxial tension; (b) uniaxial compression.

Applying the F-criterion to the problems shown in Fig.4a and Fig.5a with the assumption that  $G_{IC} = 50 \text{ J/m}^2$  and  $G_{IIC} = 500 \text{ J/m}^2$ , we obtain the F-curves (Fig.6). For a crack subjected to tension the F-criterion predicts same results as the G-criterion (Fig.6a). However, for a crack subjected to compression the F-criterion predicts that the Mode I crack propagation will occur first (Fig.6b). A local maximum of the F-value exists in the direction of the Mode II failure. If the local maximum becomes the global maximum for a certain loading condition, then the crack tends to propagate in Mode II. Hence, the F-criterion is able to predict the observed Mode I and II crack propagation which is not expressed by the G-criterion.

### NUMERICAL DETERMINATION OF $F_{\max}$ AND $\theta_0$

The maximum F-value and its direction  $\theta_0$  need to satisfy the conditions:

$$\frac{dF}{d\theta} = 0 \quad (20)$$

$$\frac{d^2F}{d\theta^2} < 0 \quad (21)$$

Equation (20) can be solved by applying the Newton-Raphson iteration method,

$$\left( \frac{d}{d\theta^i} \frac{dF^i}{d\theta^i} \right) \delta\theta = - \frac{dF^i}{d\theta^i} \quad (22)$$

where  $i$  is the iteration step and  $\delta\theta$  is the increment of  $\theta$ . In the next iteration step ( $i+1$ ), the value of  $\theta$  becomes

$$\theta^{i+1} = \theta^i + \delta\theta. \quad (23)$$

When the  $\delta\theta$  value is satisfactorily small for an iteration step, the correspondent  $\theta$ -value is then the approximate direction of the maximum F-value.

To apply the Newton-Raphson iteration method, we need to calculate both the first and the second order derivative of  $F(\theta)$ . They can be estimated by:

$$\frac{dF}{d\theta} \approx \frac{F(\theta + \Delta\theta) - F(\theta - \Delta\theta)}{2\Delta\theta} \quad (24)$$

$$\frac{d^2F}{d\theta^2} \approx \frac{F(\theta + \Delta\theta) - 2F(\theta) + F(\theta - \Delta\theta)}{\Delta\theta^2} \quad (25)$$

where  $\Delta\theta$  is a small increment of the rotation angle  $\theta$ ;  $F(\theta - \Delta\theta)$ ,  $F(\theta)$  and  $F(\theta + \Delta\theta)$  are the F-values for a crack that has grown with an unit length in the directions  $\theta -$

$\Delta\theta$ ,  $\theta$  and  $\theta+\Delta\theta$ , respectively. The F-values can be determined by applying DDM and eqs.(15), (16) and (17).

There are often two maxima (Fig.6b), one for Mode I failure and another for Mode II failure, which are usually  $90^\circ$  apart. Hence, after obtaining one maximum F-direction  $\theta_0$  we can add (or subtract)  $90^\circ$  to determine the other maximum F-direction. By comparing the F-values in these two directions, the mode of failure can then be determined.

## RESULTS

The following two examples are designed to simulate, by using the F-criterion, the tensile and shear crack propagation observed in laboratory experiments: example No.1 for the tensile and shear failure from a single crack and example No.2 for the coalescence between two cracks. In both these examples we assume that the existing cracks are flaws without surface contact, and that the initiated cracks have very-high normal stiffness and a zero friction angle, which means that only open and sliding displacement are allowed.

*Example No.1, propagation of an inclined crack subjected to compression.*

An inclined crack in an infinite elastic body is subjected to uniaxial compression. The crack has the length of 1.0 cm and is inclined  $45^\circ$  from the loading direction. The mechanical properties of the medium are taken as follows:

Young's modulus,  $E = 6200 \text{ MPa}$

Poisson's ratio,  $\nu = 0.28$

Mode I crack toughness,  $G_{Ic} = 50 \text{ J/m}^2$

Mode II crack toughness,  $G_{IIc} = 500 \text{ J/m}^2$ .

The Mode I and Mode II crack propagation from the existing crack tips is predicted by the F versus  $\theta$  plot (Fig.7). When the compressive stress is less than 15MPa, there exist two maxima in the F- $\theta$  plot: one associated with the potential tensile failure which is approximately perpendicular to the pre-existing crack, and one associated with the potential shear failure in the same direction of the pre-existing crack. When the compressive stress exceeds 15MPa the F-value in the direction of potential tensile failure will be the first to satisfy the

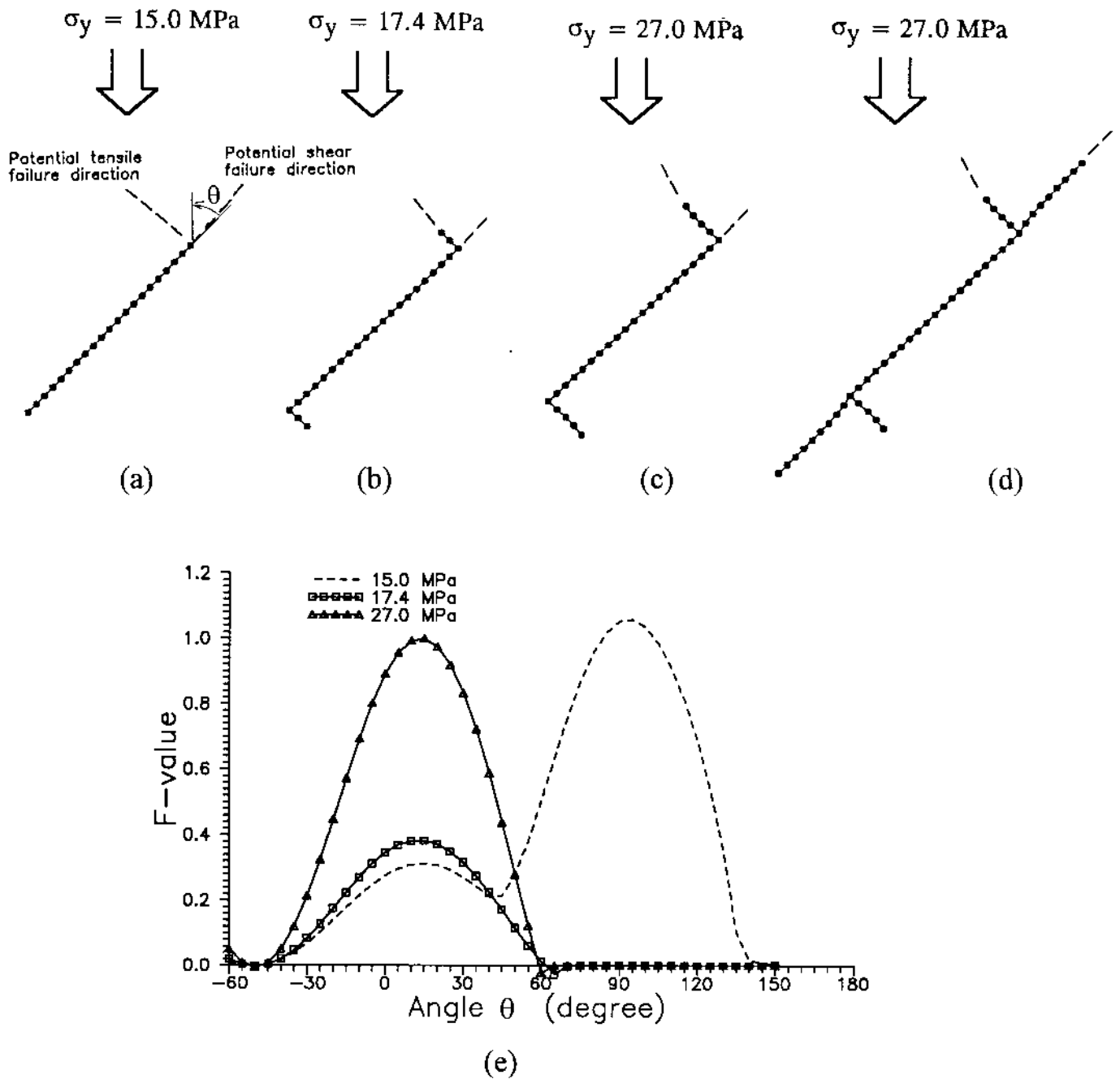


Fig.7. Stages of crack propagation in uniaxial compression and corresponding  $F$ - $\theta$  curves. (a) Initial state; (b) and (c) tensile cracks are initiated and propagate; (d) shear cracks develop and the tensile cracks stop; and (e) curves of  $F$  versus  $\theta$  at the up-right tip of the inclined crack for stages (a), (b) and (c).

propagation criterion,  $F_{\max} \geq 1.0$ , and therefore Mode I propagation will occur. This will result in the release of tensile stress at the crack tip and therefore the maximum  $F$ -value due to tension will disappear. The tensile crack has minor influence on the shear stress and the maximum  $F$ -value due to shearing will still exist. In order to maintain Mode I propagation, the load must be constantly increased. With increasing load, the maximum  $F$ -value in the direction of maximum shearing will also be increased. When it satisfies the criterion  $F_{\max} \geq$

1.0 at the stress level of 27MPa, Mode II propagation will be initiated in the direction of the initial crack. This simulated mixed Mode I and II propagation process, by using the F-criterion and the numerical method DDM, is consistent with the actual observations in laboratory experiments (Fig.1).

*Example No.2, coalescence of two inclined cracks in compression.*

Coalescence between non-overlapping cracks was recently observed by Reyes & Einstein [3] in gypsum specimens. One typical specimen after the crack coalescence is shown in Fig.8. When the tensile and shear fracture toughness are assumed to be:  $G_{Ic} = 30\text{J/m}^2$  and  $G_{IIc} = 550\text{J/m}^2$ , then the F-criterion simulation predicts the same propagation process observed in the laboratory experiment. The followings are the experimental failure process described by Reyes & Einstein, which are compared with the numerically predicted results shown in Fig.9.

1. When the uniaxial loading reaches 11.2 MPa, tensile cracks were first observed at the tips of existing cracks. (compared with Fig.9b)

2. With an increasing load, the tensile cracks grew. When the loading reaches 24.1 MPa, a sudden coalescence between the two inner existing crack tips occurs. (compared with Fig.9d,e,f)

3. After coalescence, the tensile cracks which had initiated at the outer tips extend to the boundary of the specimen (the specimen length =  $9 \times$  crack length). The cracks from the inner tips were closed and had no further propagation. (compared with Fig.9f)

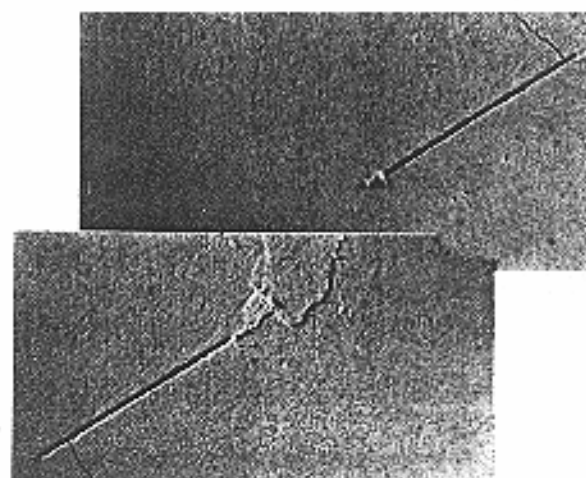


*Fig.8. Coalescence of two cracks of a gypsum model due to uniaxial compression. The closed inner tensile cracks can not be observed after coalescence. From Reyes and Einstein, 1991 [3].*

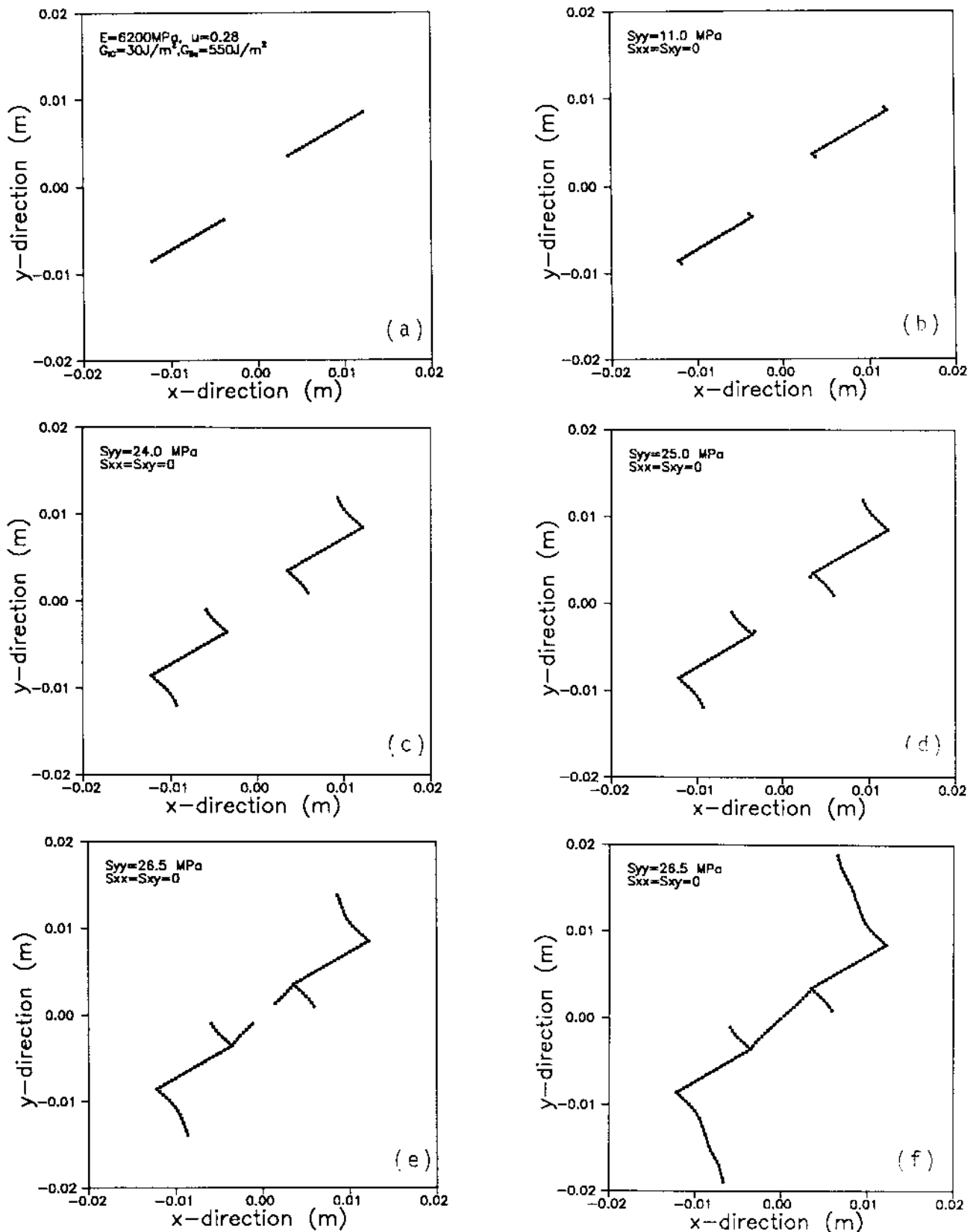


*Fig.9. Simulation of propagation and coalescence of two non-overlapping cracks subjected to uniaxial compression. (a) Initial state; (b) tensile crack initiation; (c) tensile crack propagation; (d) and (e) shear crack initiation and propagation and tensile cracks extension; (f) crack coalescence at 26.5 MPa and resulted tensile crack extension.*



## CONCLUSIONS

- (1) Cracks subjected to compression in brittle materials can propagate in Mode I and Mode II. The previously existing criteria could not predict certain aspects of the mixed Mode I and II crack propagation.
- (2) The F-criterion proposed in this paper, which uses the normalized strain energy release rate for Mode I and Mode II deformations, can successfully predict both Mode I and Mode II crack propagation. The predicted Mode I and Mode II propagation process is consistent with the experimental results observed in rock and gypsum models.
- (3) Implemented into DDM, the F-criterion has great potential for studies of the strengths of fractured rock masses, especially the stability of fractured rock slopes.

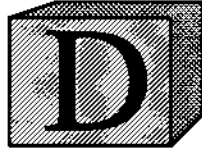
**Acknowledgments** — This study is part of the Sino-Swedish Research Cooperation on Metallic Materials and Mining and supported by the Swedish National Board for Industrial and Technical Development. The authors are thankful to H.H. Einstein for providing experimental data and for encouraging discussions. Valuable comments by J. Fernlund, F. Nilsson, E. Johnson and S. Melin are gratefully acknowledged.

## REFERENCES

- [1] A. Ingraffea and F. Heuze, Finite element models for rock fracture mechanics. *Int. J. Numerical and Analytical Method in Geomechanics*, **4**, 24-43 (1980).
- [2] J.-P. Petit and M. Barquins, Can natural faults propagate under mode II conditions? *Tectonics*, **7(6)**, 1243-1256 (1988).
- [3] O. Reyes and H.H. Einstein, Failure mechanisms of fractured rock — A fracture coalescence model. *Proc. 7th Int. Con. on Rock Mechanics*, **1**, 333-340 (1991).
- [4] F. Eordgan and G. C. Sih, On the crack extension in plates under plane loading and transverse shear. *ASME J. Bas. Engng* **85**, 519-527 (1963).

- [5] G. C. Sih, Strain-energy-density factor applied to mixed mode crack problems. *Int. J. Crack.* **10(3)**, 305-321 (1974).
- [6] K. Hellan, *Introduction to fracture mechanics*. McGraw-Hill International Editions, Singapore (1984).
- [7] B. Shen and O. Stephansson, Deformation and propagation of finite joints in rock masses. *Proc. Int. Con. Fractured and Jointed Rock Masses* (1992). (in press)
- [8] M. A. Hussain, S. L. Pu and J. Underwood, Strain energy release rate for a crack under combined mode I and mode II. *Fracture Analysis, ASTM-STP. 560*, 2-28. Am. Soc. Testing Materials, Philadelphia (1974).
- [9] S. Melin, The infinitesimal kink. Report LUTFD2/(TFHF-3022)/1-19/(1985). (Division of Solid Mechanics, Lund Institute of Technology, Lund.)
- [10] W. T. Chiang, Fracture criteria for combined mode cracks. *Fracture, ICP4*, Waterloo, Canada, **4**, 135-154 (1977).
- [11] W. W. El-Tahan, G. H. Staab, S. H. Advani and J. K. Lee, A mixed mode local symmetric fracture criterion for geo-materials. *Proc. 32th U.S. Symp. Rock Mechanics*. 455-462 (1990).
- [12] S. L. Crouch and A. M. Starfield, *Boundary element methods in solid mechanics*. George Allen & Unwin, London (1983).
- [13] R. A. Schultz, Stress intensity factors for curved cracks obtained with the displacement discontinuity method. *Int. J. Fracture*, **37**, R31-34 (1988).
- [14] H. Guo, N. I. Aziz and L. C. Schmidt, Linear elastic crack tip modelling by the displacement discontinuity method. *Engineering Fracture Mechanics*, **36(6)**, 933-943 (1990).
- [15] C. Scavia, A numerical technique for the analysis of cracks subjected to normal compressive stresses. *Int. J. Numerical Methods in Engineering*, **33**, 919-942 (1992).
- [16] B.H.G. Brady and E.T. Brown, *Rock mechanics for underground mining*. George Allen & Unwin, London. (1985)
- [17] V. C. Li, Mechanics of shear rupture applied to earthquake zones. *Fracture mechanics of rock (ed. B.K. Atkinson)*. Academic Press, London, 351-428.(1991).





# **Numerical analysis of Mode I and Mode II propagation of rock fractures**

*B. Shen and O. Stephansson*

*Int. J. Rock Mech. Min. Sci. (special issue for the 34th U.S. Symposium on rock  
mechanics) (in press) (1993).*

# Numerical Analysis of Mixed Mode I and Mode II Fracture Propagation

B. Shen  
O. Stephansson

Engineering Geology, The Royal Institute of Technology, Stockholm, Sweden.

## Abstract

Previous experiments have shown that both Mode I and Mode II fracture propagation can occur when a fracture in brittle material such as rock is subjected to compression. In this paper, the mixed mode fracture propagation has been successfully simulated with a new numerical approach using the Displacement Discontinuity Method (DDM) and a fracture criterion based on  $G_{Ic}$  and  $G_{IIc}$ . The experimental results of fracture coalescence observed by Reyes and Einstein are simulated using this new approach. Both the coalescing paths and critical loads in the simulation are similar to the experimental results. The new approach has also been used to study the influence of loading conditions and material properties on the propagation mode. Low Mode II fracture toughness and high confining stress are shown to favor Mode II fracture propagation.

## INTRODUCTION

In two dimensions, Mode I and Mode II are the two basic modes of fracture propagation. However, Mode II propagation is to a lesser extent discussed in the literature than Mode I propagation. The main reason for this is that Mode II fracture propagation has rarely been observed in laboratory experiments in most engineering materials such as steel, glass, ceramics, etc. However, the recent experiments conducted on rocks or similar materials, such as concrete and gypsum, show that Mode II propagation does occur [1-6]. Lajtai [1] observed two types of shear fractures after the occurrence of tensile fractures during uniaxial tests on pre-fractured plaster-of-paris specimens: the inclined shear fractures and the normal shear fractures. Later Petit and Barquins [2] obtained shear fractures in sandstone specimens in uniaxial tests, which are similar to the

inclined shear fractures in Lajtai's experiments. Reyes [3] and Reyes and Einstein [4] observed coalescence between two non-overlapping flaws in gypsum specimens. A microscopic examination of the surface of coalescence indicated that both Mode I and Mode II failure type were involved in the process. When the two parallel flaws have a small offset, coalescence seems to be dominated by shearing. Furthermore, in shear tests of double-edge notched beams of concrete, granite and sandstone, shear failure occurred between the notches (Bazant and Pffeifer [5], Jung et al [6]).

The above observations have recently brought special interest to the study of the mixed Mode I and Mode II propagation. The classical criteria in macro-mechanic fracture mechanics can predict Mode I propagation and mixed mode propagation dominated by Mode I, but they can not be directly applied to Mode II and Mode II dominated propagation. In an attempt to overcome this problem, Reyes [3] has successfully used a damage mechanics approach with a strain-based damage criterion to predict the coalescence of two flaws. Another attempt to simulate the mixed Mode I and Mode II problem was made in the macro-approach by Shen and Stephansson [7]. They proposed a new form of the strain energy release rate criterion, namely the F-criterion which considers both the Mode I and Mode II fracture toughness, which will be used in this paper.

This paper will first describe the F-criterion and the announced numerical technique. The F-criterion approach is then used to simulate the experiments conducted by Reyes [3]. The influence of the fracture toughness ratio ( $G_{IIc}/G_{Ic}$ ), the applied stress ratio ( $\sigma_3/\sigma_1$ ) and some other factors related to the change of the propagation mode will also be investigated.

## THE F-CRITERION

The fracture criteria in the macro-approach can be classified into two groups: the principal stress (strain)-based criteria and the energy-based criteria. The first group consists of the Maximum Principal Stress Criterion [8] and the Maximum Principal Strain Criterion [9]; the second group includes the Maximum Strain Energy Release Rate Criterion (G-criterion) [10] and the Minimum Strain Energy Density Criterion (S-criterion) [11]. The principal stress (strain) -based criteria are only applicable to Mode I or Mode I dominated mixed mode fracture propagation which relies on the principal tensile stress (strain). To be applicable

to the Mode II propagation, the fracture criterion has to consider the shear stress (strain) and not only the principal stress (strain). From this point of view, the energy based criteria seem applicable to both Mode I and Mode II propagation because the strain energy in the vicinity of a fracture tip is related to all the components of stress and strain.

Both the G-criterion and the S-criterion have been tested for Mode I and Mode II propagation, and neither of them is directly suitable. This study has concentrated on trying to improve the G-criterion. The original G-criterion states that when the strain energy release rate in its maximum direction reaches the critical value  $G_C$  then the fracture tip will propagate in that direction. It does not distinguish between Mode I and Mode II fracture toughness of energy ( $G_{IC}$  and  $G_{IIC}$ ). In fact, for a certain material, the Mode II fracture toughness is much higher than the Mode I toughness due to the differences in the failure mechanism. In rocks, for instance,  $G_{IIC}$  is found in laboratory scale to be at least two orders of magnitude higher than  $G_{IC}$  [12]. Applied to the mixed mode fracture propagation, the G-criterion is difficult to use since the critical value  $G_C$  must be carefully chosen between  $G_{IC}$  and  $G_{IIC}$ .

In our previous study [7] we proposed the F-criterion to simulate the mixed-mode fracture propagation. The F-criterion divides the resultant strain energy release rate ( $G$ ) at a fracture tip into two parts, one due to Mode I deformation ( $G_I$ ) and one due to Mode II deformation ( $G_{II}$ ). Then the sum of their normalized values is used to determine the failure load and its direction.  $G_I$  and  $G_{II}$  can be expressed as follows (Fig.1): if a fracture grows an unit length in an arbitrary direction and the new fracture opens without any surface dislocation, the strain energy loss in the surrounding body due to the fracture growth is  $G_I$ . If the new fracture has only a surface dislocation, the strain energy loss is  $G_{II}$ . The principle of the F-criterion can be stated as follows:

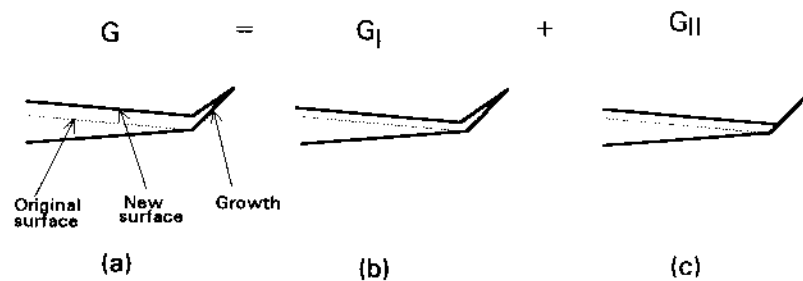


Fig.1. Definition of  $G_I$  and  $G_{II}$  for fracture growth. (a)  $G$ , the growth has opening and dislocation; (b)  $G_I$ , the growth has only opening; (c)  $G_{II}$ , the growth has only dislocation.

1. In an arbitrary direction ( $\theta$ ) at a fracture tip there exists a F-value, with that

$$F(\theta) = \frac{G_I(\theta)}{G_{Ic}} + \frac{G_{II}(\theta)}{G_{IIc}}. \quad (1)$$

2. The possible direction of propagation of the fracture tip is the direction for which the F-value reaches its maximum.

$$F(\theta) \Big|_{\theta=\theta_0} = \max. \quad (2)$$

3. When the maximum F-value is equal to or larger than 1.0, then the fracture tip will propagate, i.e.

$$F(\theta) \Big|_{\theta=\theta_0} \geq 1.0 \quad (3)$$

The F-criterion can be used to predict both the Mode I and Mode II failure of a fracture tip. An application of this criterion to the mixed mode fracture propagation where an inclined fracture is subjected to uniaxial compression is demonstrated in Fig.2. Before failure at one tip of the fracture there exist two maximum F-values (Fig.2e). One is about in the direction of the existing fracture plane and is due to shearing and the other is directed at  $90^\circ$  away from the existing fracture and is due to tension. The F-value in the direction of maximum tension at the tip reaches condition (3), therefore, Mode I fracture propagation occurs (Fig.2b). Failure in the direction of maximum tension has little influence on the existing shear stress at the tip. The maximum F-value in the shearing direction still exists. With increased load, the F-value in the shear direction increases and when it finally satisfies condition (3) shear failure occurs (Fig.2c,d). The shear failure development as demonstrated in this example, is similar to the inclined shear fracture of Lajtai [1], the shear fracture of Petit and Barquins [2], and the coalescing fracture (or secondary fracture as it was called) of Reyes [3]. The sequence of failure process is also similar to the experimental observations, namely that the tensile fracture appears first and is followed by shear fracture.

The F-criterion is actually a special form of the G-criterion which allows us to consider Mode I and Mode II propagation simultaneously. In most cases, the F-value reaches its peak either in the direction of maximum tension ( $G_{Ic} = \text{maximum while } G_{IIc}=0$ ) or in the direction of maximum shearing ( $G_{IIc} = \text{maximum while } G_{Ic}=0$ ).



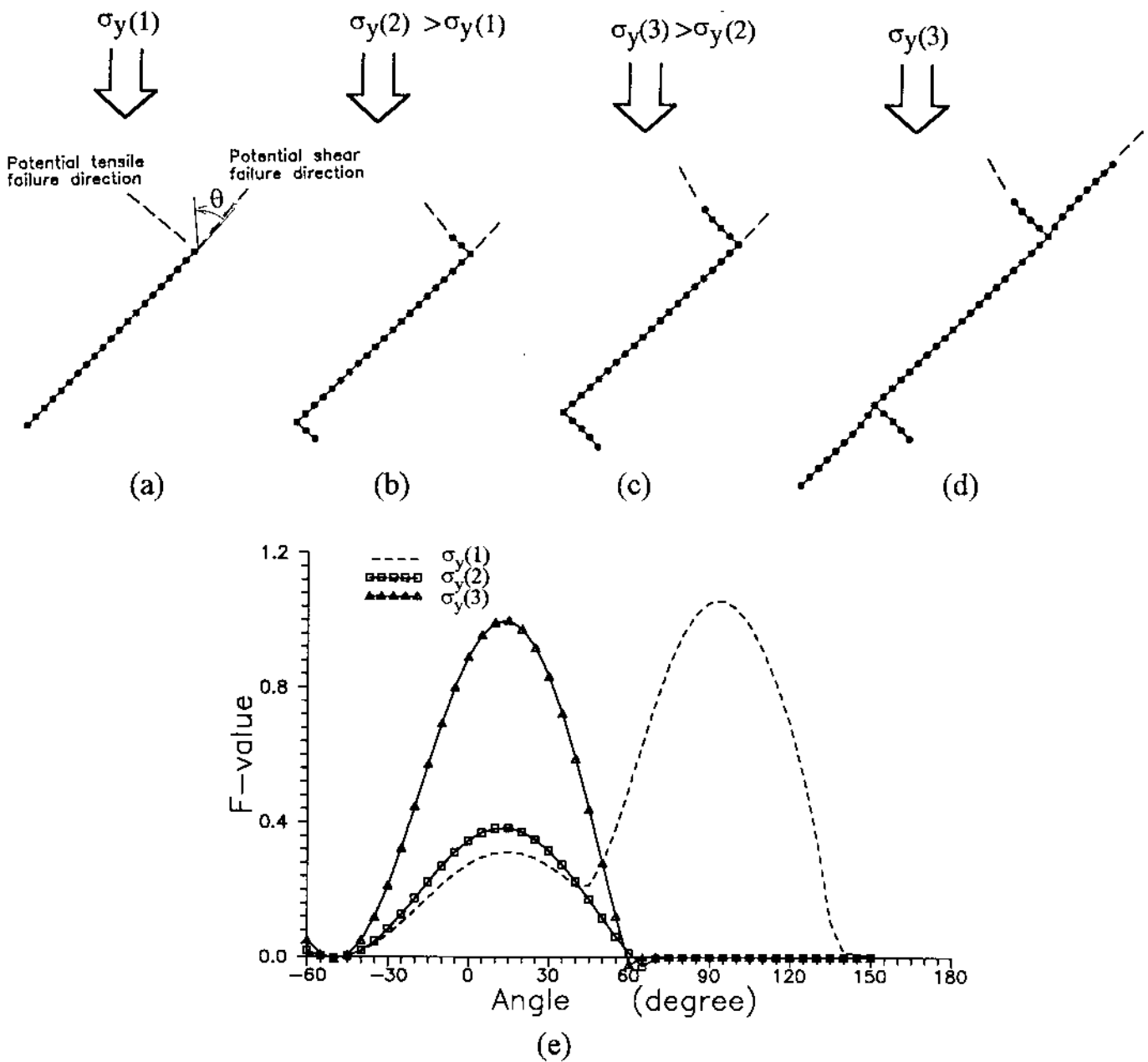


Fig.2. Process of fracture Mode I and Mode II propagation in uniaxial compression and corresponding  $F-\theta$  curves. (a) Initial state; (b) and (c) tensile fractures are initiated and propagate; (d) shear fractures develop and tensile fractures stop; and (e) curves of  $F$ -value versus  $\theta$  at a tip of the inclined fracture in stages (a), (b) and (c).

## THE NUMERICAL TECHNIQUE TO APPLY THE F-CRITERION

### 1. Determination of $G_I$ and $G_{II}$ .

The most difficult step in using the  $F$ -criterion is the computation of  $G_I$  and  $G_{II}$  in an arbitrary direction at a fracture tip. This a computation is almost

impossible when using analytical methods. Therefore a numerical method had to be applied. In the example shown in Fig.2, we have applied the Displacement Discontinuity Method (DDM) [13] to calculate the  $G_I$  and  $G_{II}$  in an arbitrary direction. The DDM has two main advantages when dealing with fractures and fracture propagation: *i)*, it directly simulates the fractures with the displacement discontinuity elements, and the two surfaces of a fracture need not be simulated separately; *ii)*, when a fracture is propagating, a re-meshing process near the fracture tip is not required. By using the DDM we can also easily handle the contact and friction between the fracture surfaces. For surface contact we introduce fracture stiffness into the DDM's coefficient matrix. For friction we apply to each element a friction force, which is related to the normal stress and friction angle of the fracture. An alternative method to handle friction, the iteration method developed by Crouch [13], is also applicable but it requires more computation time.

When using the DDM we can estimate the strain energy release rate in the following way:

(a). calculate the strain energy  $W(a)$  of a given fracture system by applying the Clapeyron's strain energy theory. It states that when an elastic body is in equilibrium, the strain energy due to deformation is equal to one half of the work caused by the external forces, acting through the displacement from the unstressed state to the state of equilibrium.

$$W(a) = \frac{1}{2} \sum_{i=1}^m a^i (\sigma_s^i D_s^i + \sigma_n^i D_n^i) \quad (4)$$

where  $m$  is the total number of displacement discontinuity elements,  $a^i$  is the length of  $i$ th element,  $\sigma_s^i, \sigma_n^i$  are the shear and normal stresses on  $i$ th element, and  $D_s^i, D_n^i$  are the shear and normal displacement discontinuities of the  $i$ th element.

(b). introduce a small "fictitious" element with length  $\Delta a$  to a fracture tip in a direction  $\theta$  (Fig.3) to simulate the possible fracture propagation. Re-calculate the stresses and displacement discontinuities of the fracture system with this "fictitious" element. Using eq.(4) the strain energy  $W(a+\Delta a)$  after the fracture propagation  $\Delta a$  can be obtained.

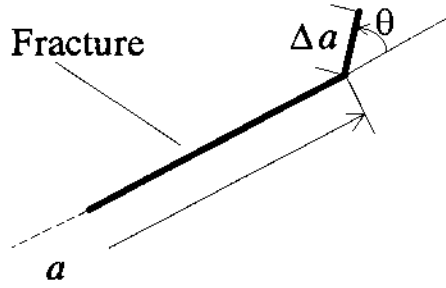


Fig.3. Fictitious fracture increment  $\Delta a$  in direction  $\theta$  with respect to the initial fracture orientation.

(c). estimate the strain energy release rate  $G$ ,

$$G = \frac{\partial W}{\partial a} \approx \frac{W(a + \Delta a) - W(a)}{\Delta a} \quad (5)$$

If we restrict the shear displacement discontinuity of the "fictitious" element to zero,  $G_I$  can be obtained. If the normal displacement discontinuity is set at zero, then  $G_{II}$  can be obtained.

## 2. Determination of the magnitude and direction of the maximum $F$ -value

If  $G_I$  and  $G_{II}$  at the crack tip are known for a certain direction, then the  $F$ -value can be calculated by eq.(1). However, calculating the  $F$ -value in all possible directions would be very time consuming. Therefore the Newton-Raphson iteration technique is used, i.e.,

$$\left( \frac{d}{d\theta} \frac{dF^i}{d\theta} \right) \delta\theta = - \frac{dF^i}{d\theta} \quad (6)$$

$$\theta^{+1} = \theta + \delta\theta \quad (7)$$

where  $i$  is the iteration step and  $\delta\theta$  is the increment of  $\theta$ . To apply this technique it is necessary to determine the first and second order derivatives of the  $F$ -value

regarding the direction  $\theta$ , i.e.,  $\frac{dF}{d\theta}$ ,  $\frac{d^2F}{d\theta^2}$ . This is done numerically.

Normally there are two maximum  $F$ -values in two different directions, one for the Mode I failure and the other for the Mode II failure. Both of them need to be determined. Therefore, to find the two maximum  $F$ -values the Newton-Raphson technique has to be used twice with different initial  $\theta$ -value. Caution is needed in defining the two initial  $\theta$ -values.

## SIMULATION OF FRACTURE COALESCENCE WITH THE F-CRITERION APPROACH

Recently, Reyes [3] and Reyes and Einstein [4] performed laboratory experiments to study fracture coalescence. They used gypsum specimens and observed the coalescence of non-overlapping fractures during uniaxial compression test. The dimensions of the gypsum specimen were: height×width×thickness =152.4×76.2×30 mm. The original fractures (flaws) were 12.7 mm long and arranged in the central part of the specimen. The resulting coalescence was due to the growth of secondary fractures.

In this study the numerical technique based on the F-criterion is used to simulate the experimental results. A comparison is made between the experimental and simulated results as well with those from the strain-based damage approach presented by Reyes [3]. Two examples are described:

a). *A specimen containing two offset open flaws (flaw inclination =30°, the inclination of a rock bridge between the two flaws =45°, namely specimen 30°-45° in Reyes [3]).*

With this flaw geometry, coalescence occurred during the experiment (Fig.4). The failure process was described by Reyes [3] as follows: when a compressive stress of 11.2 MPa was exerted tensile fractures near the flaw tips appeared and they were extended as the load was increased. When the compressive stress reached 24.1 MPa there was a sudden coalescence between the two inner flaw tips. Meanwhile, the outer tensile fracture extended to the boundaries of the specimen and the inner tensile fractures were closed.

This failure process was reproduced numerically by using our numerical technique with the F-criterion. The process of failure was the same as the one observed in the experiment (Fig.5). In this simulation, we assume that the two pre-existing fractures exist in an infinite body. The two pre-existing fractures are assigned zero normal and shear stiffness so that the stress free condition on the flaw surfaces during the experiment can be properly modelled. The stiffness and friction angle of the propagating shear fracture are difficult to determine. Therefore, the following assumption is made:  $K_n=100\text{GPa/m}$ ,  $K_s=10\text{GPa/m}$  and  $\phi=45^\circ$ . Results of several computations proved that changes of the stiffness and friction angle of the propagating shear fracture have a certain influence on the

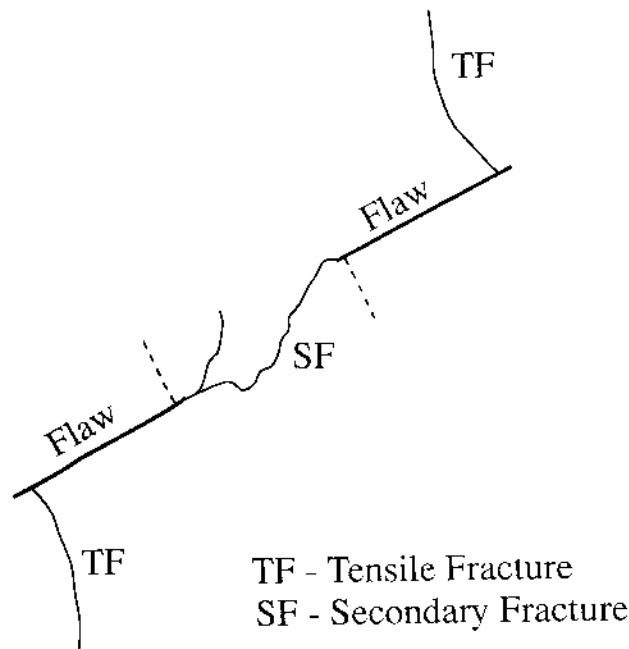


*Fig.4. Experimentally observed tensile fractures and secondary fracture after coalescence between the 30°-45° flaws. Inner tensile fractures (dash lines) were closed and invisible. The path of the secondary fracture within the specimen may be slightly different from its trace on the specimen surface. Applied stress is 24.1 MPa. After Reyes[3].*

path of coalescence but have minor influence on the critical load at coalescence. In this modelling we have also determined  $G_{IC}$  and  $G_{IIc}$  of the model material based on the experimentally observed critical loads when the tensile fractures and coalescence appeared, namely  $G_{IC}=30 \text{ J/m}^2$  and  $G_{IIc}=550\text{J/m}^2$ . These values are also used for other specimens in our numerical modelling.

*b). A specimen containing two non-offset open flaws (flaw inclination = 30°, the inclination of rock bridge = 30°, namely specimen 30°-30°).*

Flaws with this geometry did not coalesce in the experiment (Fig.6). Secondary fractures appeared but did not connect with each other. Applying to this flaw geometry the numerical technique with the F-criterion predicts similar paths of both tensile fractures and secondary fractures (Fig.7).

The numerical technique with the F-criterion has also been applied to two other experimental specimens with different flaw geometries. The toughness values used were those obtained from the 30°-45° specimen:  $G_{IC}=30 \text{ J/m}^2$  and  $G_{IIc}=550\text{J/m}^2$ . The critical loads predicted by the F-criterion approach are fairly close to the experimental results, see Table 1.

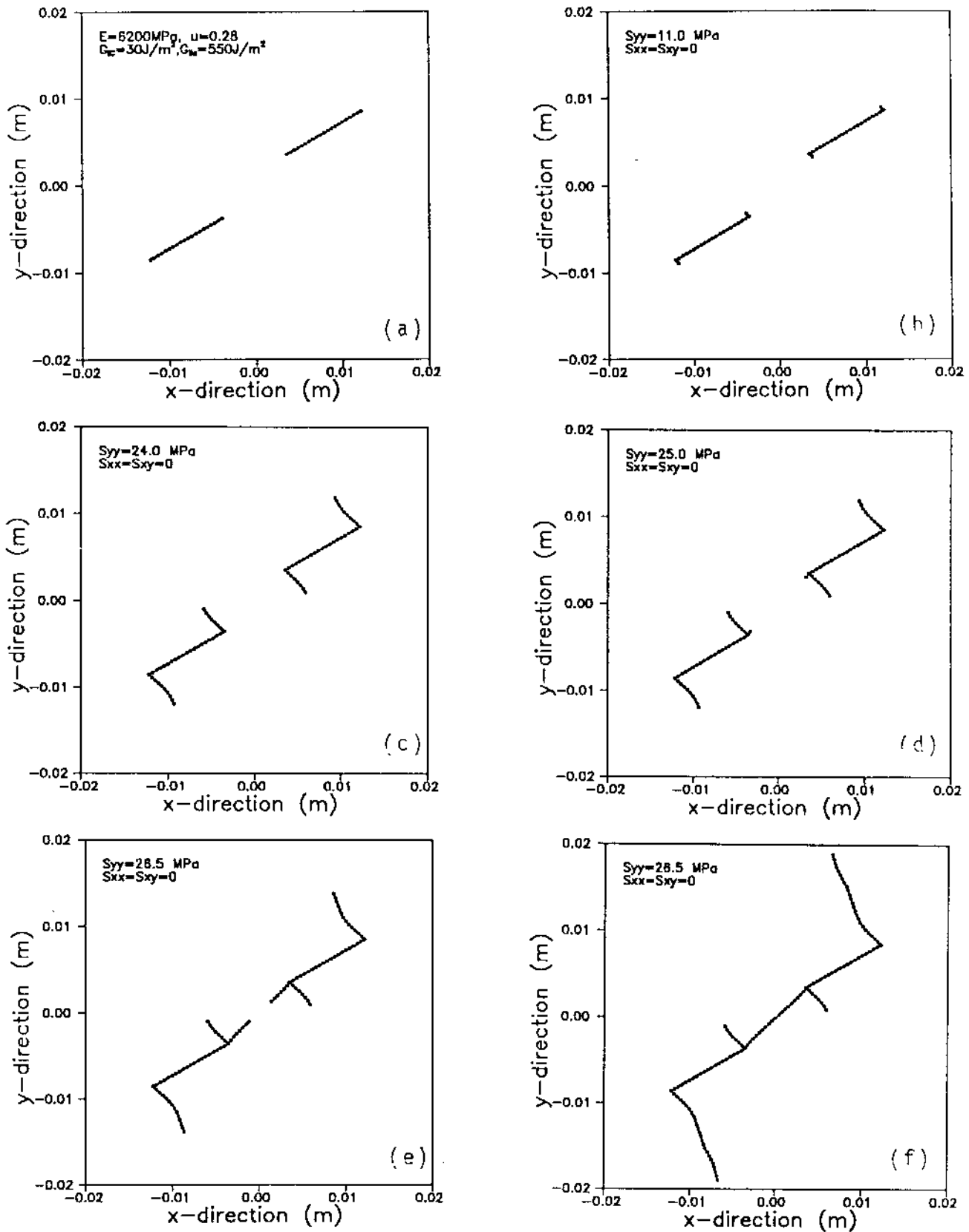


*Fig.5. Predicted process of fracture propagation and coalescence for the 30°-45° specimen using the F-criterion approach. The flaws are assumed to be located in an infinite elastic body. (a) Initial state; (b) and (c) tensile fractures initiate and propagate; (d) shear fractures initiate; (e) and (f) shear fractures propagate and finally coalesce, meanwhile the outer tensile fractures extend.*

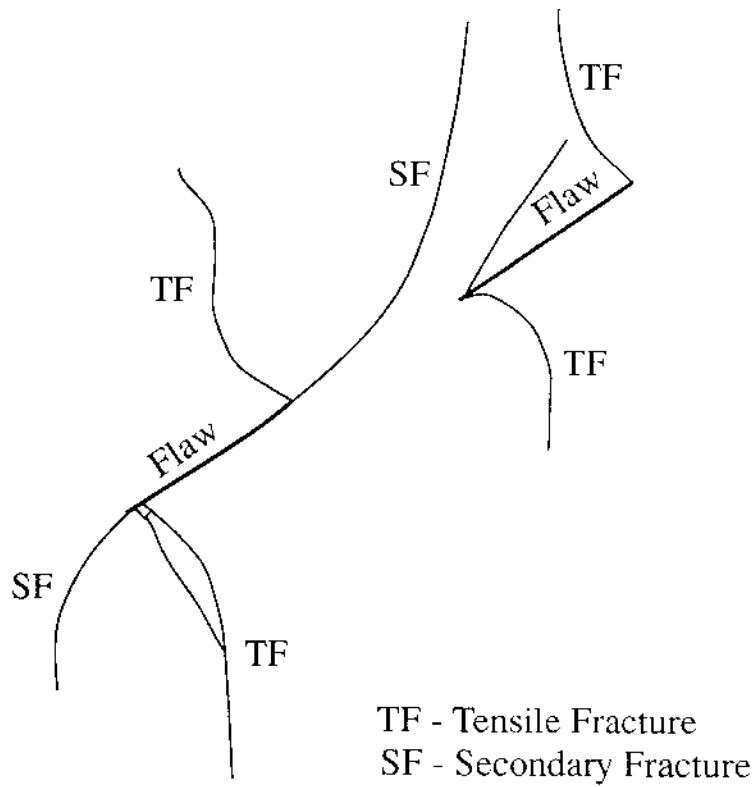


Fig.6. Experimentally observed tensile and secondary fractures after the failure of the  $30^{\circ}$ - $30^{\circ}$  specimen. The secondary fractures did not coalesce. Applied stress is 30 MPa. After Reyes[3].

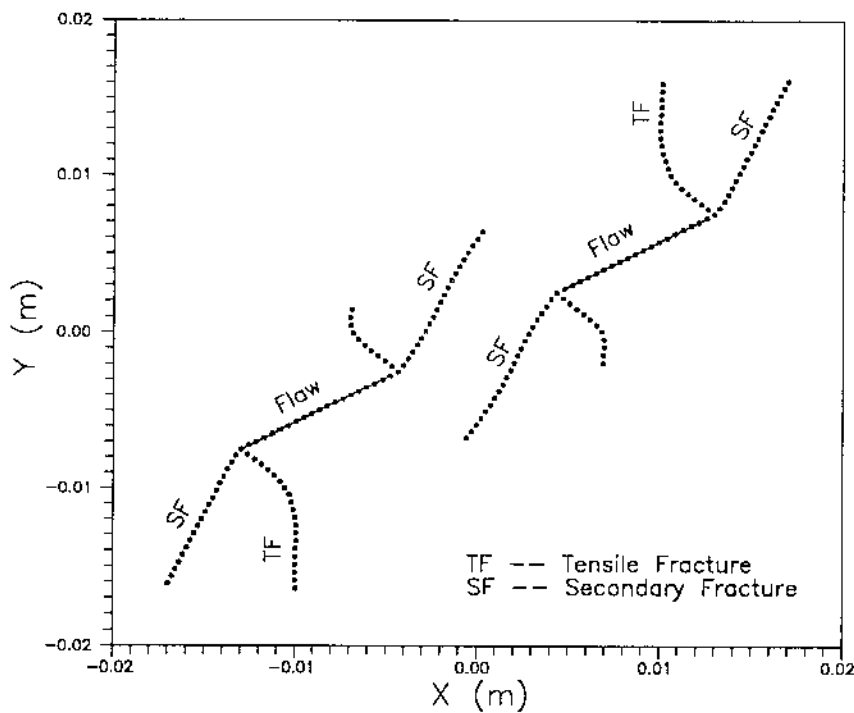


Fig.7. Predicted tensile and secondary fractures for the  $30^{\circ}$ - $30^{\circ}$  specimen using the F-criterion approach. Applied stress is 33 MPa.

*Table 1. Critical loads for the tensile fractures and coalescence with different fracture geometry. The results from experiment and different numerical approaches are compared.*

Specimen (Fracture inclination - Rock bridge inclination)	Experiment		Strain-based damage approach		F-criterion approach	
	Tensile fracture (MPa)	Coalescence (MPa)	Tensile fracture (MPa)	Coalescence (MPa)	Tensile fracture (MPa)	Coalescence (MPa)
30°-45°	11.0	24.1	—	21.4	11.0	26.5
45°-60°	16.0	23.0	—	18.0	15.5	26.5
60°-45°	30.0	31.0	—	24.5	26.5	33.6

The agreement of results between the experimental and the simulated failure strongly supports the validity of the F-criterion based numerical technique. The F-criterion can solve mixed-mode problems and predict both the tensile fracture and the secondary fracture simultaneously.

## WHICH FACTORS WILL INFLUENCE THE PROPAGATION MODE OF ROCK FRACTURES?

The factors which strongly influence the fracture propagation mode include: the toughness ratio, loading conditions, mechanical properties of the fracture ( $K_n, K_s, \phi$ , etc.) and the stiffness of the surrounding medium ( $E, \nu$ ). The toughness ratio ( $G_{IIc}/G_{Ic}$ ) is considered to be of greatest importance. Lower toughness ratios (i.e., lower  $G_{IIc}$  and higher  $G_{Ic}$ ) certainly favor the development of Mode II propagation. The toughness ratio is a material property. Materials like rocks, concrete, gypsum, etc. have low toughness ratios and hence have been observed to fail more easily by shearing.

Some other factors which influence fractures in rock material are: 1. the stress ratio ( $\sigma_3/\sigma_1$ ); 2. friction angle of the fracture ( $\phi$ ); 3. fracture inclination ( $\phi_i$ ); 4. fracture length ( $a$ ); 5. fracture normal stiffness ( $K_n$ ); 6. elastic property ( $E$ ). These six factors are studied by means of the following dimensionless parameters:  $\sigma_3/\sigma_1, \phi/\phi_i, E/(aK_n)$ . The analysis is performed with a single inclined fracture in a rock mass subjected to biaxial compressive loading (Fig.8). By using the F-criterion approach and given values of the three parameters, a



critical toughness ratio ( $G_{IIc}/G_{Ic}$ ) can be determined where the fracture initiation will be in Mode II instead of Mode I, (see  $G_{IIc}/G_{Ic}$  versus  $\sigma_3/\sigma_1$  plot, Fig.9,  $G_{IIc}/G_{Ic}$  versus  $\phi/\phi_i$  plot, Fig.10, and  $G_{IIc}/G_{Ic}$  versus  $E/(aK_n)$  plot, Fig.11). Each relationship divides the plots into two regions, Mode I and Mode II. If the critical  $G_{IIc}/G_{Ic}$  value increases with increasing the value of one of the three dimensionless parameters, this parameter favors Mode II fracture propagation.

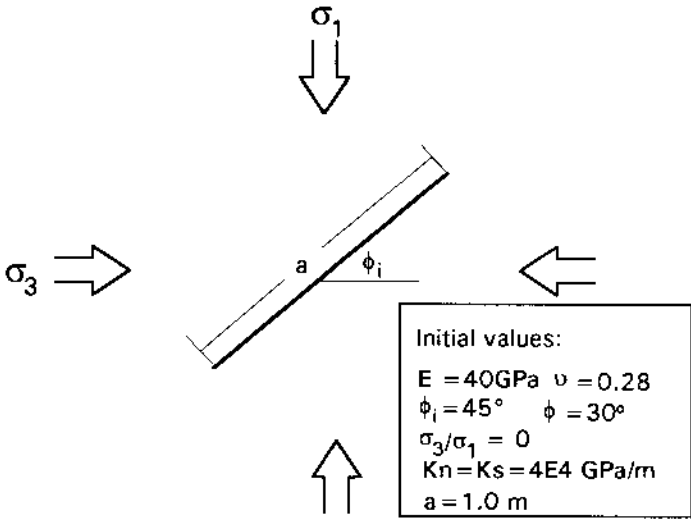


Fig.8. A rock fracture (joint) subjected to biaxial loading.

Figure 9 shows that the stress ratio  $\sigma_3/\sigma_1$  has a significant influence on the propagation mode. Especially when the ratio is larger than 0.1, i.e., the confining stress is more than 10% of the loading stress, Mode II propagation is more likely to occur. Therefore, high confining stress ( $\sigma_3$ ) favors Mode II fracture propagation. In rock masses the confining stresses are usually high, which is perhaps the main reason why shear fractures are very common. When there is no confinement or the confining stress is tensile, the material toughness ratio ( $G_{IIc}/G_{Ic}$ ) for Mode II failure is  $\leq 0.70$ . A study by Melin [14] proved that when a fracture is subjected to pure shear, the  $G_{IIc}/G_{Ic}$  ratio for Mode II failure should be  $\leq 0.67$ .

Figure 10 shows  $G_{IIc}/G_{Ic}$  versus  $\phi/\phi_i$  for a special case where  $\sigma_3=0$ . In this case, the fracture inclination is also the upper limit of the friction angle for sliding. When  $\phi/\phi_i$  is close to 1, i.e., the fracture inclination is close to and slightly larger than the friction angle of the fracture, fracture propagation is more likely to be in Mode II.

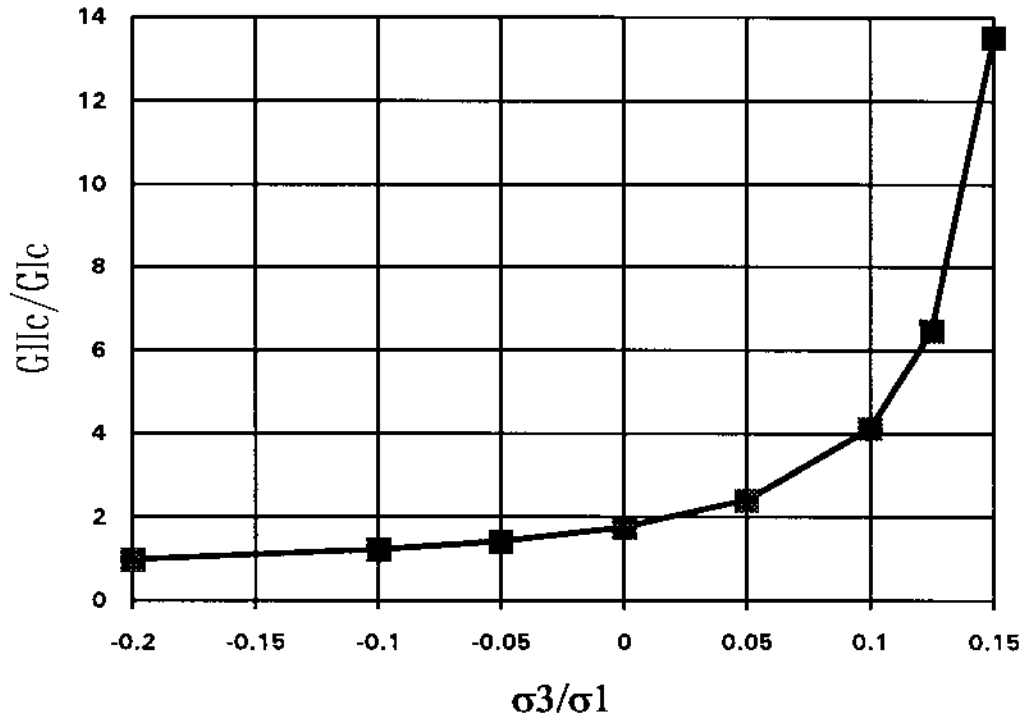


Fig.9. Critical  $G_{IIc}/G_{Ic}$  versus  $\sigma_3/\sigma_1$  for Mode II propagation. Except for the  $\sigma_3/\sigma_1$  value, initial parameters are the same as shown in Fig.8.

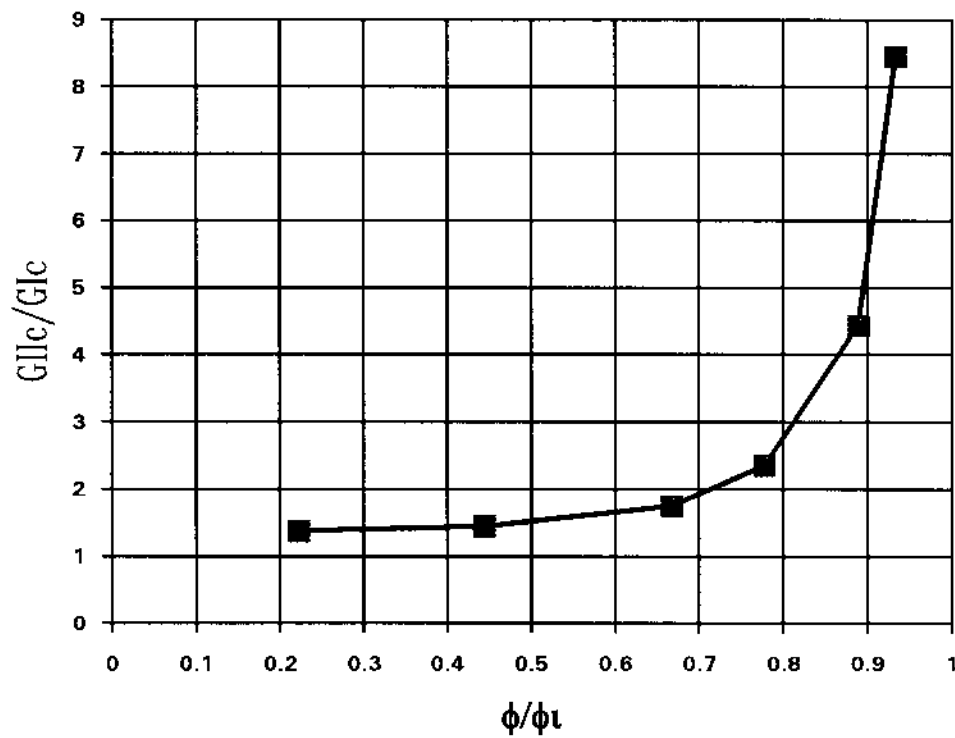


Fig.10. Critical  $G_{IIc}/G_{Ic}$  versus  $\phi/\phi_i$  for Mode II propagation. Except for the  $\phi$  and  $\phi_i$  values, initial parameters are the same as shown in Fig.8.

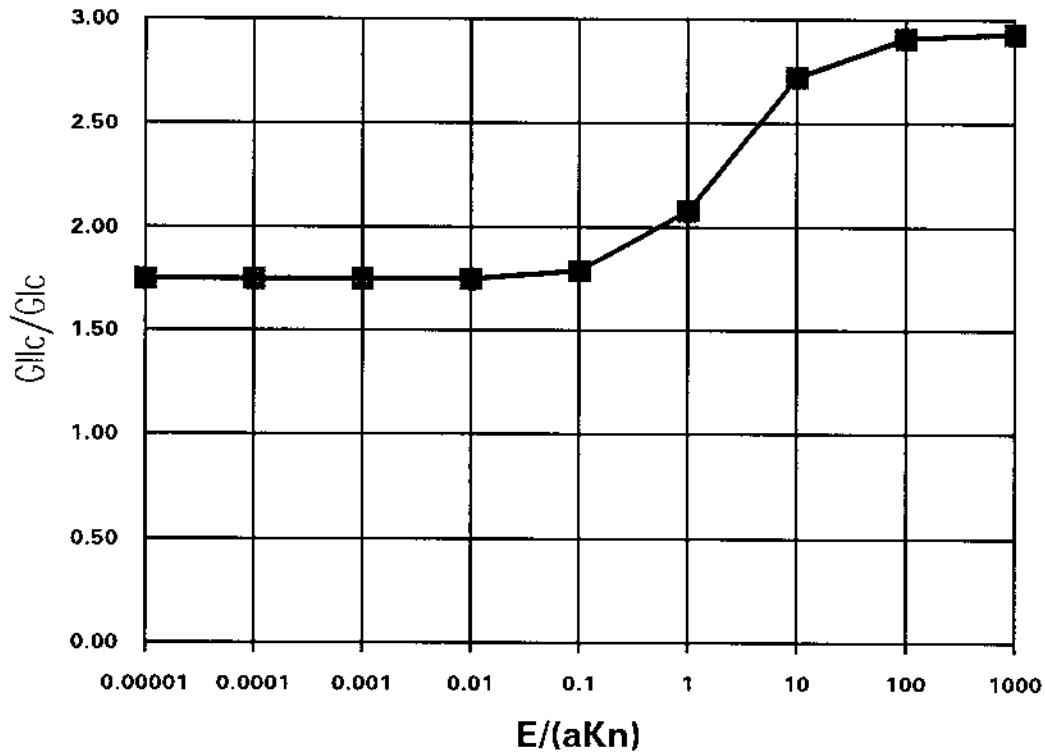


Fig.11. Critical  $G_{IIc}/G_{Ic}$  versus  $E/(aK_n)$  for Mode II propagation. Except for the  $\phi$  and  $\phi_i$  values, initial parameters are the same as shown in Fig.8.

The critical toughness ratio for Mode II propagation does not change significantly with variation of  $E/(aK_n)$  (Fig.11). This suggests that Young's modulus ( $E$ ) of intact rock, fracture normal stiffness ( $K_n$ ) and fracture length ( $a$ ) have little influence on the propagation modes of a rock fracture.

## DISCUSSION AND CONCLUSIONS

Shear (or Mode II) fracture propagation is currently debated in rock fracture mechanics. There are several interpretations of the shear failure of rocks. The most common view is that shear failure is caused by the linkage of many small tensile cracks or flaws. According to this interpretation, the classical Mode II fracture propagation may not exist on a micro-scale. However, this does not exclude the possibility that Mode II failure can occur on the macro-scale. Micro-scale tensile fracturing and linkage can be looked upon as shear fracturing on the macro-scale. In this case, it is sufficient to handle the process by using the macro-scale fracture mechanics approach. The work presented in this paper is

based on this idea and the results demonstrate that the macro-scale approach can predict shear fracturing of rock and other brittle materials.

The F-criterion approach has provided to be a powerful tool for studying mixed-mode fracture propagation. In contrast to other methods the F-criterion together with the numerical method DDM can predict both the tensile fractures and shear fractures. The F-criterion approach has been used to successfully simulate the fracture coalescence observed in experiments. The failure paths and critical loads predicted by the F-criterion approach are similar to those observations in experiments.

Both the fracture toughness ratio ( $G_{IIc}/G_{Ic}$ ) and the stress ratio ( $\sigma_3/\sigma_1$ ) have a significant effect on the mode of fracture propagation. The occurrence of Mode II failure in laboratory experiment requires materials with both low toughness ratio ( $G_{IIc}/G_{Ic}$ ) and high confining stress.

The F-criterion approach can be applied to studies of the deformability and strength of fractured rock masses. The F-criterion approach is capable at simulating the complete process of pre-failure—failure—post-failure of a rock mass with a defined fracture network.

#### ACKNOWLEDGMENTS

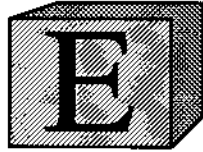
This study is supported by the Swedish National Board for Industrial and Technical Development. The authors are thankful to H.H. Einstein for providing experimental data, for encouraging discussions and for his comments about our manuscript. Valuable comments from J. Fernlund, L. Myer and an anonymous reviewer are also gratefully acknowledged.

#### REFERENCES

1. Lajtai E. Brittle fracture in compression. *Int. J. Fracture*. **10(4)**, 525-536 (1974).
2. Petit J.-P. and Barquins M. Can natural faults propagate under mode II conditions? *Tectonics*, **7(6)**, 1243-1256 (1988).

3. Reyes O. Experimental study and analytical modelling of compressive fracture in brittle materials. Ph.D. Thesis of Massachusetts Institute of Technology (1991).
4. Reyes O. and Einstein H.H. Failure mechanisms of fractured rock — A fracture coalescence model. *Proc. 7th Int. Con. on Rock Mechanics*, **1**, 333-340 (1991).
5. Bazant Z.P. and Pfeiffer P.A. Shear fracture tests of concrete. *Mater. Constr.* **19**(110), 257-263 (1987).
6. Jung S.J., Enbaya M. and Whyatt J.K. The study of fracture of brittle rock under pure shear loading. *Proc. Fractured and Jointed Rock Masses (Preprint)*, 458-475 (1992).
7. Shen B. and Stephansson O. Modification of the G-criterion for fracture propagation in compression. Manuscript submitted to *Engineering Fracture Mechanics*. (1993)
8. Eordgan F. and Sih G.C. On the crack extension in plates under plane loading and transverse shear. *ASME J. Bas. Engng* **85**, 519-527 (1963).
9. Chang K.J. On the maximum strain criterion - A new approach to the angled crack problem. *Engineering Fracture Mechanics*. **14**, 107-124(1981).
10. Hellan K. *Introduction to fracture mechanics*. p.301. McGraw-Hill International Editions, Singapore (1984).
11. Sih G.C. Strain-energy-density factor applied to mixed mode crack problems. *Int. J. Fracture*. **10**(3), 305-321 (1974).
12. Li V.C. Mechanics of shear rupture applied to earthquake zones. *Fracture mechanics of rock* (ed. Atkinson B.K), Academic Press, London, 351-428.
13. Crouch S.L. and Starfield A.M. *Boundary element methods in solid mechanics*. p. 322. George Allen & Unwin, London (1983).
14. Melin S. When does a crack grow under mode II condition? *Int. J. Fracture*, **30**, 103-114 (1986).





# **Coalescence of open and closed cracks — A laboratory investigation**

*B. Shen , O. Stephansson, H. Einstein and B. Ghahreman*

*Int. J. Rock Mech. Min. Sci. (1993) (Submitted)*

# Coalescence of Open and Closed Cracks — A Laboratory Investigation

B. Shen and O. Stephansson

Engineering Geology, Royal Institute of Technology, Stockholm, Sweden

H.H. Einstein and B. Ghahreman

Department of Civil Engineering, Massachusetts Institute of Technology,  
MA02139, U.S.A.

## Abstract

To study the failure mechanism of joints and rock bridges in jointed rock masses, a series of uniaxial compression tests were performed using gypsum specimens with pre-existing cracks. The coalescence mechanism of two cracks was investigated. Results show that both open and closed cracks can coalesce by shear failure or tensile failure. The coalescence load of closed cracks is about 25% higher than that of open cracks. The coalescence path mainly depends on the inclination of the rock bridge between two cracks. With low bridge inclination, coalescence is generated by shear failure. The path of wing cracks, the coalescence load, and the stress-strain relation is different for specimens with open and closed cracks.

## Introduction

The initiation, propagation and coalescence of rock cracks is commonly recognised to govern mechanical behaviour of brittle rocks. Numerous experimental and analytical investigations on microcrack initiation, growth and coalescence have been conducted since Griffith [1] proposed the mechanism, see e.g. [2,3,4]. Studies on cracked rock do not only help to explain crack propagation mechanism, but they can also serve as models for the behavior of jointed<sup>1</sup> (fractured) rock masses. Joint extension and coalescence can reduce the stiffness of jointed rock masses [5], cause the shear failure of rock slopes [6], and induce earthquakes by forming shear faults [7]. Coalescence of cracks has been

---

<sup>1</sup> The term "joint", rather than fracture, will be used throughout this paper.



investigated by many researchers both experimentally and analytically. Lajtai [8] performed direct shear tests on natural rock specimens with two parallel slots, Segall & Pollard [9] investigated analytically the stress field in rock bridges between two stepped cracks, Horri & Nemat-Nasser [10] studied the coalescence behaviour of multi-cracks in polymer specimens, and Reyes & Einstein [11] conducted uniaxial tests on gypsum specimens with two inclined flaws. These studies have increased our knowledge about the behaviour of multi-fractured rock. However, most of the previous studies, especially the experimental studies, were carried out by using pre-existing slots and flaws whose surfaces were not in contact. Hence, we do not know under what conditions cracks or fractures with surface contact and friction propagate and coalescence. The answer to this question is of special significance for the understanding of the failure of rock masses, where joints or other discontinuities have surface contact and friction in most situations.

In this study, we conduct a series of uniaxial loading tests on gypsum specimens containing two cracks. Two types of cracks are used: i) cracks without surface contact and friction, named *open cracks*, and ii) cracks with surface contact and friction, named *closed cracks*. The results from testing specimens with open cracks and closed cracks are compared. Cracks with different configuration (inclination of cracks and inclination of the bridge between the cracks) are investigated. The failure process is monitored with a microscope and video camera and the failure mechanism is evaluated.

## Specimen Preparation and Testing

### *Specimen preparation*

Specimens are made from gypsum, water and celite at ratios gypsum/water/celite = 165/70/2 in weight. This mixture has been previously reported to behave similarly to brittle rock [12] and was used by Reyes and Einstein [11] in their study of coalescence of open cracks. The size of the prismatic specimens is 152.4×76.2×30 mm (Fig. 1a). Two cracks with lengths of 12.7 mm each are created in the center of the specimens during casting (Fig. 1b). The length of the bridge between the two inner tips is also 12.7 mm. The design of the specimens and cracks simulates plane strain conditions and minimizes the influence of free boundaries. Different cracks and bridges inclinations are used to investigate the influence of crack geometry on failure mode and failure load.

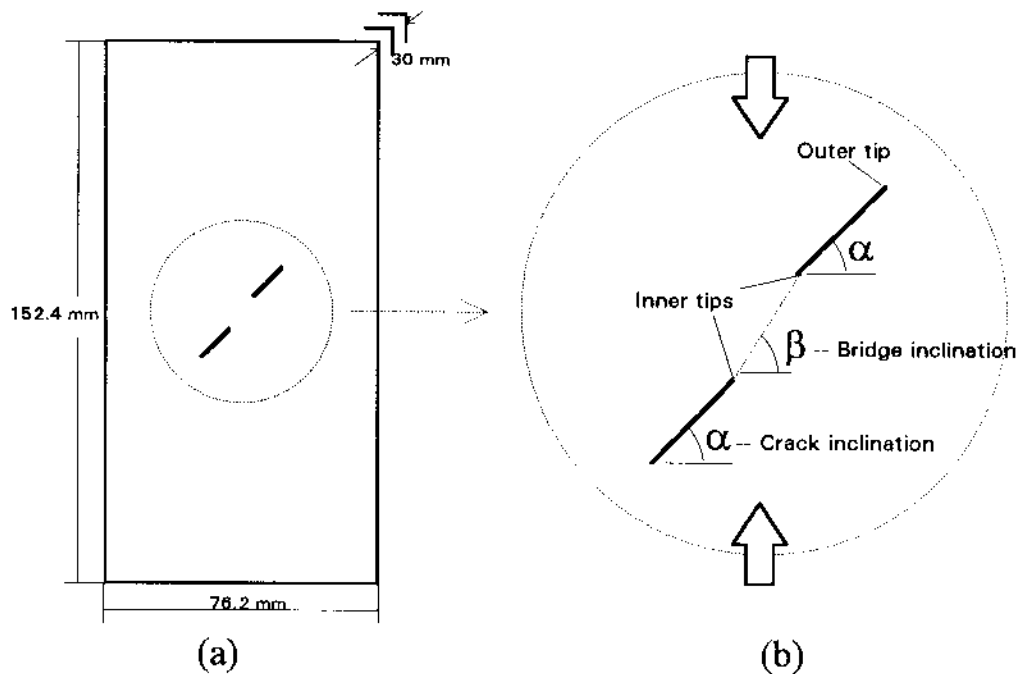


Fig.1. Geometry of specimens and pre-existing cracks

Open cracks in the specimen can be created by positioning two thin (0.04 mm) steel sheets in the mould before casting and pulling them out when the gypsum mixture becomes hard. Closed cracks are much more difficult to produce. A number of methods to generate closed cracks have been investigated by Ghahreman [13], including: (a) cracking by impact; (b) pre-installation of wax papers in the crack position and leaving the paper in the specimen; (c) back and forth movement of a thread during curing; and (d) pre-installation of polyethylene sheets and removal of the sheets during curing. Only the last method was found suitable for creating closed cracks with similar properties to natural rock joints. In this method, we pre-install two tightly stretched polyethylene sheets (thickness 10 $\mu$ m) in the desired crack positions before casting. After casting and 30 minutes of curing when the gypsum mixture starts to become hard, the polyethylene sheets are pulled out. The expansion of the gypsum mixture closes the thin slots and hereby creates the closed cracks. Additional loading tests of small specimens showed that the closed cracks made in this way have approximately a friction angle of 35° and a cohesion of 3.5 MPa.

#### *Testing and recording*

The uniaxial tests are performed in an INSTRON (Model 1331) servo-controlled hydraulic loading machine. Displacement control is used to avoid a

sudden failure of the specimens. The crack initiation and propagation are monitored by a microscope connected to a video recorder. The whole process of failure is recorded and studied by re-playing it in slow motion (the coalescence process is usually very fast and cannot be seen). Simultaneously, the load and displacement are recorded and the complete loading and unloading curve can be drawn. Fig. 2 is a schematic loading and monitoring system.

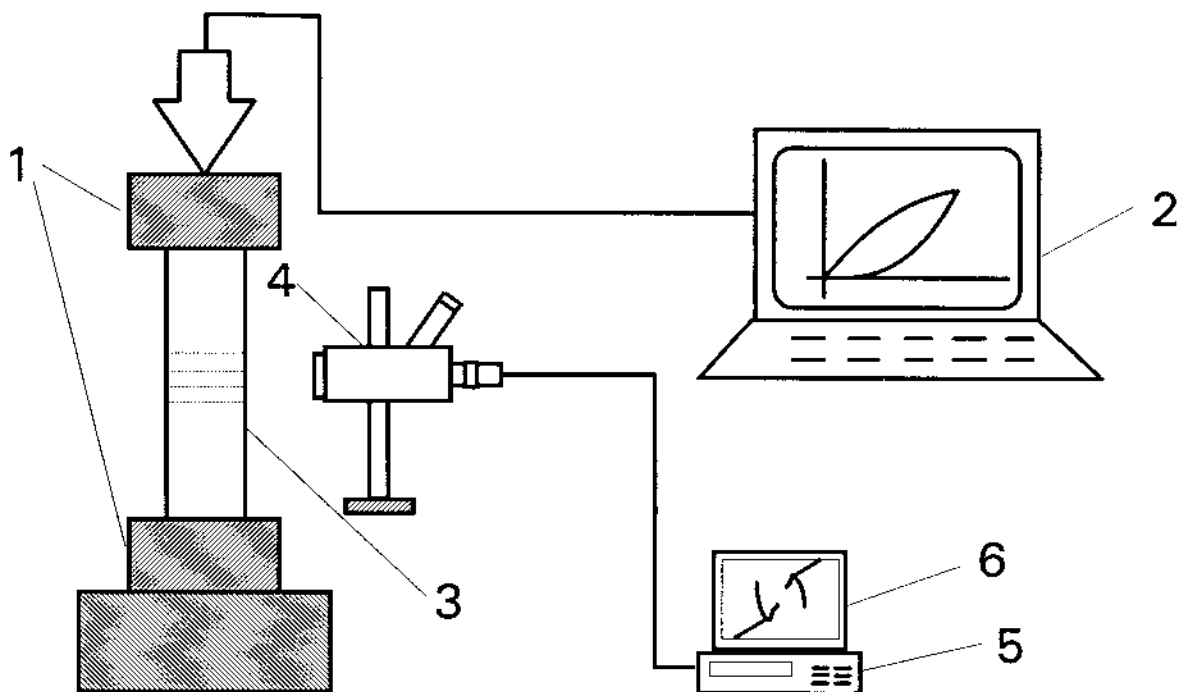


*Fig.2. Loading and monitoring system of the crack coalescence test. 1 — load cell; 2 — operating and recording device; 3 — specimen with pre-existing cracks; 4 — microscope; 5 — video recorder; 6 — TV.*

## Results

The tests are performed with different crack-bridge geometries. The selected crack inclinations ( $\alpha$ ) are  $30^\circ$ ,  $45^\circ$  and  $60^\circ$ , and the bridge inclinations ( $\beta$ ) vary from  $45^\circ$  to  $120^\circ$  in steps of  $15^\circ$ . For each crack-bridge geometry, a minimum of three specimens are tested, one with open cracks and two with closed cracks. Different specimens with the same crack-bridge geometry and crack condition (open or closed) have shown a good reproducibility for both failure pattern and failure load.

## 1. Process of crack propagation and coalescence.

Crack initiation, propagation and coalescence are observed during the tests. A typical sequence of the fracturing process is shown in Fig.3.

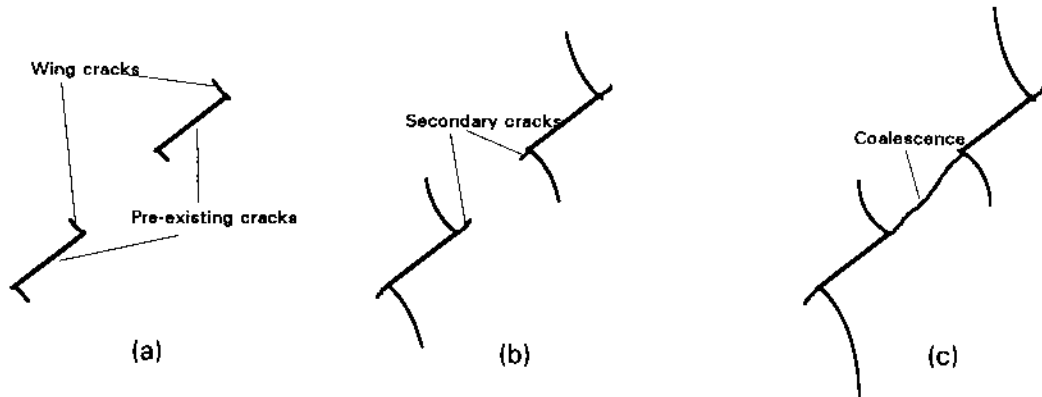


*Fig.3. Typical sequence of crack initiation, propagation and coalescence. (a) Wing cracks initiate from the pre-existing crack tips at low uniaxial load; (b) wing cracks propagate with increasing load and secondary cracks appear at the pre-existing tips; and (c) secondary cracks propagate very quickly and coalesce, meanwhile the outer wing cracks extend.*

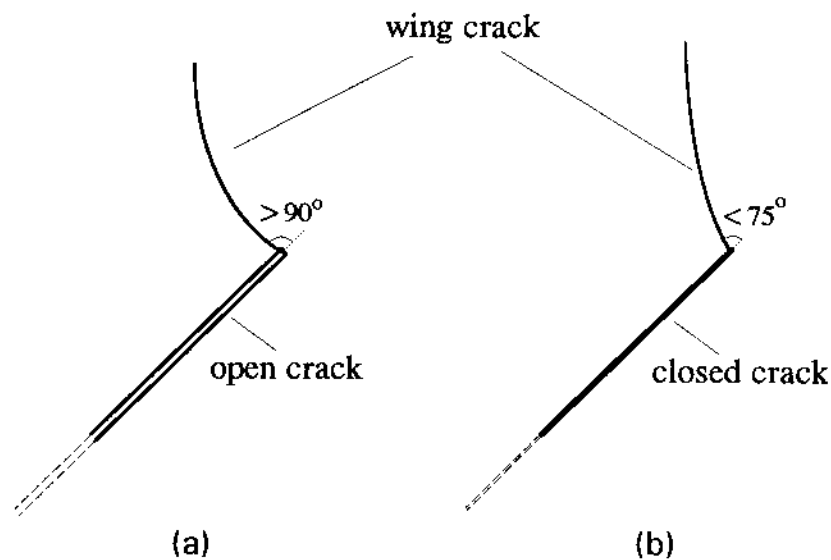
The failure process shown in Fig. 3 is only representative when the inclination of the bridge is low ( $\beta \leq 60^\circ$ ). The observed failure processes for open and closed cracks and for different crack-bridge geometries are rather different. Some of the most interesting results which will be discussed in more detail below, are summarized as the follows:

- Wing cracks have different paths for open and closed pre-existing cracks.
- The coalescence mechanism is very different when the bridge inclination varies from a low angle ( $\leq 60^\circ$ ) to a high angle ( $\geq 90^\circ$ ) for both open and closed cracks. The secondary cracks are initiated from the pre-existing crack tips or from the bridge center, depending upon the bridge inclination.
- For closed cracks, when the crack inclination ( $\alpha$ ) is less than the friction angle, crack propagation and coalescence do not occur.
- The load at coalescence of closed cracks is higher than that of open cracks.

## 2. Wing cracks.

All specimens in our tests show that the wing cracks emanating from pre-existing open cracks have smaller curvature than those propagating from the pre-existing closed cracks. Wing cracks emanating from pre-existing open cracks form a greater angle between wing crack and pre-existing crack plan than wing crack

propagating from closed pre-existing cracks (see Fig.4). The wing cracks initiated from a closed crack take a path close to a straight line almost parallel to the direction of uniaxial load. The wing crack initiation from a pre-existing closed cracks generally requires a higher uniaxial load than that from pre-existing open crack. Also, the initiation load of wing cracks is higher when the inclination of the pre-existing cracks increases.



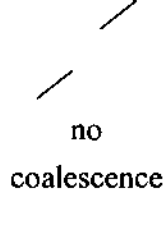
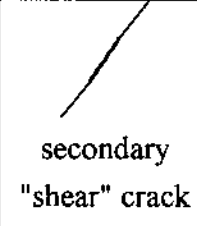
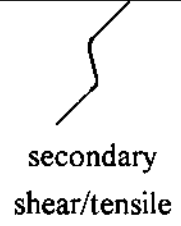
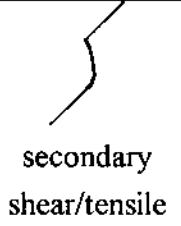
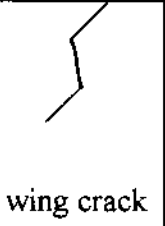
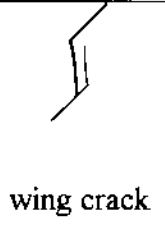
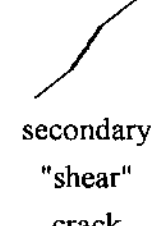
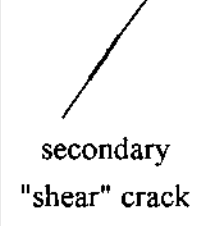
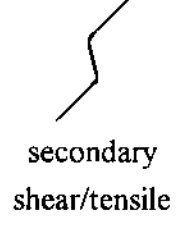
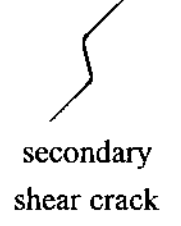


*Fig.4. Path difference of wing crack developing from an open pre-existing crack or a closed pre-existing crack.*

### 3. crack coalescence

Coalescence is found to occur in different modes, depending upon the geometry of cracks, see Table 1. There are evidently four major modes of coalescence:

- a). Apparent shear coalescence for flatly inclined pre-existing cracks.
- b). Combined shear/tension or shear/wing crack coalescence for pre-existing cracks with intermediate inclination.
- c). Wing crack coalescence for steeply inclined and overlapping pre-existing cracks.
- d). Other coalescence for very strongly overlapping pre-existing cracks.
- e). No coalescence.

*Table 1. Summary of the mode of coalescence observed in different specimens*

$\alpha/\beta$	30°/45°	45°/45° (45°/60°, 60°/45°, 60°/60°)	45°/75° (60°/75°)	45°/90° (60°/90°)	45°/105° (60°/105°)	45°/120°
Closed pre-existing cracks	 no coalescence	 secondary "shear" crack	 secondary shear/tensile crack	 secondary shear/tensile crack	 wing crack	 wing crack
Open pre-existing cracks	 secondary "shear" crack	 secondary "shear" crack	 secondary shear/tensile crack	 secondary shear crack +wing crack	 wing crack	 other crack

*a). Coalescence caused by apparent shearing*

For both open and closed cracks, when the bridge inclination  $\beta \leq 60^\circ$ , the coalescence is through so called secondary cracks. Two secondary cracks initiate at the two inner tips of the pre-existing cracks and propagate toward each other. Finally they meet somewhere in the bridge and coalesce. This process is shown in Fig.5 for a specimen with open cracks and a bridge inclination of  $45^\circ$ . The secondary cracks are initiated and propagate in the direction perpendicular to wing cracks. The propagation of the secondary cracks is often a fast and unstable process. Also, the surfaces of the secondary cracks are usually very rough and stepped, which is different from the smooth surface of a wing crack (Fig.6b). In some specimens which have undergone complete shear failure after the coalescence, the coalescence surface contains pulverized material and striations or traces of shear displacement. All these features of the secondary cracks suggest that they are caused by shearing.

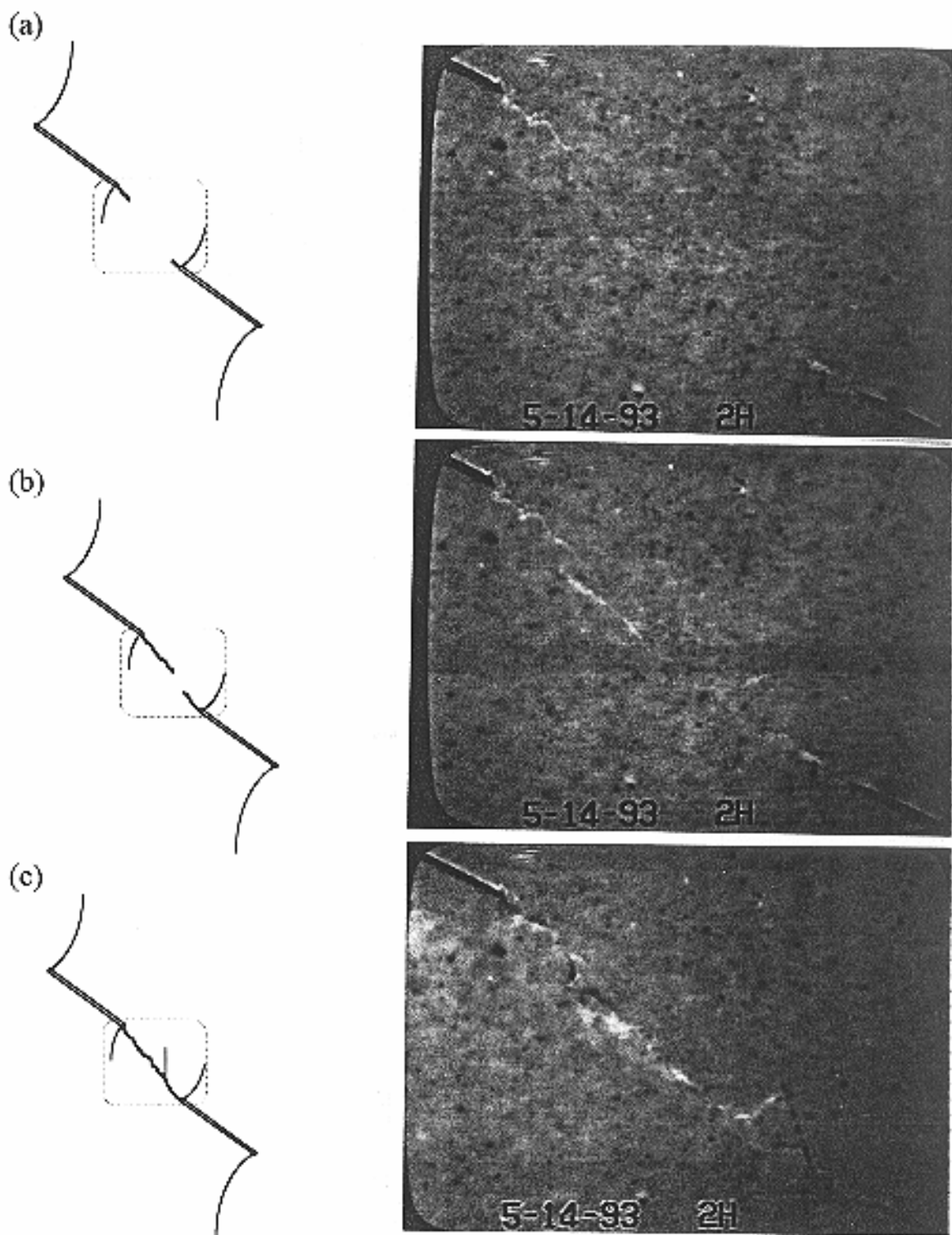


*Fig.5. Successive video recording of the coalescence process. Specimen  $30^\circ/45^\circ$  (crack inclination/bridge inclination) with open cracks. (a) After wing cracks have propagated, two secondary cracks start from the pre-existing crack tips; (b) the secondary cracks propagate toward each other in a straight path; and (c) the two secondary cracks meet at the bridge center and coalescence occurs.*

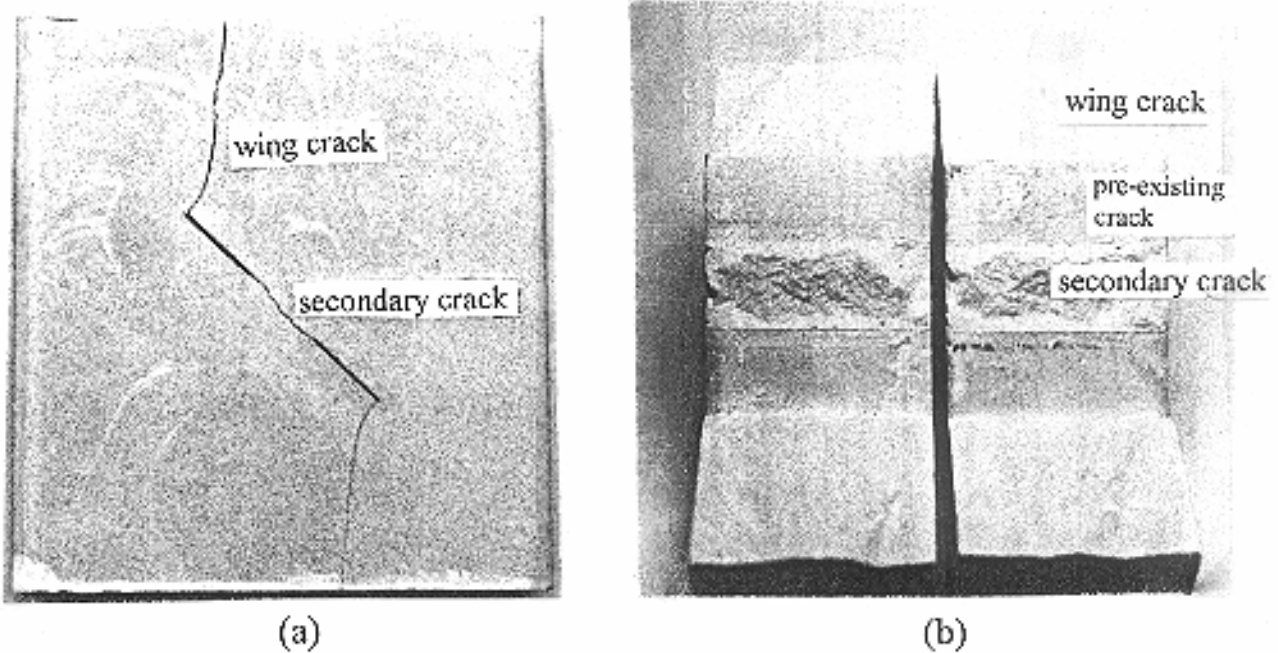


Fig.6. Failure path and failure surface topography of the specimen  $45^\circ/45^\circ$  (crack inclination/bridge inclination) with open cracks. (a) Path of wing cracks and coalescence; (b) Separation of specimen showing the surface topography of wing cracks and secondary cracks by shearing.

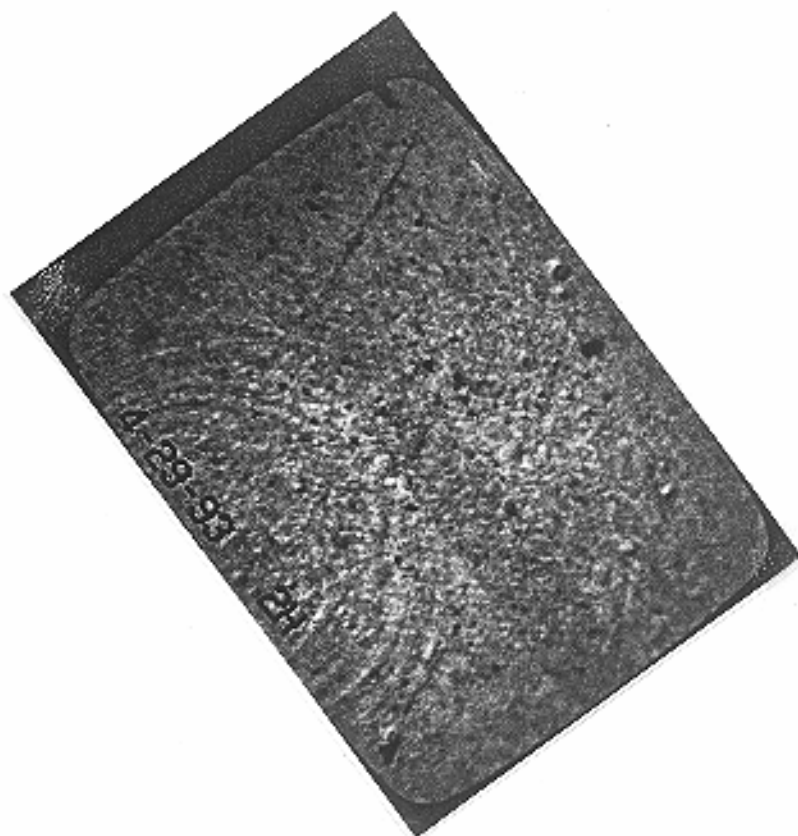
b). Coalescence caused by combined shear and tension.

In specimens with the bridge inclination of  $75^\circ$  and  $90^\circ$  the coalescence is caused by mixed shear and tension. In most of these specimens, a secondary crack emanates at the center part of the bridge and finally links the two pre-existing cracks. A typical crack development is demonstrated for one of the two  $45^\circ/90^\circ$  specimens with closed cracks, see Fig.7. The pre-existing cracks in this specimen are believed to have weaker contact than that in other specimens, because the polyethylene sheets were left longer in the mould during specimen preparation.

For the test presented in Fig. 7, two wing cracks are first observed when the uniaxial load reaches 9.6 MPa. With increasing load, the wing cracks extend and form an elliptical solid core between the two pre-existing crack tips. When the load is 16.8 MPa, a secondary crack appears at the center of the bridge and quickly propagates in the direction almost parallel to the wing cracks. The secondary crack in the center of the bridge shows a clear separation between the two surfaces similar to the wing cracks. But close to the pre-existing crack tips, the secondary crack becomes curved to the direction of the pre-existing cracks.



(a)



(b)

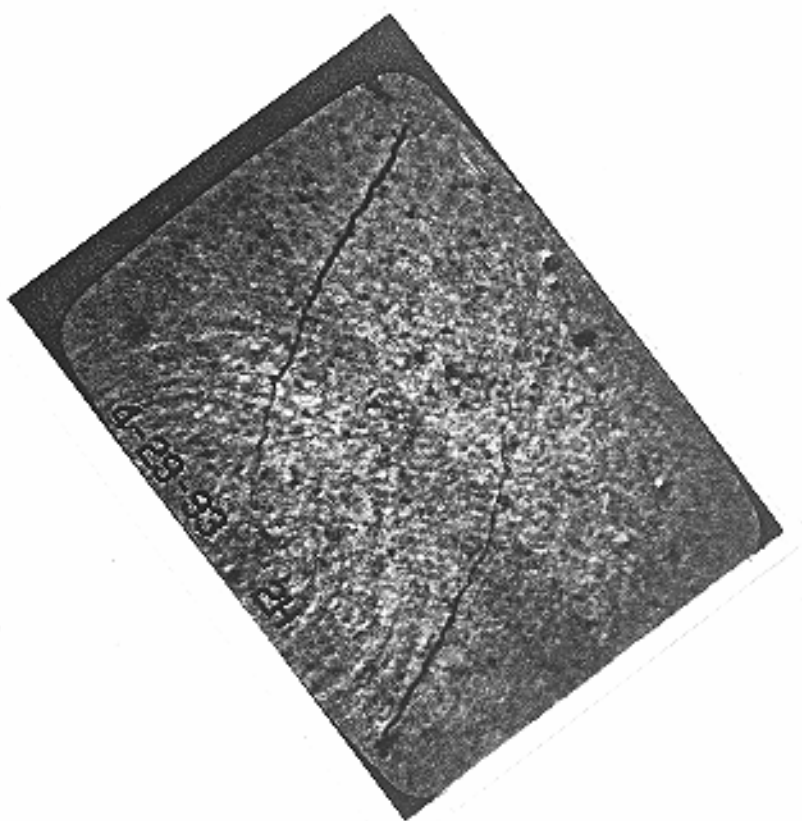


(Fig.7, see also next page)

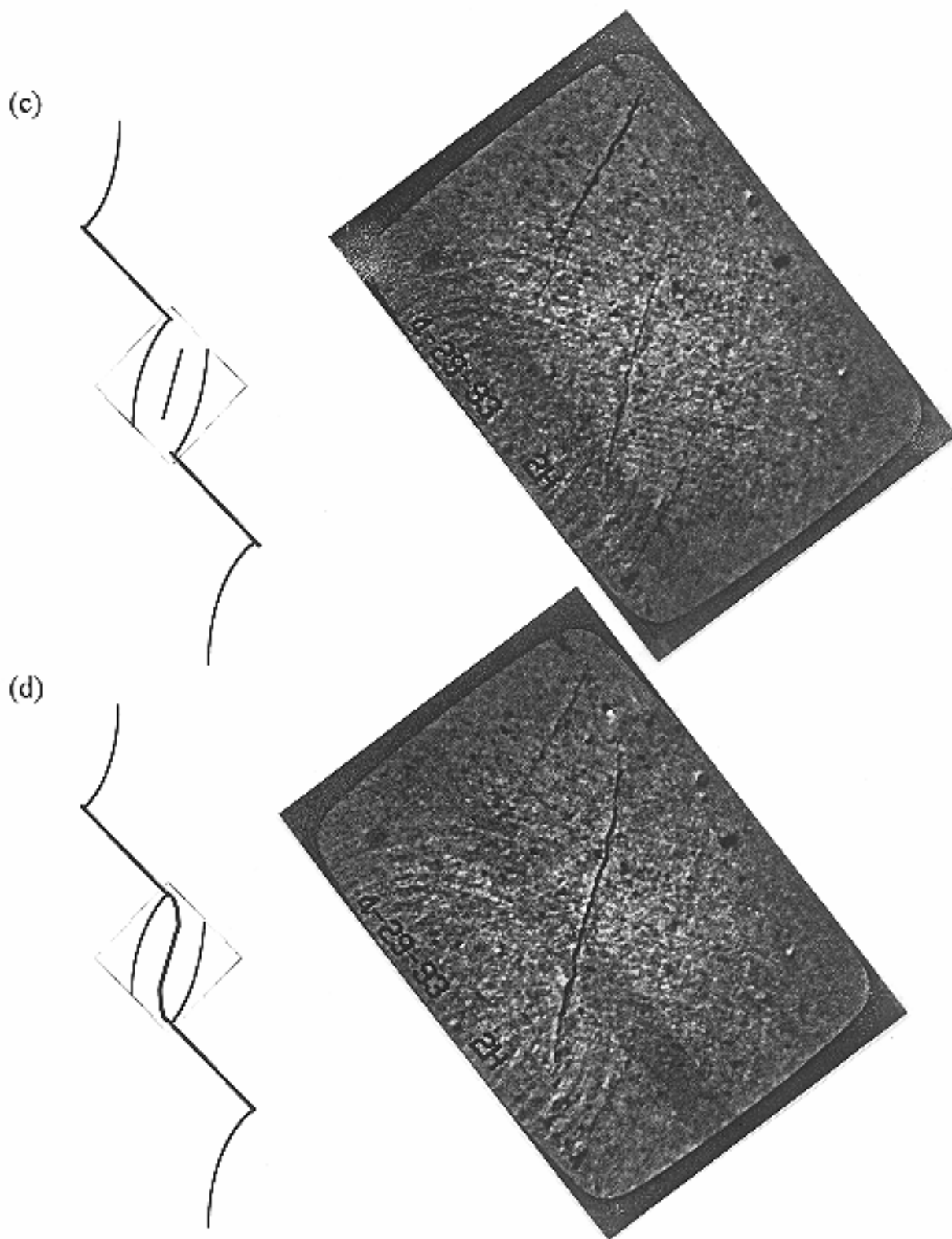


*Fig.7. The process of coalescence of one 45°/90° specimen (crack inclination/bridge inclination) with closed cracks. The closed cracks in this specimen have weaker contact than the other 45°/90° specimen. (a),(b) wing crack initiation and propagation; (c) secondary cracks originate inside the bridge and propagate toward the pre-existing crack tip; and (d) final coalescence.*

The failure surfaces near the crack tips show a manner of closing and sliding, differing from the failure surfaces in central part of the bridge. The wing cracks are closed after coalescence.

The results presented in Fig.7 show a different mechanism of fracture development with that presented in Fig.5. The secondary crack seems to be initiated by tension inside the bridge and it propagates through the main portion of the bridge. Near the pre-existing crack tips the failure is caused by shearing, but it is not obvious whether the shear failure occurs from the pre-existing crack tips or from the tips of the secondary cracks.

Another  $45^{\circ}/90^{\circ}$  specimen with ordinary closed cracks shows somehow different manner of coalescence (Fig.8). A secondary crack develops from a pre-existing crack tip and connects a wing crack appeared from another pre-existing crack tip. The surface of secondary crack contains evidence of shear failure. Comparing Fig.8 and Fig.7 for the same crack/bridge geometry but with different contact condition of pre-existing cracks, it can be observed that the coalescence mode is different when the contact condition changes.

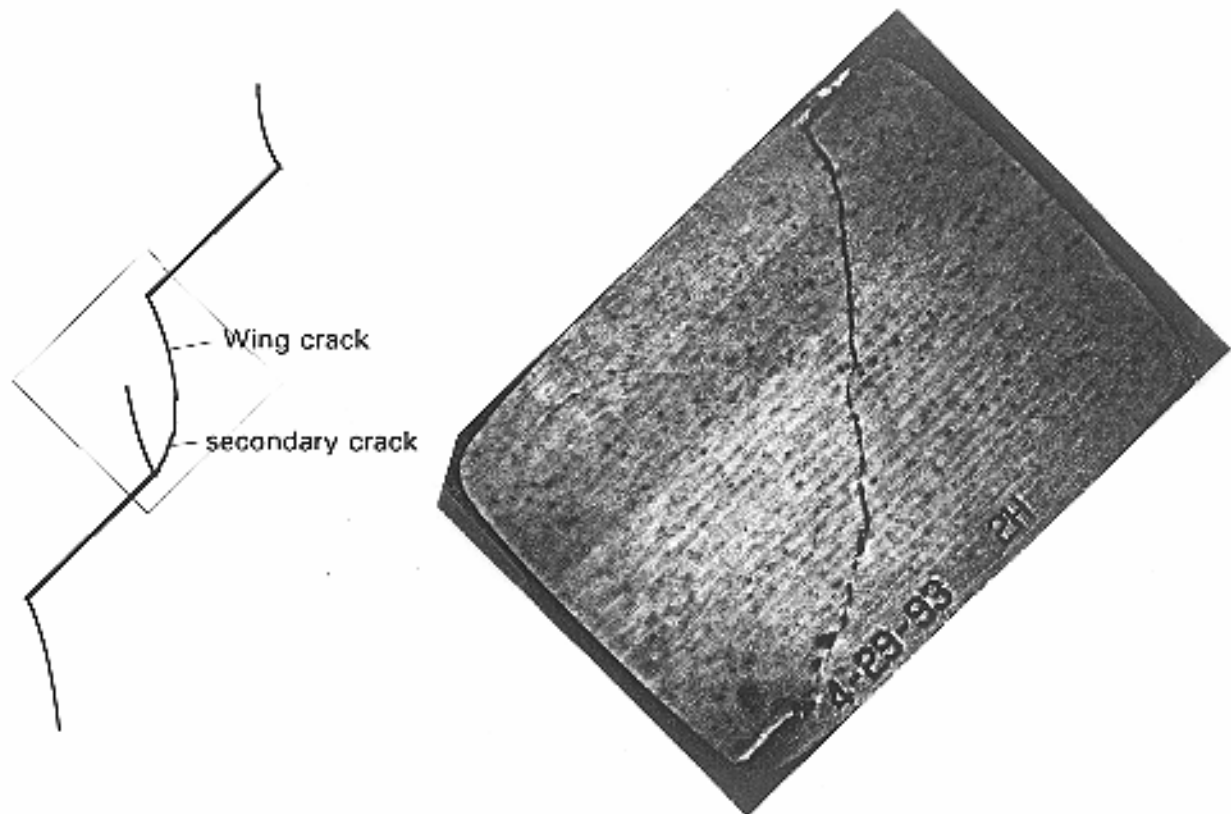


*Fig.8. Coalescence caused by a wing crack and a secondary crack. Specimen  $45^{\circ}/90^{\circ}$  with closed cracks. The closed cracks are believed to have stiffer contact than the specimen shown in Fig.7.*

c). *Coalescence caused by wing cracks.*

In the case with a bridge inclination of  $\beta \geq 105^\circ$ , coalescence is not caused by secondary cracks but by wing cracks. Coalescence by wing cracks can develop in three ways (see Fig.9): i) **wing crack**  $\rightarrow$  **pre-existing crack tip**, i.e., a wing crack is initiated from one pre-existing tip and propagates to the other tip and forms the coalescence, Fig.9a; ii) **wing crack**  $\rightarrow$  **wing crack**, i.e., two wing cracks are initiated from the two inner tips and meet inside the bridge, Fig.9b; and iii) **wing crack**  $\rightarrow$  **pre-existing crack**, i.e., a wing crack propagates from the inner tip of one crack to approximately the center of the other pre-existing crack, Fig.9c. The conditions of the pre-existing cracks, i.e. the fact if they are open or closed, has a strong influence on which kind of coalescence will occur (Fig.9a,b). Closed pre-existing cracks make the wing cracks less curved and more likely to connect with each other inside the bridge.

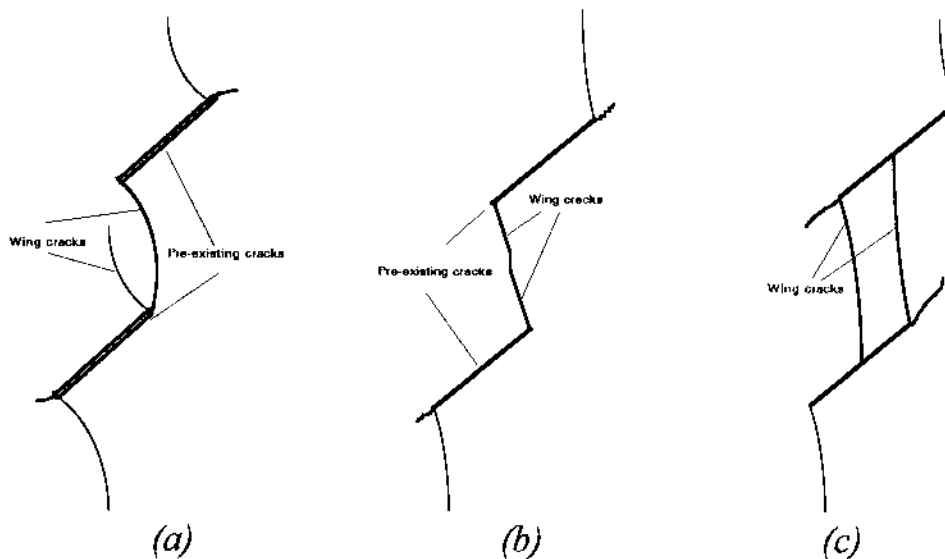
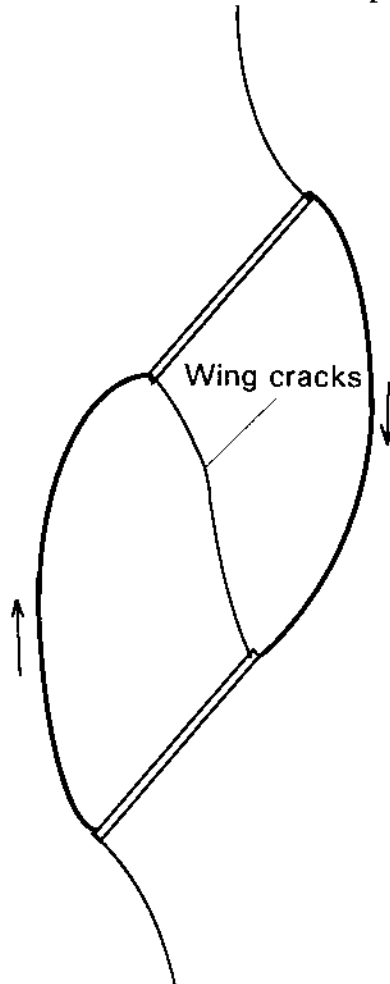


Fig.9. *Coalescence caused by wing cracks. (a) wing crack  $\rightarrow$  pre-existing crack tip, specimen  $45^\circ/105^\circ$  with open cracks; (b) wing crack  $\rightarrow$  wing crack, specimen  $45^\circ/105^\circ$  with closed cracks; (c) wing crack  $\rightarrow$  pre-existing cracks, specimen  $45^\circ/120^\circ$  with closed cracks.*

d). *Coalescence caused by other cracks*

The specimen  $45^\circ/120^\circ$  with open cracks shows different type of coalescence (Fig.10). In this specimen, there are two secondary cracks which develop at the outer tips in the direction opposite to the wing cracks and finally reach the inner

tips of the other pre-existing cracks. The surface of these two secondary cracks is much smoother than that of wing cracks and is not stepped as are the shear cracks. The direction of initiation of the two cracks suggests that they may be caused by compression or a combination of compression and shearing.



*Fig.10. Coalescence by other cracks, specimen  $45^{\circ}/120^{\circ}$  with open cracks. Additional coalescence occurs along two cracks which are possibly caused by compression.*

*e). No coalescence.*

When the inclination of pre-existing cracks is  $30^{\circ}$ , neither wing cracks nor secondary cracks are obtained if the cracks are closed. Specimens with such pre-existing cracks fail at a high stress level, caused by intact material failure. As mentioned before, the closed cracks in our specimens have a friction angle of approximately  $35^{\circ}$ , therefore, closed cracks with the inclination of  $30^{\circ}$  can not slide. This phenomenon suggests that the sliding or the failure of the closed crack

itself is the essential condition for the occurrence of wing cracks and secondary cracks.

#### 4. Critical load of coalescence

The coalescence loads of different specimens are plotted in Fig.11. The data in Fig.11 can be summarized as follows: i). The occurrence of coalescence of closed cracks requires a higher uniaxial stress than that of open cracks. The difference is about 4MPa or 25%. ii). Coalescence occurs at lower loads when the bridge inclination is within the range 60°-90°. In this case, coalescence is caused mainly by mixed tensile and shear failure. When the bridge inclination is 45° (coalescence is through secondary apparent shear cracks) or 105° (coalescence is through wing cracks), the coalescence load is higher. iii). Variation of crack inclination has a minor influence on the coalescence load.

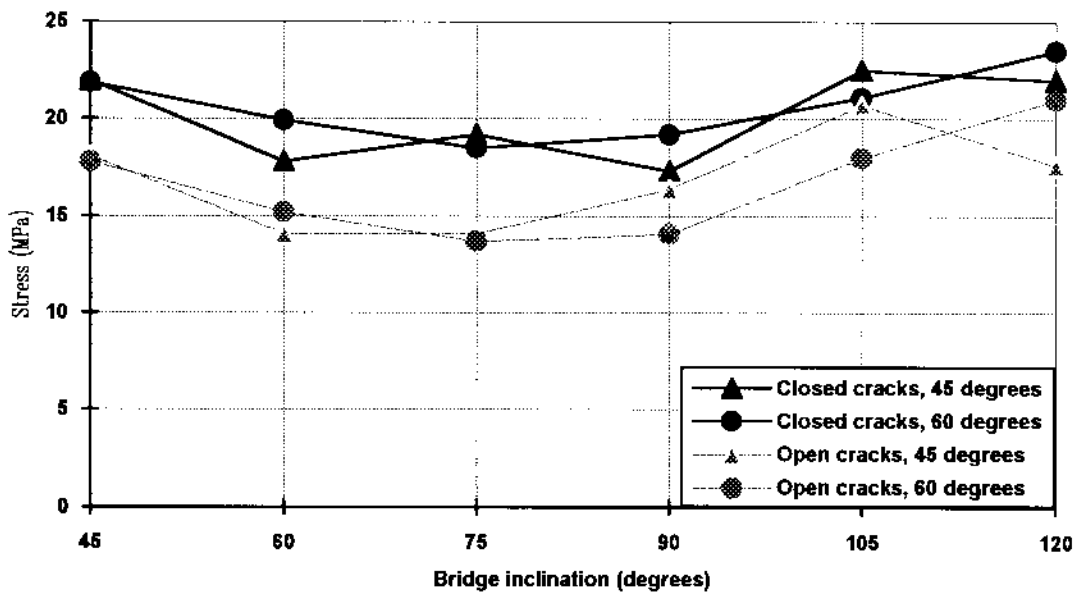


Fig.11. The critical uniaxial stress of coalescence for open and closed cracks.

Fig.12 shows typical stress-strain curves for two specimens, one with open cracks and the other with closed cracks. The loading curve before coalescence shows a slight non-linearity for both specimens, which is possibly caused by wing crack initiation and propagation. The specimen with closed cracks has a slightly steeper stress-strain curve than the specimen with open cracks. This is because the open cracks make the specimen more deformable than the closed cracks. A strong hysteresis is observed for both cases during unloading. The

friction along pre-existing cracks and/or the coalescence cracks is believed to be the main reason for such a hysteresis, (see Shen and Stephansson [5][14]).

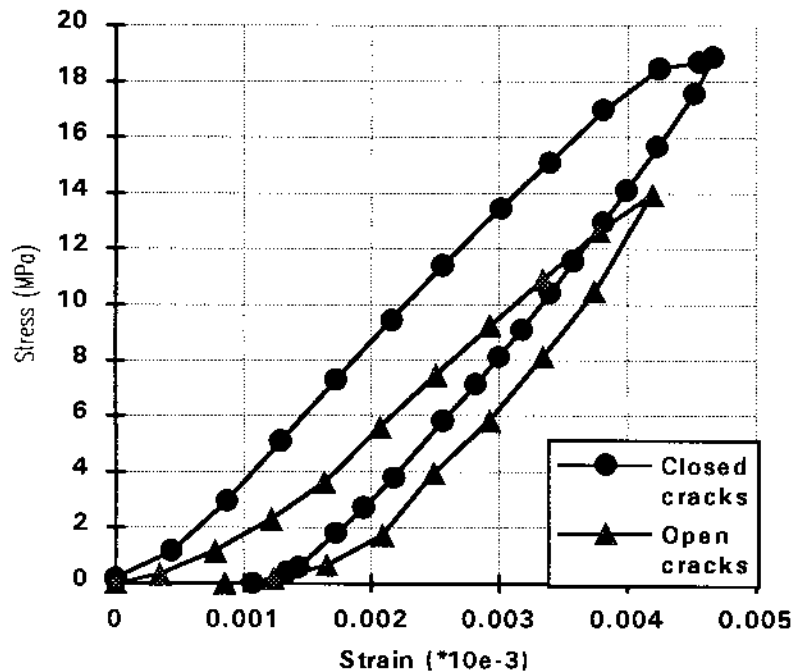


Fig.12. Loading and unloading curves of two  $60^{\circ}/75^{\circ}$  specimens with open cracks and closed cracks, respectively.

Another important conclusion can be drawn from the loading and unloading curves in Fig.11: the energy loss during the process of loading—coalescence—unloading, which is equal to the area enclosed by the curve, for closed cracks is approximately twice of that for open cracks. This can be explained by the sliding along the pre-existing closed cracks.

##### 5. Crack branching and the change of propagation mode.

In one of the  $45^{\circ}/120^{\circ}$  specimens with closed cracks, we have observed a crack branching, see Fig.13. The branching is actually caused by the change of propagation mode. The initial crack developed from the pre-existing crack tip is parallel to the loading direction and has an evident opening between its surfaces. This crack is believed to be a tensile crack. Then the tensile crack branches to a shear crack, followed by the occurrence of another tensile crack. The shear crack is characterized by a narrow damage zone. Along this damage zone we do not observe any opening between crack surfaces which a tensile crack always has. By carefully examining the pre-existing polishing marks on specimen surfaces,

we find small shear dislocations along this zone. The shear crack in this specimen has not extended to the boundary but terminates inside the specimen.

Even though there are many observations of shear fracturing and change of fracture mode in natural rock masses, the evidences of a mode II crack propagation and the changes of propagation mode have rarely been obtained in the laboratory. The results presented in Fig.13 prove that crack propagation with changing mode can occur during uniaxial loading of small specimens.

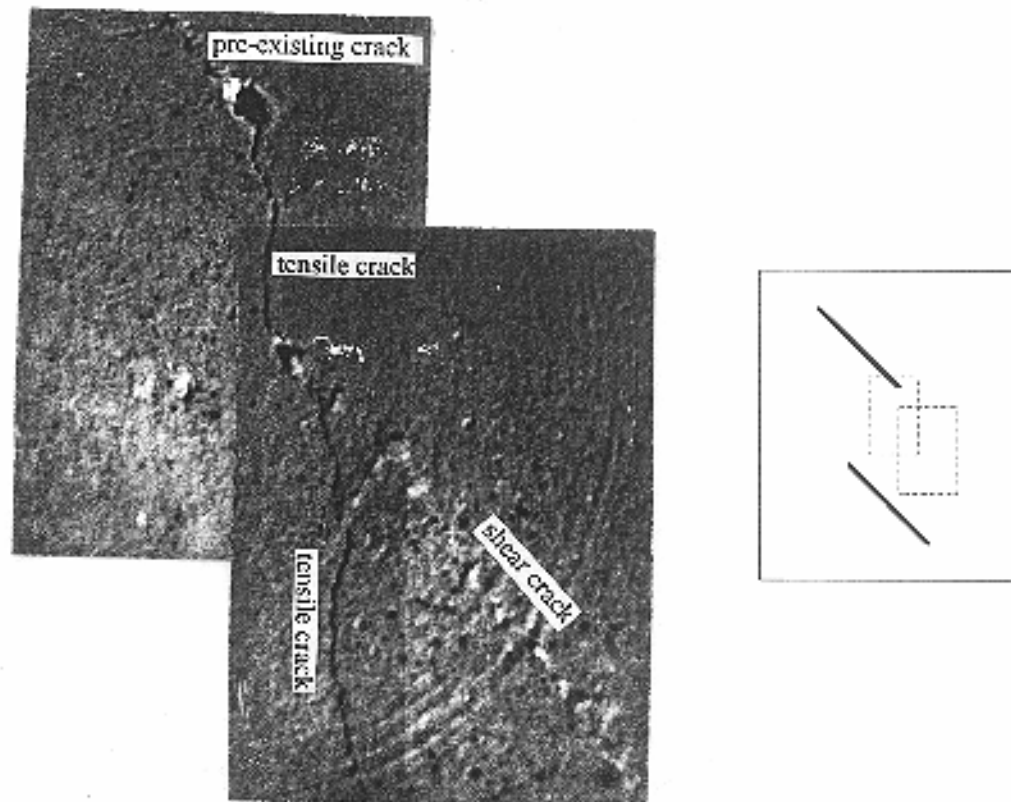


Fig.13. Crack propagation with changing failure mode and crack branching. Specimen  $45^\circ/120^\circ$  with closed cracks.

## Explanation and Discussion

### 1. Wing cracks

We have observed during the tests that the wing cracks developed from a closed pre-existing crack have a smaller angle relative to the pre-existing cracks and are thus less curved than those developed from an open crack. This difference can be explained by looking at the stress distribution in the vicinity of the pre-existing crack (Fig.14). An open pre-existing crack redistributes the



stress field and the wing cracks have to take a curved path to follow the maximum principal stress (Fig.14a). A closed pre-existing crack, however, does not cause a significant change of the stress-field, and therefore, the direction of the maximum principal stress near the crack tips is close to the direction of loading. The wing cracks are then initiated and propagate in almost the same direction as the applied load and along a straight path (Fig.14b).

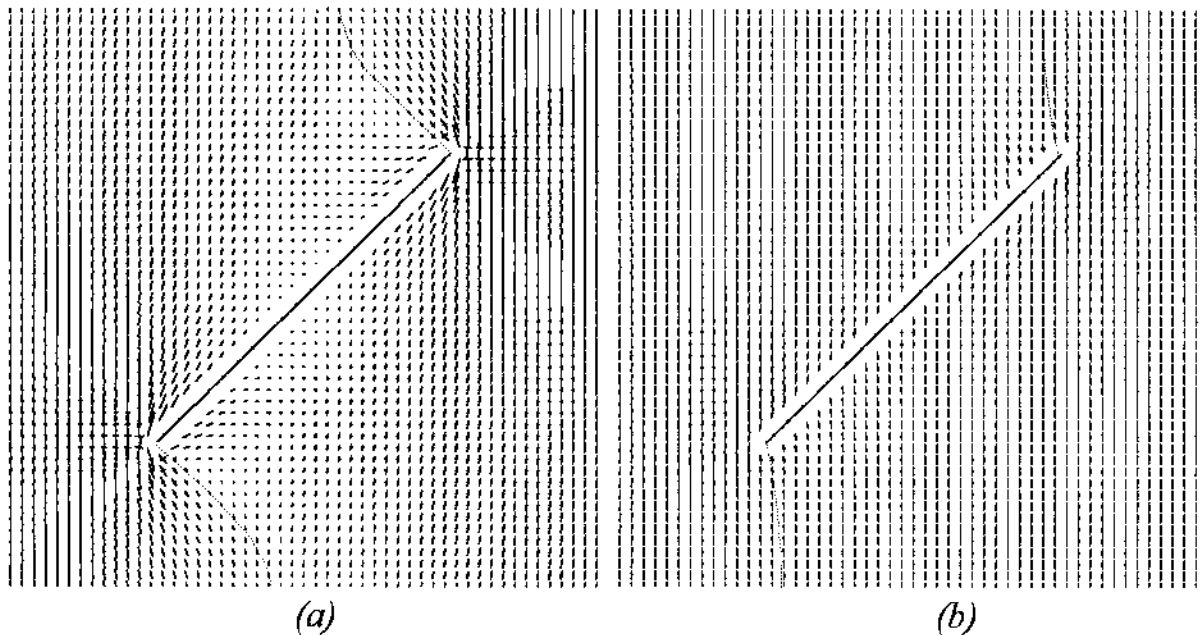


*Fig.14. Principal stress distribution in the vicinity of an open crack (a) and a sliding crack (b) under uniaxial compressive loading.*

We also applied an existing numerical method [15][16] to simulate the different wing crack path for open and closed pre-existing cracks (Fig.15). This numerical simulation suggests that the curvature of wing cracks mainly depends on the normal stiffness of the pre-existing cracks. High normal stiffness favours straight wing cracks. Since closed cracks have high contact stiffness while open cracks have zero contact stiffness, this explain also why closed cracks are associated with straight wing cracks and, to generalize, why joints in rock masses are usually straight and planar.

## *2. Coalescence caused by secondary cracks in shearing.*

It has been discussed in this paper that with low bridge inclination coalescence is caused by secondary cracks, which are apparently shear cracks. The reason why such a geometry induces shear cracks can be found from stress analysis, see Fig.16. After the occurrence of wing cracks there is no tensile stress along the

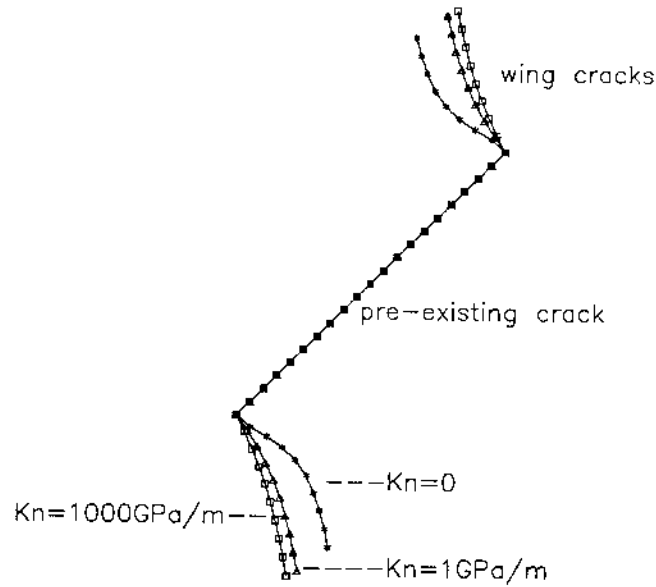


Fig.15. Numerical simulation of wing cracks at different normal stiffness of a pre-existing crack. The pre-existing crack is 2.83 m long, has no cohesion and friction and is loaded in uniaxial compression.

coalescence path. However, high shear stresses exist inside the bridge and the maximum shear stress appears at the crack tip and is directed along the path of coalescence. The secondary cracks are initiated at the crack tips where the shear stress reaches its maximum, and they propagate in the direction of maximum shear stress, i.e. the direction parallel to the pre-existing cracks. Coalescence occurs when the secondary cracks meet inside the bridge.

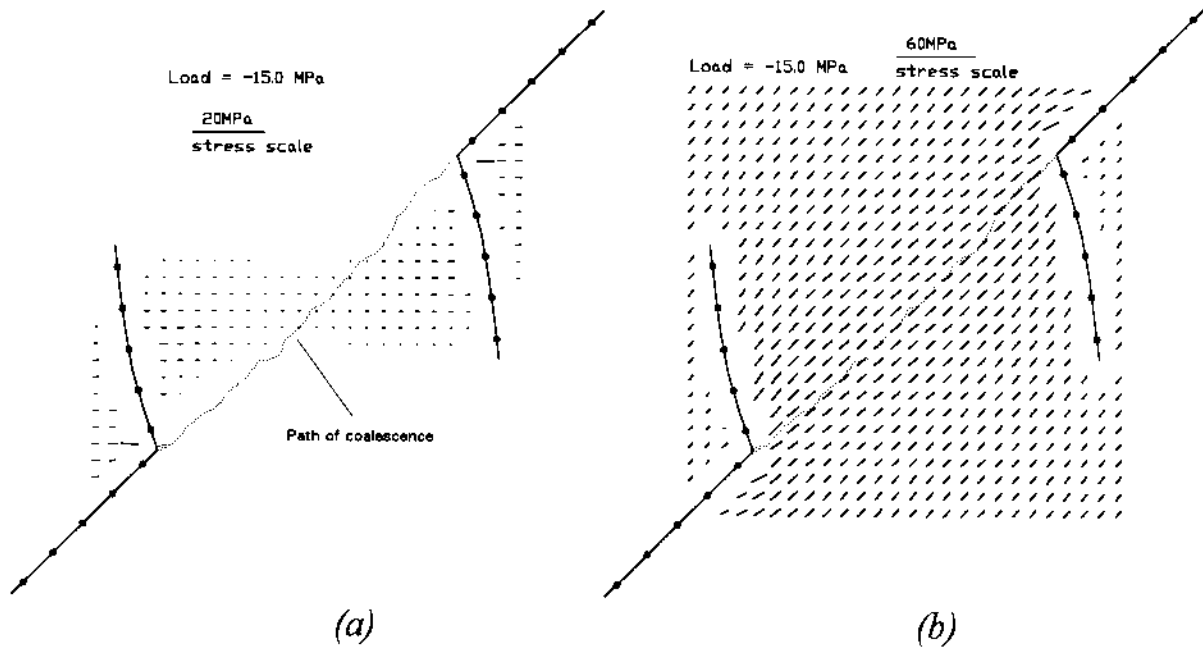


Fig.16. Stress distribution in the bridge between two closed  $45^{\circ}/45^{\circ}$  cracks after the occurrence of wing cracks. (a) Tensile stress field; (b) maximum shear stress field.

### 3. Coalescence caused by secondary cracks in combined tension and shear.

The secondary crack shown in Fig.7 can be explained by the stress distribution inside the bridge, see Fig.17. The extension of wing cracks causes an almost uniformly distributed tensile stress field in the bridge. The maximum tensile stress appears at the center of the bridge and reaches 2.85 MPa when the applied load is 15 MPa. The gypsum mixture was reported to have the tensile strength of about 2.3 MPa [12]. Therefore, a tensile failure can occur in the central part of the bridge. Close to the pre-existing crack tip there is zero tensile stress (Fig.17a) but the shear stress reaches a maximum (Fig.17b). Consequently, the failure in this part of the bridge is caused by shearing. This confirms the experimental observations that the secondary crack at the center of the bridge is a tensile crack while the failure near the crack tips is caused by shearing.

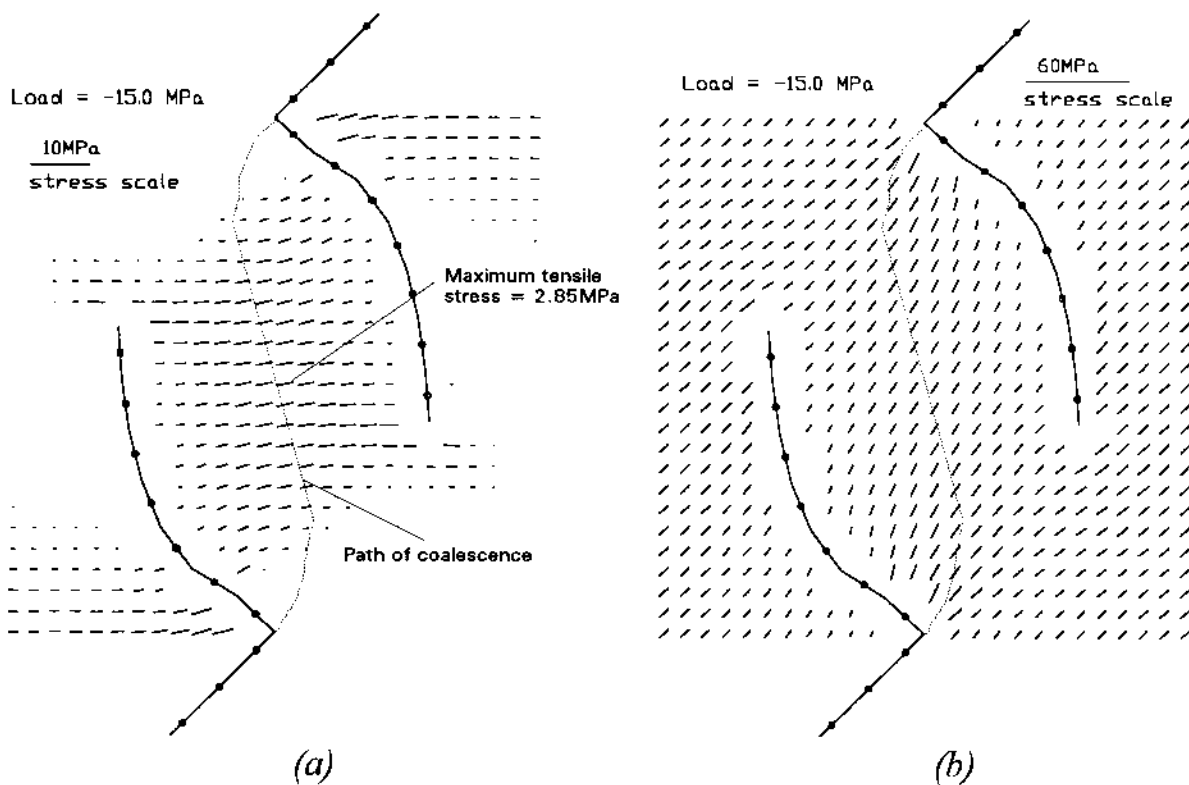


Fig.17. Calculated stress distribution in the vicinity of the bridge between two  $45^\circ$  closed cracks after the occurrence of wing cracks, as shown in Fig.7. The pre-existing cracks have been assigned with the stiffness  $K_n=K_s=10\text{GPa/m}$ , and the friction angle is  $\phi=35^\circ$ . (a) Tensile stress; (b) maximum shear stress.

#### *4. Mode II crack propagation.*

Whether mode II crack propagation can occur in nature is still a topic of discussion in the field of fracture- and rock mechanics. Laboratory tests in materials such as steel, glass, ceramics, polymer, etc. do not produce mode II cracks. However, this study with gypsum material shows that mode II crack can occur. Tests on other earth materials like rock and concrete have also produced mode II cracks [17][18]. Whether mode II crack can occur or not seems thus to depend on the type of material [19][20]. The authors' explanation of this phenomenon is because of the porosity of a material. The first group of materials (steel, glass, etc.) have almost zero porosity and smaller grain size, while the second group (rock, concrete, gypsum etc.) have larger porosity and grain size. The porosity of a material is thought to enhance mode II crack development and propagation. Mode II crack propagation is always accompanied by dilation and volume increase in the fracture process zone. If a material has zero porosity, dilation will be transferred into high stresses which resist the development and propagation of mode II cracks. In a material with high porosity, however, the increase of volume in the process zone will be absorbed by the existing voids and flaws and, therefore, resisting stresses cannot develop. To validate this explanation, further physical or numerical experiments for materials with different porosities would be interesting and helpful.

## Conclusions

The experimental study demonstrates that specimens with closed cracks have two major characteristics which are different from specimens containing open cracks: i) they generate straight wing cracks instead of curved ones; ii) the coalescence load of closed cracks is about 25% higher than that of open cracks.

The mechanism of coalescence for two pre-existing cracks is fairly complicated and it is highly dependent upon the inclination of the bridge. With low rock bridge inclination, coalescence is apparently caused by shear failure, while opposite for high bridge inclination coalescence is generated in tension. The coalescence induced by shear failure develops from the tips to the bridge center, while coalescence induced by combined tensile and shear failure often starts from the bridge center and to the crack tips.

## Acknowledgement

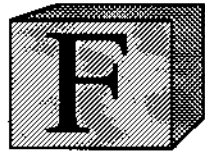
The authors would like to thank Prof. J. Hudson for his comments to the first draft of this manuscript.

## References

1. Griffith A.A. The phenomena of rupture and flow in solid. *Phil. Trans. Roy. Soc.* **A221**, 163-197. (1921)
2. Kachanov, M.L. A microcrack model of rock inelasticity — Part I and Part II. *Mech. Mater.* **1**, 29-41. (1982)
3. Kemeny J.M. and Cook N.G.W. Effective moduli, non-linear deformation, and strength of a cracked elastic solid. *Int. J. Rock Mech. Min. Sci.* **23**, 107-118. (1986)
4. Wong T-F. Micro-mechanics of faulting in Westerly granite. *Int. J. Rock Mech. Min. Sci.* **19**, 49-64. (1982)
5. Shen B. and Stephansson O. Deformation and propagation of finite joints in Rock masses. *Proc. Fractured and Jointed Rock Masses (preprint)*, 312-318. (1992)
6. Einstein H.H., Veneziano D., Baecher G.B. and O'reilly K.J. The effect of discontinuity persistence on rock stability. *Int. J. Rock Mech. Min. Sci. & Geomech. Abs.* **20(5)**, 227-237. (1983)
7. Deng Q. and Zhang P. Research on the geometry of shear fracture zones. *J. Geophy. Res.* **89**, 5699-5710.
8. Lajtai E.Z. Shear strength of weakness planes in rock. *Int. J. Rock Mech. Min. Sci. & Geomech. Abs.* **6**, 299-515. (1969).
9. Segall P. and Pollard D. Mechanics of discontinuous faults. *J. Geophy. Res.* **85(B8)**, 4337-4350. (1980)
10. Horri H. and Nemat-Nasser S. Brittle failure in compression: splitting, faulting and brittle-ductile transition, *Phil. Trans. Roy. Soc.*, **319 (1549)**, 337-374. (1986)
11. Reyes O. and Einstein H.H. Failure mechanism of fractured rock — A fracture coalescence model. *Proc. 7th Int. Con. on Rock Mechanics*, **1**, 333-340. (1991)
12. Nelson R. Modelling a jointed rock mass. S.M. Thesis, Massachusetts Institute of Technology. (1968)

13. Ghahreman B. Some suggested methods for producing gypsum specimens containing closed cracks. Internal report, Massachusetts Institute of Technology, 1992.
14. Shen B. and Stephansson O. Cyclic loading characteristics of joints and rock bridges in a jointed rock specimen. *Proc. Int. Symp. Rock Joints* (ed. N. Barton and O. Stephansson). 725-729.(1990)
15. Shen B. and Stephansson O. Modification of the G-criterion for crack propagation subjected to compression. *Engineering Fracture Mechanics*. (1993) (in press)
16. Shen B. and Stephansson O. Numerical analysis of mixed mode I and mode II fracture propagation. *Int. J. Rock Mech. Min. Sci. & Geomech. Abstr.* (Special issue for 34th U.S. Symp. on Rock Mech.). (1993) (in press)
17. Bazant Z.P. and Pfeifer. P.A. Shear fracture tests of concrete, *Materials and structures*, **19**, 111-121. (1986)
18. Jung S.J., Enbaya M. and Whyatt J.K. The study of fracture of brittle rock under pure shear loading. *Proc. Fractured and Jointed Rock Masses* (preprint), 458-475. (1992)
19. Melin S. Why are crack paths in concrete and mortar different from those in PMMA? *Material and Structure*, **22**, 23-27. (1989)
20. Reyes O. Experimental study and analytical modelling of compressive fracture in brittle material. Ph.D Thesis, Massachusetts Institute of Technology. (1991)





**The mechanism of fracture coalescence in  
compression — Experimental study and  
numerical simulation.**

*B. Shen*

*Int. J. Eng. Frac. Mech. (1993) (Submitted)*



# **The Mechanism of Fracture Coalescence in Compression — Experimental Study and Numerical Simulation**

B. Shen

Engineering Geology, Royal Institute of Technology, S-10044 Stockholm

## **Abstract**

The mechanism of fracture coalescence is reported from uniaxial compression of gypsum samples with two open or closed cracks. Coalescence can be caused by tensile failure, shear failure or mixed tensile and shear failure. In this paper, the coalescence observed in the tests are modelled numerically by using a modified G-criterion and displacement discontinuity method (DDM). The numerically predicted path and critical load of coalescence are in good agreement with the experimental results. It is also unveiled by this study that mode II failure is the key reason for the coalescence between two non-overlapping cracks.

## **Introduction**

Fracture coalescence means the connection or merging of two or more fractures (or cracks) due to fracture propagation. The failure of a material with pre-existing fractures, such as jointed rock masses, is usually controlled by the coalescence of fractures [1]. Therefore, study of the mechanism of fracture coalescence is of crucial importance in the study of the strength of fractured and jointed material such as rock masses and in particular the stability analysis of underground excavations and other rock engineering.

A number of experimental studies of fracture coalescence have been carried out [2-7]. Lajtai [2] studied the failure mode between two parallel slots in rock samples by using shear box tests. Bazant and Pfeiffer [3] and Jung et al [4] performed direct shear test of double-notched beams in concrete and rocks. Horii and Nemat-Nasser [5] carried out biaxial compressive loading tests in polymer material with a number of small flaws. Reyes and Einstein [6] performed uniaxial compressive loading tests of gypsum samples with two inclined flaws. In these tests, the fractures were simulated by using slots or flaws without surface contact and friction. To study the coalescence of rock fractures with surface contact and friction, Shen et al [7] recently conducted a series of uniaxial compression tests

of gypsum samples and systematically studied the coalescence of open and closed fractures generated from pre-existing cracks. It was observed that, depending on the configuration and the contact condition (open or closed) of the pre-existing cracks, coalescence can be caused by tensile failure, shear failure or mixed mode failure. The coalescing fractures can start from the tip of pre-existing cracks or from the center of the bridge between the pre-existing cracks.

Some numerical studies were reported to simulate the coalescence by using damage model [6] and mode I failure model [8]. In our previous study, we introduced a modified G-criterion and combined it with the displacement discontinuity method (DDM) to predict the mixed mode I and mode II propagation [9]. This approach has been demonstrated to predict the fracture coalescence caused by both tensile failure and shear failure [10] and it will be applied in this study.

### Experiments

The experiments were conducted by using pre-cracked gypsum samples subjected to uniaxial loading. The size of the samples is length/width/thickness = 152/76/30 mm. Two cracks were created during sample curing with the length of 12.7 mm each and separated by 12.7 mm between their inner tips (Fig.1). Two

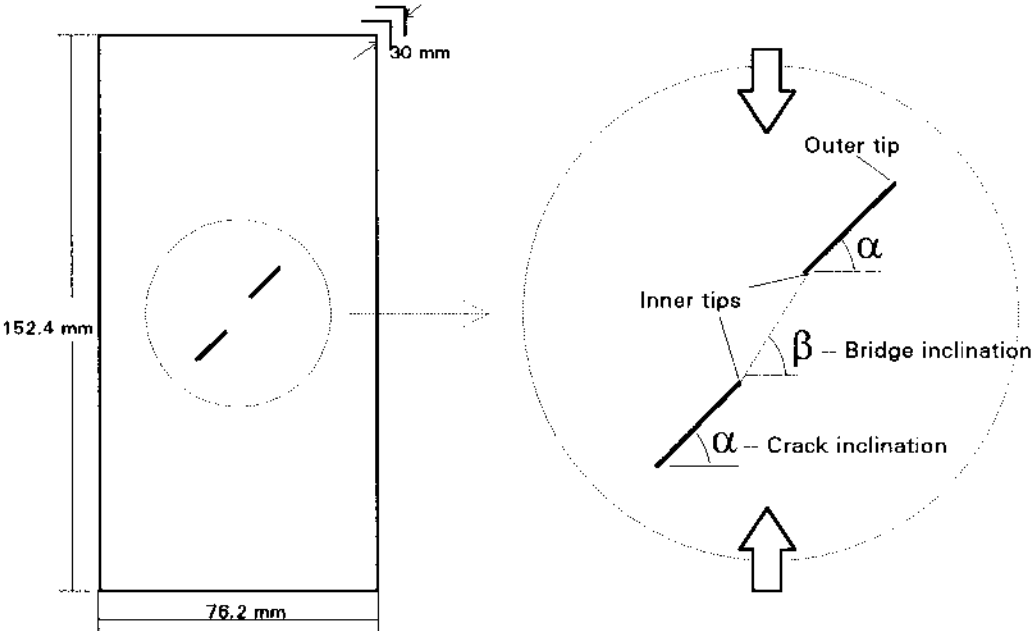


Fig.1. Geometry of gypsum samples and pre-existing cracks.

types of pre-existing cracks were used: 1) open crack, which was created by pre-installing a thin steel sheet (0.04mm) and pulling it out *after* curing the gypsum mixture; 2) closed crack, generated by pre-installing a stretched polyethylene sheet (thickness 10 $\mu$ m) and pulling it out *during* curing. The pull-out time controlled the contact condition of the closed crack. The bridge inclination ( $\beta$ ) varied from 45° to 120° and the crack inclination ( $\alpha$ ) from 30° to 60°, both with an interval of 15°. The process of coalescence and failure mechanism was monitored during the test by using a microscope and video recorder. The failure process can be studied by replaying the recorded message at a speed 480 times slower than the real speed.

Fracture coalescence occurred for most crack and bridge inclinations, except for the crack inclination of 30° at which no fracture propagation was found. The coalescence was caused by different failure modes, mainly depending on bridge inclination and crack types. Three different types of coalescence were distinguished as shown in Table 1.

Table 1. Modes of the coalescence with different bridge inclination

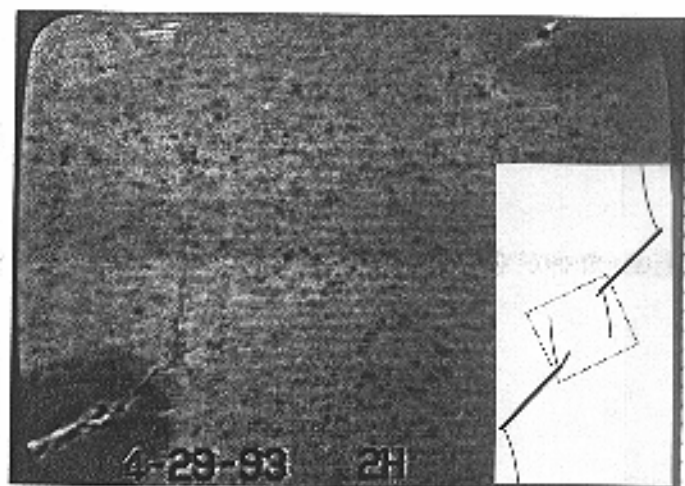
Bridge inclination	Failure mode	Description
45°, 60°	Shear failure	Failure surface was rough and stepped, and often contained pulverized material. Coalescence started from the crack tips
75°, 90°	Tensile failure + Shear failure	Failure surface in central part of the bridge was smooth while near the crack tip it was rough and stepped. Coalescence started from the center of the bridge.
105°, 120°	Tensile failure	Failure surface was smooth and clean. Coalescence started from crack tips

1) *Coalescence by shear failure.*

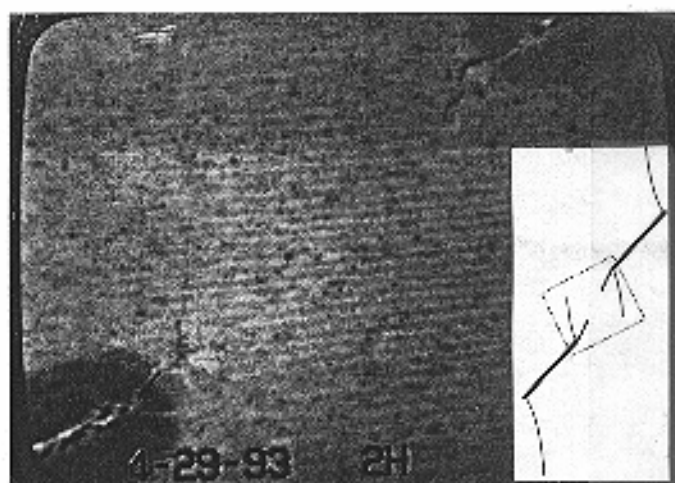
When the bridge inclination was 45° and 60°, coalescence was caused by shear failure. Open and closed pre-existing cracks produced a similar path of coalescence. The typical process of shear-induced coalescence is shown in Fig.2



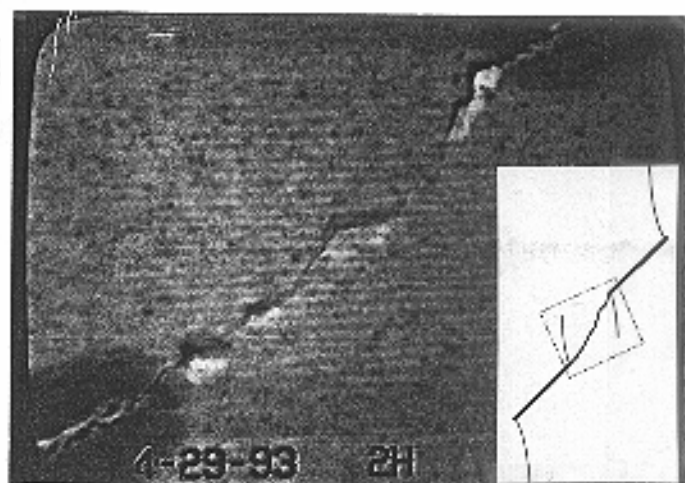
(a)



(b)



(c)



(d)

Fig.2. Development of wing cracks and coalescence from two closed cracks with crack inclination =  $45^\circ$  and bridge inclination =  $60^\circ$  subjected to uniaxial compression. (a) Overview of the gypsum sample after crack coalescence and the development of wing cracks; (b) close-eye view in the area of bridge: wing cracks and secondary cracks were initiated from the tips of pre-existing cracks; (c) the secondary cracks were propagating; (d) the secondary cracks finally coalesced. The time interval of (b), (c) and (d) was about 0.02 seconds.

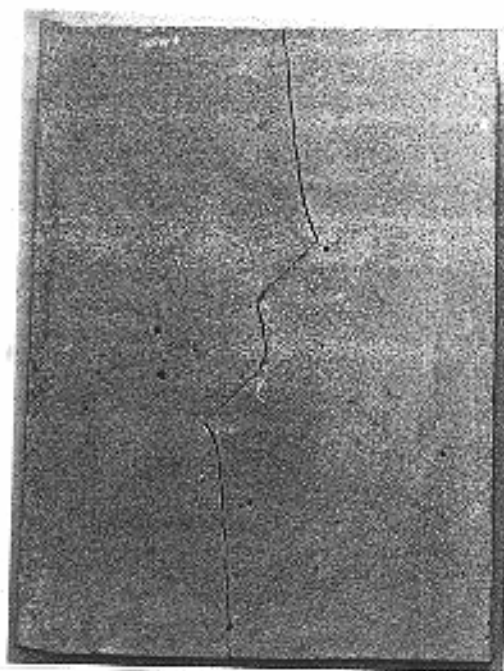
for the sample with crack inclination=45° and bridge inclination=60° (45°/60°), with closed cracks. When the uniaxial load was 18 MPa, wing cracks and secondary cracks were developed simultaneously from the tips of pre-existing crack tips. The secondary cracks propagated very quickly and merged in the bridge. Following the coalescence the wing cracks which developed from the inner tips were closed, while those from the outer tips extended to the boundary of the sample. The surface of the secondary cracks was rough and stepped, which is the characteristic of shear failure. The surface of the wing cracks was smooth and clean, indicating that the failure was caused by tension.

### *2). Coalescence by mixed tensile and shear failure.*

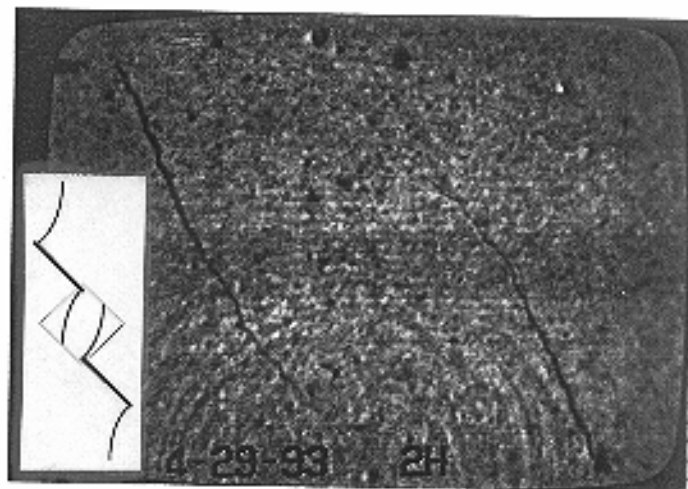
For the bridge inclinations of 75° and 90°, both tensile and shear failure were interacting in the process of coalescence. The coalescence did not start from the crack tip but from the center of the bridge, as demonstrated in Fig.3 for sample 45°/90° with closed cracks. Wing cracks were initiated from the crack tips at the stress level of 10 MPa and they grew with increasing load. At 17 MPa, the wing cracks formed an elliptical core between the two tips of pre-existing cracks. Then a tensile crack suddenly appeared at the center of the bridge and extended in the direction almost parallel to the wing cracks and finally a coalescence was formed. The coalescence near the tip of pre-existing cracks has the surface characteristics of shear failure while that in the central part of the bridge has the typical characteristics of tensile failure with smooth fracture surface.

### *3). Coalescence by tensile failure.*

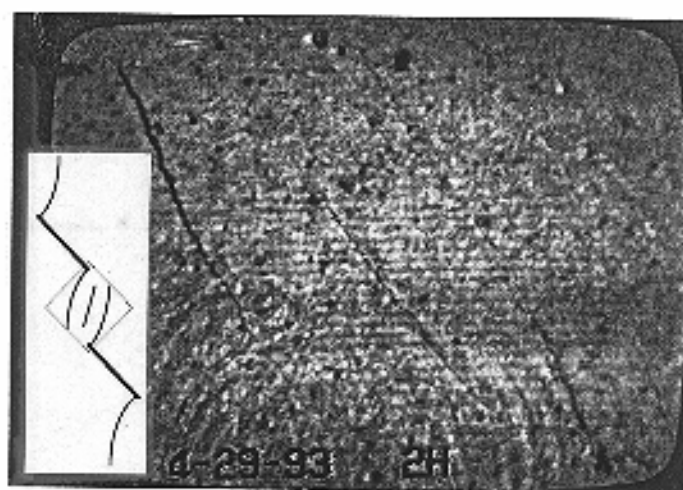
For bridge inclinations of 105° and 120°, coalescence was caused by wing cracks initiated from the crack tips and propagating in the bridge (Fig.4). For some of the experiments the coalescence was formed by a wing crack from one inner tip to the other inner tip, or from one inner tip to the center part of another pre-existing crack. The type of the pre-existing cracks (open or closed) has a strong influence on the path of the failure. Open pre-existing cracks produced strongly curved wing cracks, while closed pre-existing cracks resulted in straight wing cracks, oriented almost parallel to the direction of loading.



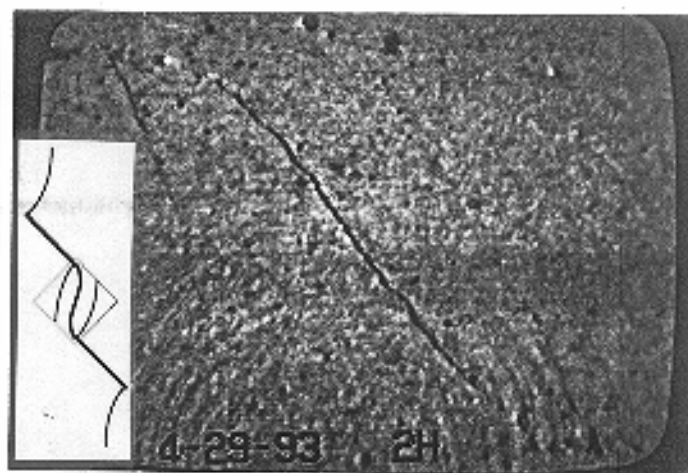
(a)



(b)



(c)



(d)

Fig.3. Coalescence of two closed cracks with crack inclination =  $45^\circ$  and bridge inclination =  $90^\circ$  subjected to uniaxial compression. (a) Overview of the sample after coalescence and development of wing cracks; (b) close-eye view of wing crack initiation and propagation; (c) occurrence of secondary crack inside the bridge; and (d) final coalescence.

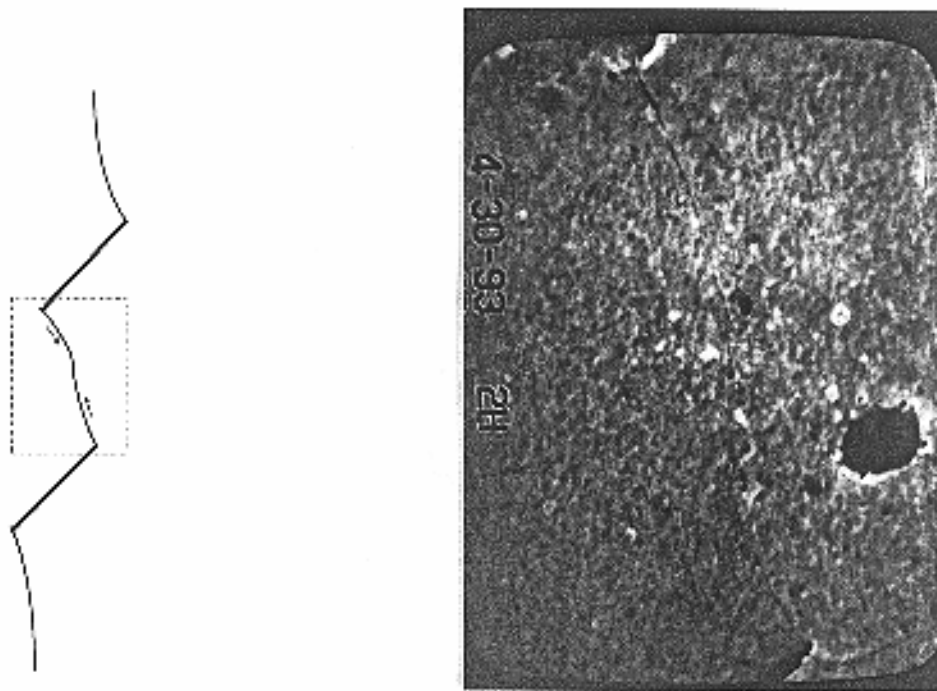


Fig.4. The path of coalescence of two 45°/105° closed cracks. Coalescence was formed by two wing cracks initiated from the two inner tips.

Open and closed pre-existing cracks had different load when coalescence occurred. The average load at coalescence of two closed cracks is about 25% higher than that of two open cracks, Fig.5. When the inclination of pre-existing cracks was 30°, which is less than the friction angle of the closed cracks (about 35°), closed pre-existing cracks did not coalesce while the open pre-existing cracks did. This means that the sliding of the pre-existing cracks is the essential condition for crack coalescence. Beyond the strength of pre-existing cracks, no crack initiation and propagation can occur.

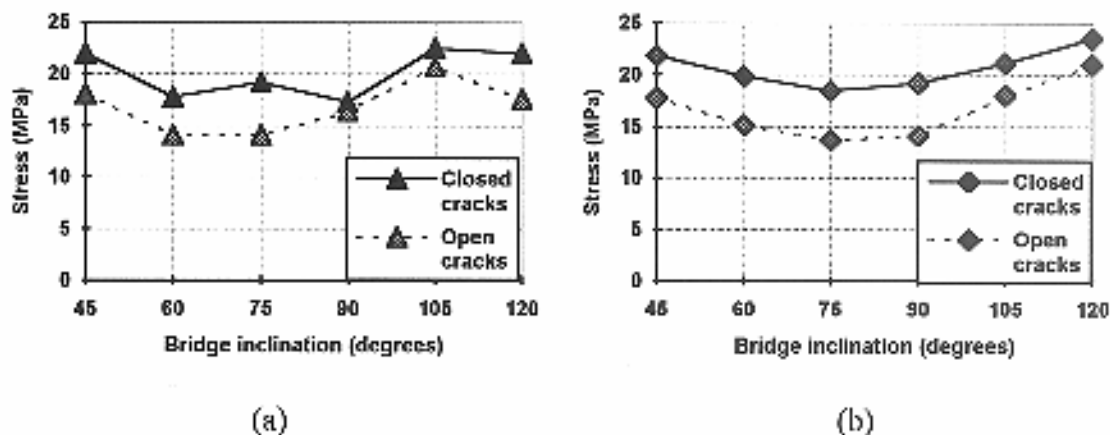


Fig.5. The average uniaxial stress of coalescence of open and closed cracks. (a) Crack inclination = 45°; (b) crack inclination = 60°.

## Crack Propagation Criterion and Numerical Technique

There exist many fracture propagation criteria, among which the most commonly used are: (1) the maximum tensile stress criterion [11]; (2) the maximum strain energy release rate criterion (G-criterion) [12]; and (3) the minimum strain energy density criterion (S-criterion) [13]. A criterion must enable the prediction of both mode I and mode II crack propagation to be applicable to the crack coalescence described above .

The maximum tensile stress criterion takes into account only the tensile stress and, therefore, does not predict mode II crack propagation. The G-criterion and the S-criterion are energy-based criteria and they have the potential to predict both mode I and mode II failure. The G-criterion is considered in our studies. However, our previous studies [9] have shown that, when applied to crack propagation under compressive load, the original G-criterion can lead to wrong results, especially for the direction of wing crack initiation. The original G-criterion does not consider the difference between mode I surface energy ( $G_{Ic}$ ) and mode II surface energy ( $G_{IIc}$ ). Therefore, a modified G-criterion, called the F-criterion, has been proposed (see Shen and Stephansson [9]). The F-criterion takes the form

$$F = \frac{G_I}{G_{Ic}} + \frac{G_{II}}{G_{IIc}} \geq 1.0 \quad (1)$$

where  $G_I$  and  $G_{II}$  are the loss of strain energy due to crack growth with pure open displacement and with pure shear displacement respectively.  $F$  is a dimensionless factor which searches for its maximum value from different directions of crack growth. The propagation occurs in the direction of maximum  $F$ -value.

The F-criterion has proved to predict both tensile and shear crack propagation [9] and to handle crack initiation from kink tips by means of "fictitious crack growth", Fig.6. Here we assume there is a small crack growth in a certain direction, and then calculate the change of strain energy due to the small crack growth. If the two terms of energy ( $G_I$  and  $G_{II}$ ) satisfy Eq.(1), the "fictitious crack growth" represents a true crack growth.



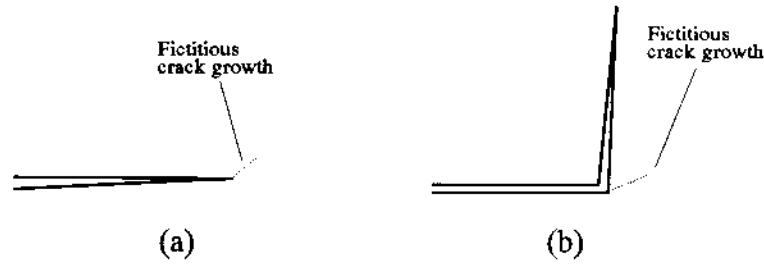


Fig.6. The method of fictitious crack growth to predict crack initiation by using the F-criterion. (a) Sharp crack tip; (b) crack tip with kink.

The F-criterion is implemented into the numerical method DDM to simulate automatic crack growth. In the DDM simulation we consider the fictitious crack growth as a fictitious DDM element with a small length. The fictitious element is allowed to rotate in any direction to find the maximum F-value. When the maximum F-value is found to be greater than 1, a failure is defined and a real DDM element is introduced to represent the new crack in the direction of maximum F-value.

With the DDM technique we can consider the contact and friction along the closed cracks. The contact normal stiffness  $K_n$  and shear stiffness  $K_s$ , friction angle ( $\phi$ ) and cohesion ( $c$ ) are given to the DDM elements. The crack follows Coulomb's friction law, i.e. when the following condition is met, the crack will slide.

$$\sigma_s \geq c + \sigma_n \tan \phi \quad (2)$$

where  $\sigma_n$  and  $\sigma_s$  are the normal and shear stresses acting on crack surface. The use of contact stiffness allows a closed crack to have a 'soft' surface contact in the numerical simulation, i.e., crack surface can contact with small normal and shear displacement. The stress-displacement relation for a closed crack takes the following forms.

Elastic crack:

$$\begin{aligned} \sigma_n &= K_n D_n \\ \sigma_s &= K_s D_s \end{aligned} \quad (3)$$

Sliding crack:

$$\begin{aligned} \sigma_n &= K_n D_n \\ |\sigma_s| &= \sigma_n \tan \phi = K_n D_n \tan \phi \end{aligned} \quad (4)$$

where  $D_n$  and  $D_s$  are the normal and shear displacement of the crack surfaces.

## Simulation Results

The F-criterion and the DDM technique are applied to the experimental tests. Two cracks with different crack inclination and bridge inclination are in an infinite elastic medium subjected to far-field uniaxial compression. The mechanical properties of the elastic material and cracks used in the simulation are listed in Table 2.

Table 2. Mechanical properties used in numerical simulation.

	Intact material	Pre-existing cracks			New developed cracks
		Closed (A)	Closed (B) <sup>§</sup>	Open	
E (MPa)	6200 *				
$\nu$	0.28 *				
$\sigma_t$ (MPa)	2.3 *				
$K_n$ (GPa/m)		500	50	0	10000
$K_s$ (GPa/m)		500	50	0	10000
$\phi$ (°)		35 #	30	0	30
$c$ (MPa)		2.0 #	1.0	0	0
$G_{Ic}$ (J/m <sup>2</sup> )	5 □				
$G_{IIc}$ (J/m <sup>2</sup> )	100				

\* Values according to test results for gypsum material by Nelson [14].

# Values according to tests with small samples containing through-going cracks by Shen et al [7].

□ Value obtained from three-point bending tests of notched gypsum samples.

§ This type of properties is only assigned to the closed cracks in the sample 45°/90° where the crack contact is weaker due to longer curing time before the polyethylene sheets were pulled out during sample preparation.

The simulation is carried out mainly with the crack inclination of 45° and different bridge inclination. A few cases when the crack inclination is 60° are also modeled. In general, the numerical simulation by using the F-criterion and DDM produced the same process of coalescence as has been observed in the experiments. The simulation results for three representative samples are presented.

*1) Coalescence caused by shear failure for sample 45°/60° with closed cracks.*

The simulation results for this crack/bridge inclination are shown in Fig.7. When the uniaxial load reaches 18 MPa, the pre-existing cracks start to slide. Consequently, mode I cracks are initiated from the pre-existing tips and propagate with an almost straight path in the direction of loading. With mode I crack growing, mode II cracks are developed from the kink tips left by the pre-existing cracks and mode I cracks. Mode II cracks from the inner tips propagate in a direction toward the center of the bridge, Fig.7c-e. Finally the mode II cracks coalesce, Fig.7f. The mode I cracks from the inner tips stop and those from outer tips extend longer.

The reasons why the mode II cracks develop at the tips of the pre-existing cracks and propagate to inside the bridge can be found by analyzing the maximum shear stress distribution of the bridge area, see Fig.8. The maximum shear stress in the bridge is directed approximately parallel to a line between the tips of two pre-existing cracks with maximum magnitude at the tips. The extension of the mode I cracks does not influence the maximum shear stress distribution significantly. The maximum shear stress causes the mode II crack initiation and propagation, and this is in agreement with the experimental results at the same uniaxial loading presented in Fig.2.

*2) Coalescence caused by tensile and shear failure for samples 45°/90° with closed cracks.*

The closed pre-existing cracks are assigned the properties of type B (Table 2) to simulate the weaker contact condition observed in the experiment. The simulation results are shown in Fig.9, where mode I cracks are initiated when the uniaxial load is about 6 MPa. The occurrence of mode I cracks induces high tensile stress inside the bridge (Fig.10b). When the load is 15 MPa, the tensile stress is evenly distributed in the bridge (Fig.10c) and the magnitude at the center of the bridge is about 2.4 MPa, which reaches the tensile strength of intact material (2.3 MPa). Therefore, a tensile failure should occur. To simulate the tensile failure, we introduce a small crack inside the bridge along the direction perpendicular to the principal tensile stress. The length of the crack is the critical crack length ( $a$ ) for the material and it is estimated by using the equation for a central crack in an infinite medium under maximum tensile stress ( $\sigma_t$ ):

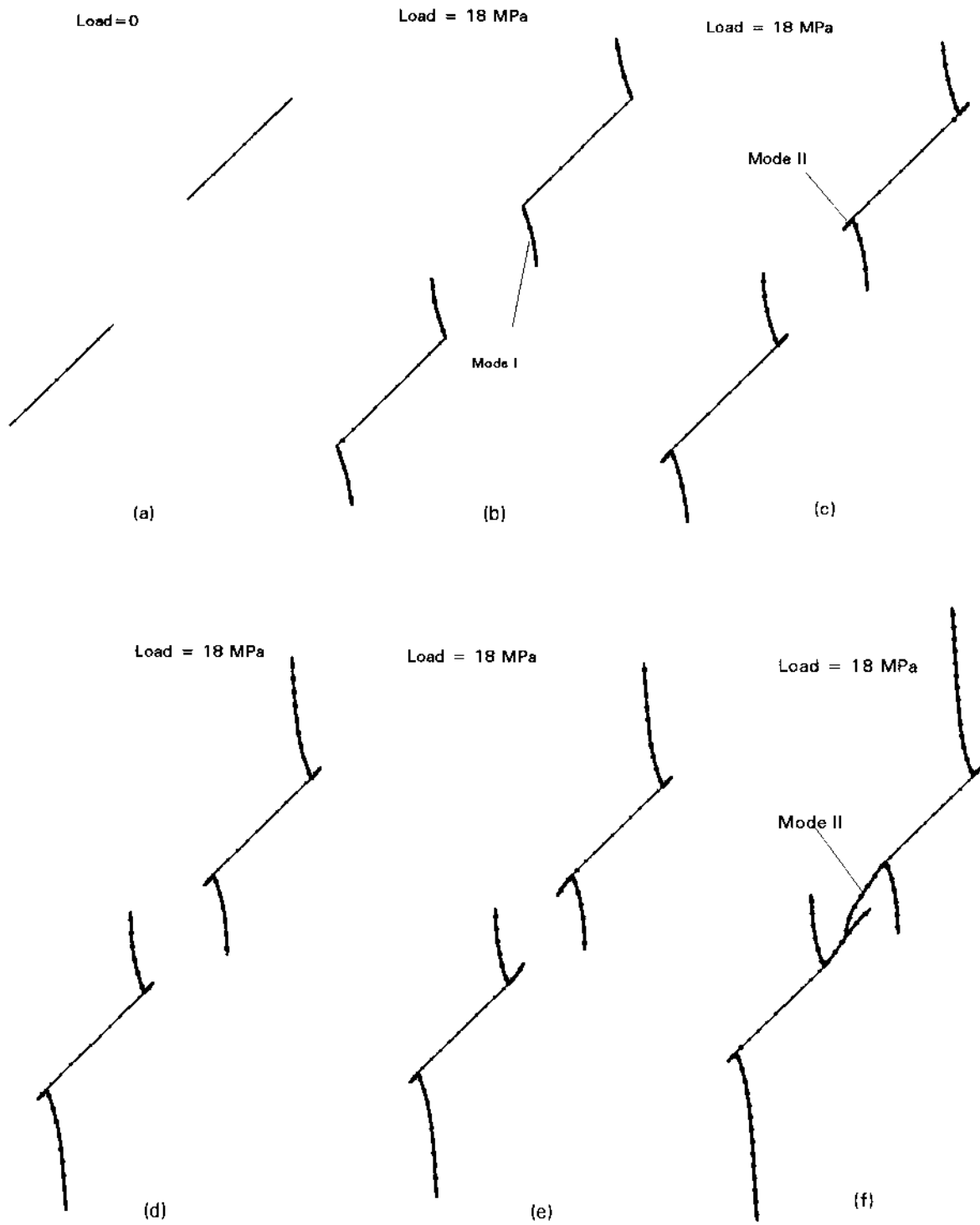


Fig.7. Simulation of coalescence between two 45°/60° closed cracks. (a) Initial state; (b) mode I crack propagation; (c)-(f), mode II crack initiation, propagation and coalescence. Compare with the experimental results in Fig.2.

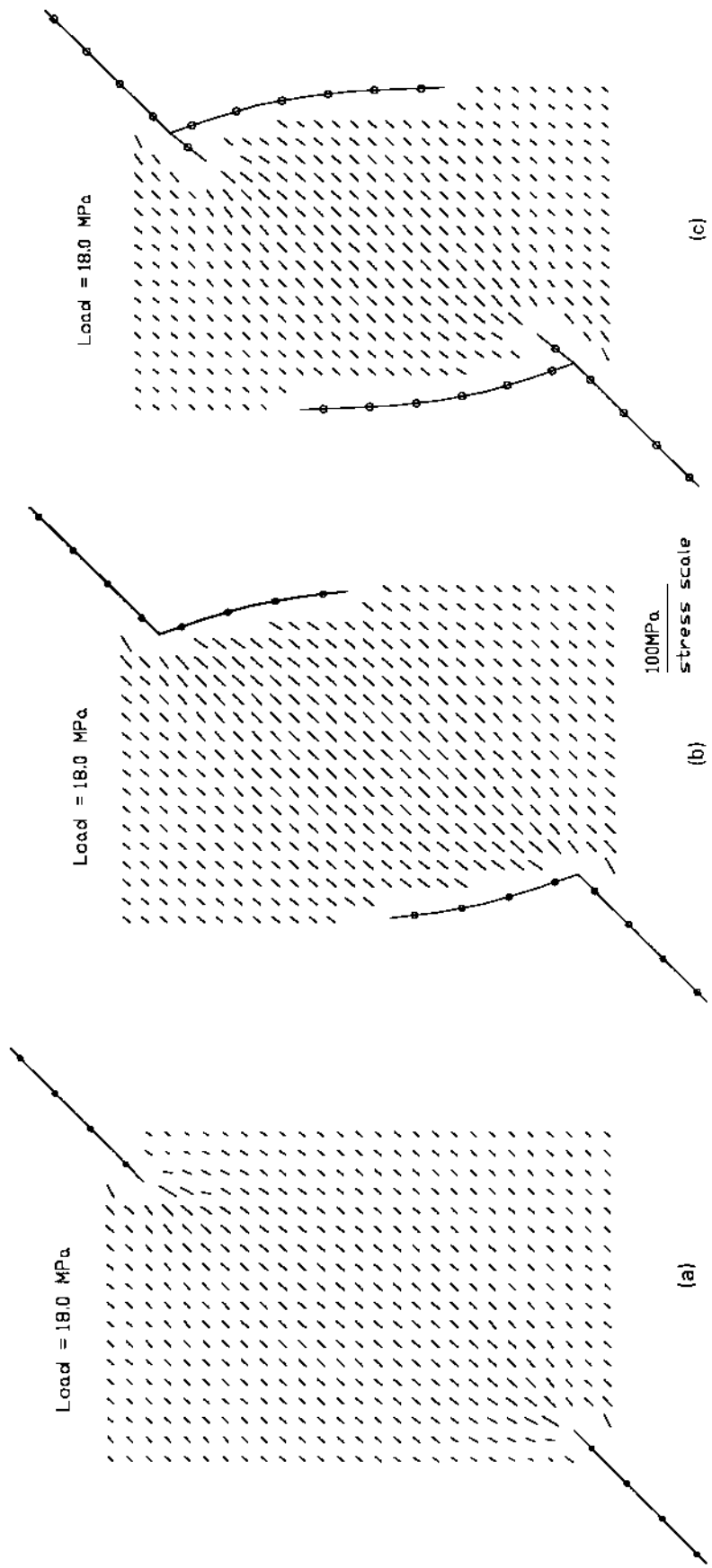


Fig. 8. Maximum shear stress distribution in the bridge area between two 45°/60° closed cracks. (a) Initial state; (b) mode I crack propagation; (c) mode II crack initiation and propagation along the maximum shear stress.

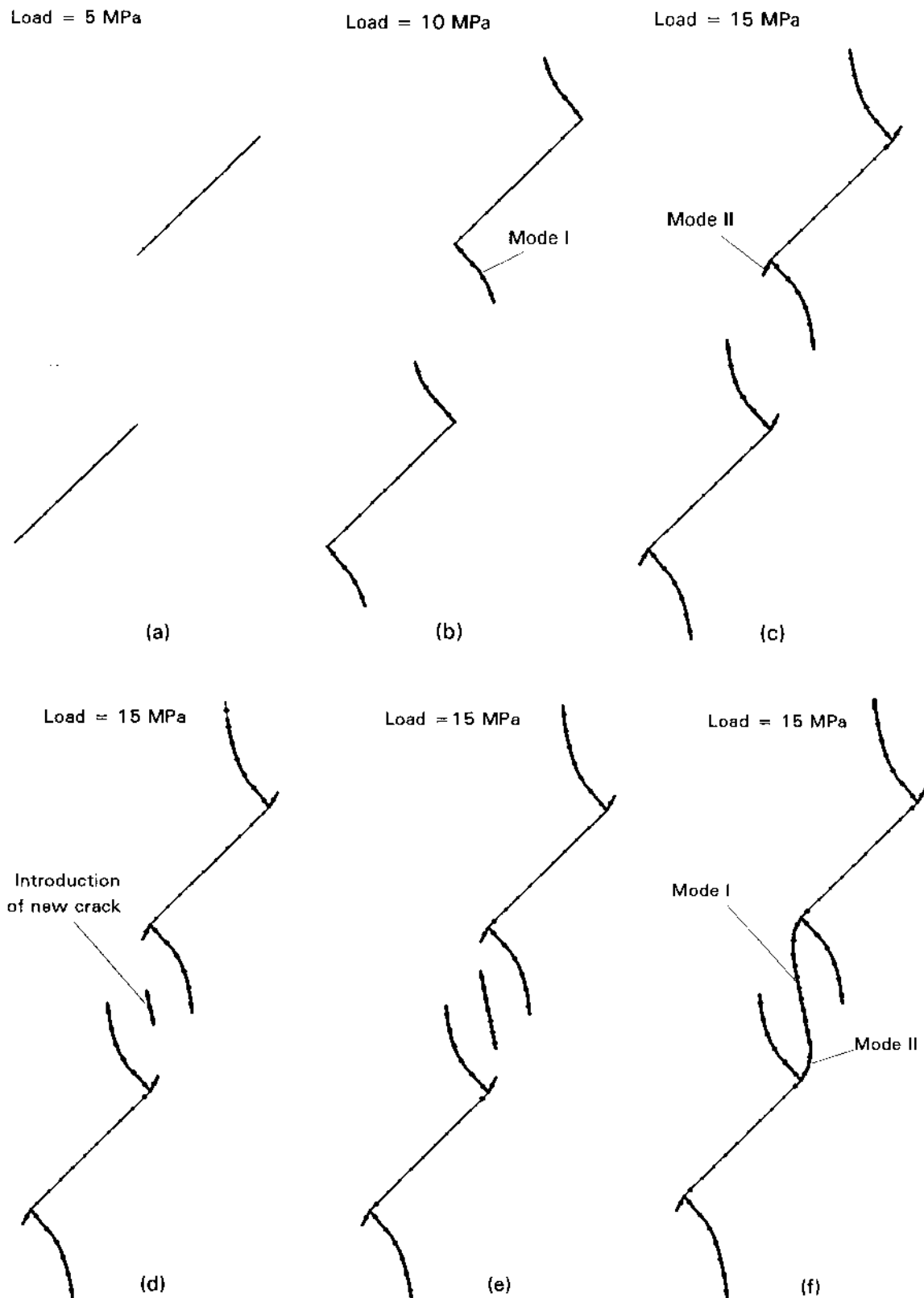


Fig.9. Simulated process of coalescence of two 45°/90° closed cracks in uniaxial loading. (a) Initial state; (b) mode I crack initiation and propagation; (c) mode II crack initiation; (d) tensile failure inside the bridge; (e) growth of the new crack; and (f) final coalescence. Compare with the experimental results in Fig.3.

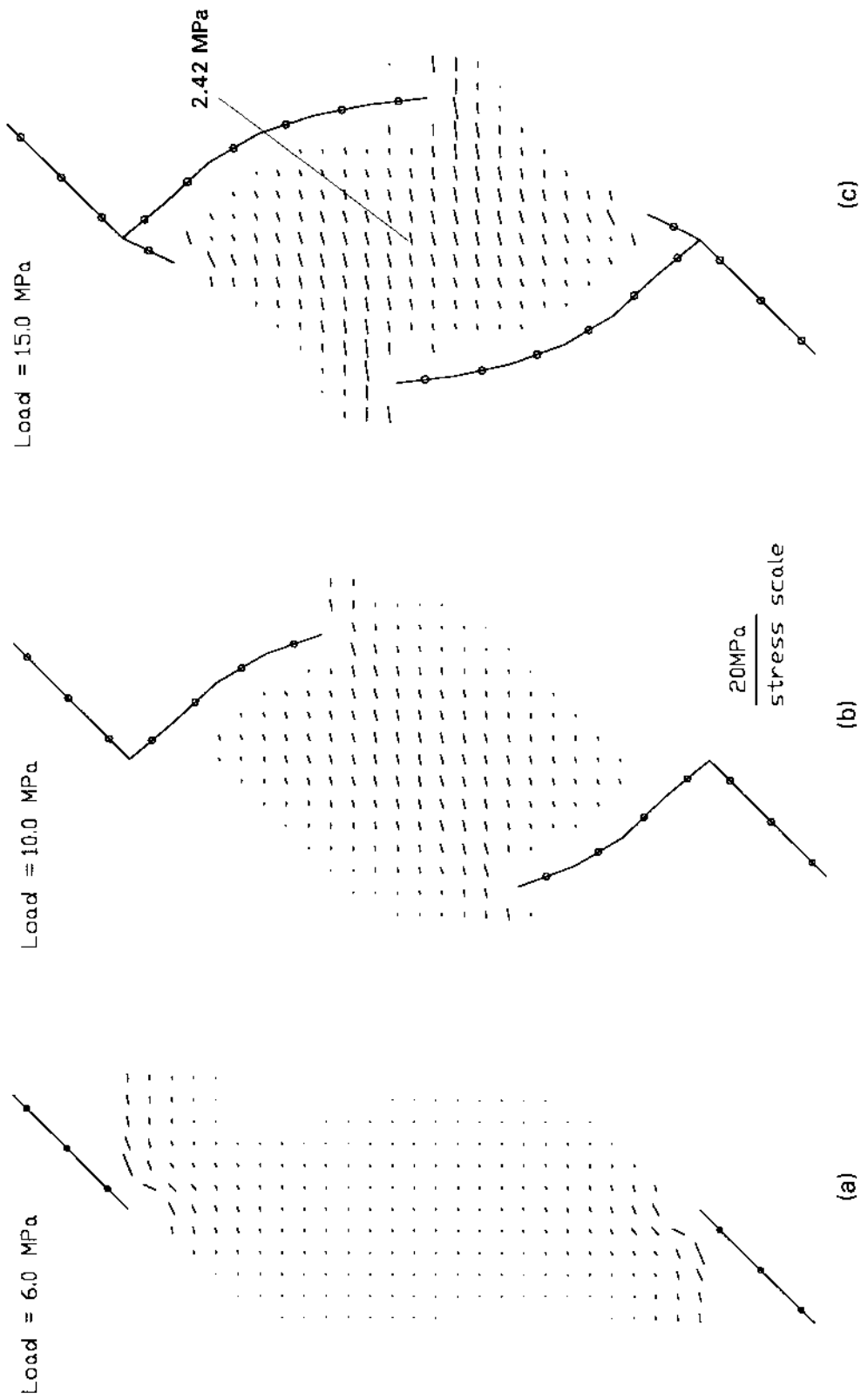


Fig.10. Tensile principal stress distribution in the bridge area between two 45/90 closed cracks for different uniaxial loads. Figures (a), (b) and (c) correspond to the same states as in Fig.9.

$$G_{Ic} = \frac{(1-\nu^2)}{E} K_{Ic}^2 = \frac{\pi(1-\nu^2)}{E} \sigma_t^2 a; \quad a = \frac{E}{\pi(1-\nu^2)} \frac{G_{Ic}}{\sigma_t^2} \quad (5)$$

Substituting the values in Table 2 into Eq.(5), the crack length is calculated to be a=2.0 mm.

The new crack propagates upward and downward at the loading stress of 15 MPa. It finally connects with the mode II crack previously developed from the pre-existing crack tips, and the coalescence occurs. It needs to be mentioned that if we do not consider the occurrence of the mode II cracks in the numerical analysis, the mode I crack developed from the center of the bridge is found to propagate upward and downward in a straight path and will not connect with the pre-existing crack tips. This indicates that even though the main part of the coalescence is caused by mode I crack propagation, mode II crack initiation and propagation play a key role in the final coalescence. The simulated process of coalescence and the level of load of 15 MPa is almost identical to that observed in the experiment shown in Fig.3.

### *3). Coalescence caused by tensile failure for sample 45°/105° with closed cracks*

The predicted process is shown in Fig.11. When the load is 20 MPa, the two pre-existing cracks start to slide. As a consequence of crack sliding, mode I cracks occur at the crack tips, and they grow into the bridge and coalesce. The predicted path agrees with the observed path from the experiments, see also Fig.4.

The simulated critical load of coalescence is also in fair agreement with the experimental results. The results are shown in Fig.12 for different bridge inclination when the inclination of pre-existing cracks is 45°. As with the experimental results, the coalescence of closed cracks is found in the simulation to require higher load than that of open cracks. The simulated load of coalescence reaches the minimum when the bridge inclination is about 75° to 90°. At these bridge inclinations, the coalescence is caused by mixed mode I and mode II failure. When the bridge inclination is 45° or 105° coalescence occurs at higher load and the coalescence is caused by pure mode II or mode I failure respectively. The result indicates that mixed mode failure controls the strength of pre-fractured material and needs to be considered in stability analysis of jointed rock masses.



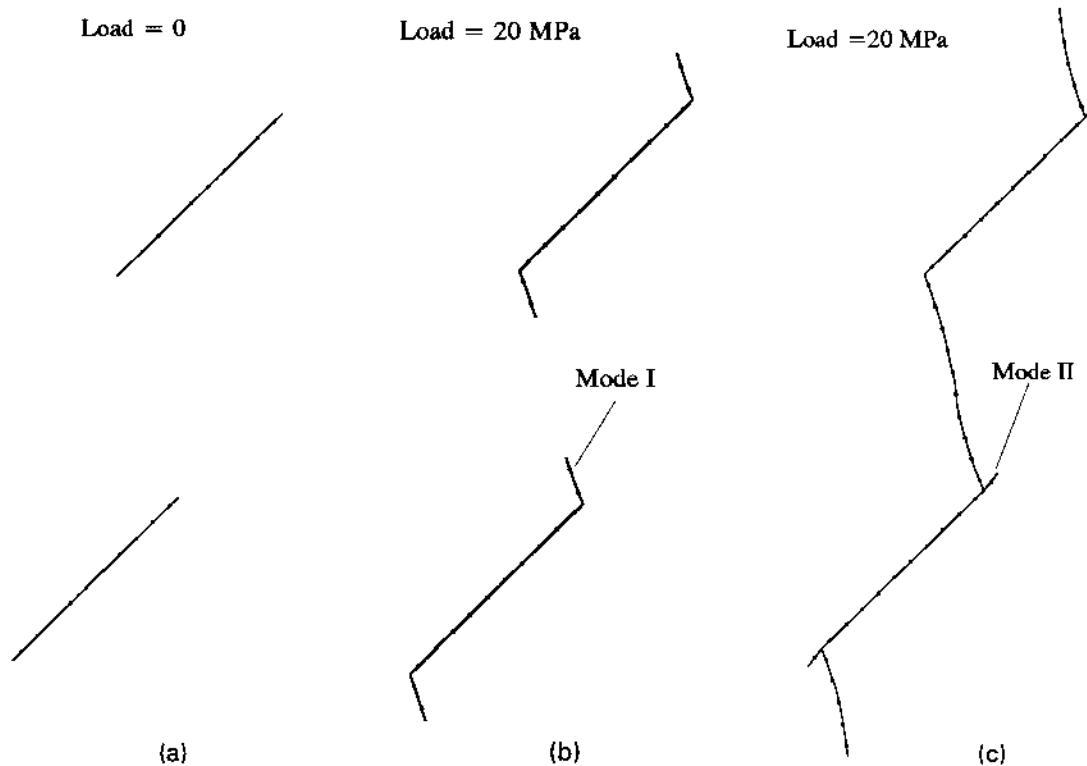


Fig.11. Simulated coalescence of two 45°/105° closed cracks. Compare with experimental results in Fig.4.

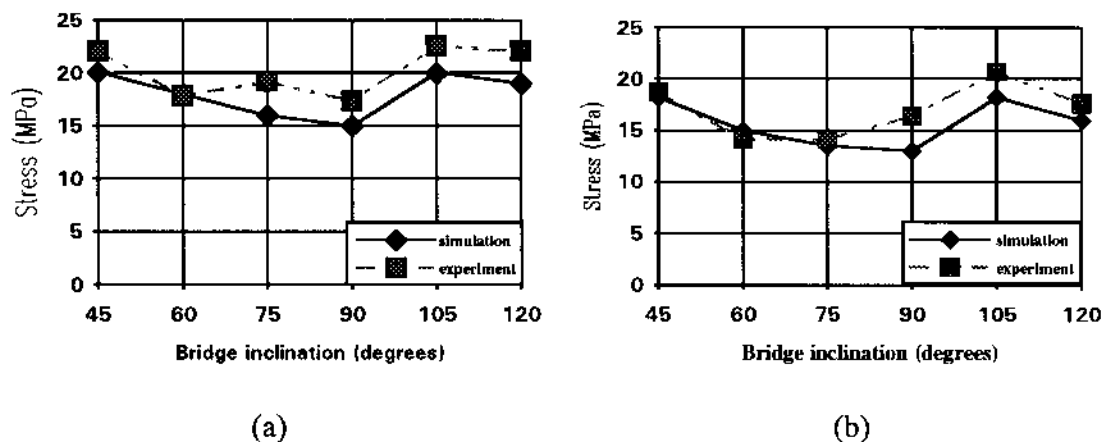


Fig.12. Comparison of numerical and experimental load of coalescence of two pre-existing cracks with inclination of 45°. (a) Closed pre-existing cracks; (b) open pre-existing cracks.

## Discussion and Conclusions

The mechanism of fracture coalescence in hard, porous material is rather complicated. As has been indicated by experiments and simulations, fracture coalescence can be generated by mode I failure, mode II failure, or mixed mode I

and II failure. The mode II failure plays an important role in the coalescence between two non-overlapping cracks. The mechanism of coalescence observed in gypsum does not agree with previous experimental results where glass and polymer have been used [5][15][16]. For those materials coalescence only occurs between overlapping cracks and is caused by mode I failure. The possible reason why mode II failure can occur in gypsum and other earth materials such as rock and concrete is the existence of voids and pores in these materials. Porous material can absorb the shear dilation in the fracture process zone and prevent the development of resistant stress due to shear dilation. The mode II fracture toughness of material with high porosity is known to be low.

The new modified G-criterion which considers both mode I and mode II surface energy can predict the complicated process of fracture coalescence. Excellent agreement is obtained between the experimental and predicted path and load magnitude of coalescence. The numerical technique by using the modified G-criterion and DDM is proved to be a powerful tool in studying fracture propagation and coalescence. This technique can also be applied to the study of the strength of jointed rock masses where joints and rock bridges widely exist.

## Acknowledgements

This work is sponsored by NUTEK for Sino-Swedish research co-operation. The author would like thank Prof. O. Stephansson for his supervision of the study and for his reviewing of the manuscript. Prof. H.H. Einstein and B. Ghahreman are also acknowledged for their guidance and help in the experimental work.

## References

- [1] H.H. Einstein, D. Veneziano, G.B. Baecher and K.J. O'reilly, The effect of discontinuity persistence on rock stability. *Int. J. Rock Mech. Min. Sci. & Geomech. Abs.* **20(5)**, 227-237. (1983)
- [2] E.Z. Lajtai, Shear strength of weakness planes in rock. *Int. J. Rock Mech. Min. Sci. & Geomech. Abs.* **6**, 299-515. (1969).
- [3] Z.P. Bazant and P.A. Pfeifer, Shear fracture tests of concrete, *Materials and structures*, **19**, 111-121. (1986)

- [4] S.J. Jung, M. Enbaya and J.K. Whyatt, The study of fracture of brittle rock under pure shear loading. *Proc. Fractured and Jointed Rock Masses (preprint)*, 458-475. (1992)
- [5] H. Horri and S. Nemat-Nasser, Brittle failure in compression: splitting, faulting and brittle-ductile transition, *Phil. Trans. Roy. Soc.*, **319 (1549)**, 337-374. (1986)
- [6] O. Reyes and H.H. Einstein, Failure mechanism of fractured rock — A fracture coalescence model. *Proc. 7th Int. Con. on Rock Mechanics*, **1**, 333-340. (1991)
- [7] B. Shen, O. Stephansson, H.H. Einstein and B. Ghahreman, Coalescence of open and closed cracks — A laboratory investigation. Manuscript submitted to *Int. J. Rock Mech. Min. Sci. & Geomech. Abs.* (1993)
- [8] B. Shen and O. Stephansson, Deformation and propagation of finite joints in Rock masses. *Proc. Fractured and Jointed Rock Masses (preprint)*, 312-318. (1992)
- [9] B. Shen and O. Stephansson, Modification of the G-criterion for crack propagation subjected to compression. *Engineering Fracture Mechanics*. (1993) (in press)
- [10] B. Shen and O. Stephansson. Numerical analysis of mixed mode I and mode II fracture propagation. *Int. J. Rock Mech. Min. Sci. & Geomech. Abstr. (Special issue for 34th U.S. Symp. on Rock Mech.)*. (1993) (in press)
- [11] F. Eordgan and G. C. Sih, On the crack extension in plates under plane loading and transverse shear. *ASME J. Bas. Engng* **85**, 519-527 (1963).
- [12] G. C. Sih, Strain-energy-density factor applied to mixed mode crack problems. *Int. J. Crack*. **10(3)**, 305-321 (1974).
- [13] K. Hellan, *Introduction to fracture mechanics*. McGraw-Hill International Editions, Singapore (1984).
- [14] R. Nelson Modelling a jointed rock mass. S.M. Thesis, Massachusetts Institute of Technology. (1968)
- [15] W. Brace and J. Byerlee, Recent experimental studies of brittle fracture of rocks. *In: Failure and Breakage of Rock. AIME*, 57-81 (1967).
- [16] S. Melin, Why are crack paths in concrete and mortar different from those in PMMA? *Material and Structure*, **22**, 23-27. (1989)

